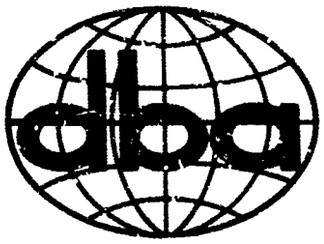

DBA SYSTEMS, INC.

ADVANCED METHODS FOR THE CALIBRATION OF METRIC CAMERAS

Photogrammetry

Computer Application

Mathematical Research

Electro-Optical Instrumentation

MAIN OFFICE
Post Office Drawer 550
Melbourne, Florida 32901
Phone: 305 727-0660

WASH. D.C. OFFICE
9301 Annapolis Road
Lanham, Maryland 20801
Phone: 301 577-3001

AD

ADVANCED METHODS FOR THE CALIBRATION OF METRIC CAMERAS

Final Report, Part 1

by

Duane C. Brown

December 1966

Submitted To:

U.S. Army Engineer Topographic Laboratories
Fort Belvoir, Virginia 22060

Contract Number: DA-44-009-AMC-1457(X)

Submitted By:

DBA Systems, Inc.
P.O. Drawer 550
Melbourne, Florida 32901

SUMMARY

A new analytical approach to the problem of the accurate calibration of metric cameras is developed and specific applications are reported. The method permits an indefinitely large number of frames from a given camera to be reduced simultaneously, yet efficiently, to produce common parameters of the inner cone for all frames, as well as independent elements of exterior orientation for each frame. Because control points may be exercised repeatedly in a common reduction, very large sets of well distributed residuals can be generated from a relatively small set of control points (in principle, a complete and accurate calibration could be performed from as few as three control points). From such large sets of residuals empirical functions can be derived to account for persistent, unmodelled systematic error. In addition, it becomes feasible to establish the variation in the accuracies of the radial and tangential components of plate coordinates throughout the format and thus to establish appropriate empirical weighting functions for subsequent applications. The method is of universal applicability and encompasses (a) calibration from aerial photographs, (b) calibrations from stellar photographs, and (c) calibrations from multicollimator photographs. Applied to stellar calibrations, the method leads to improved accuracies and convenience by completely doing away with conventional requirements for precise timing of the shutter and for stability of the camera throughout successive exposures. Applied to multicollimator calibrations, the method has far reaching implications concerning both the use of existing multicollimators and the design of future multicollimators.

FOREWORD

This is Part 1 of a final report prepared by Duane C. Brown of DBA Systems, Inc., under Contract DA-44-009-AMC-1457(X), project number 4A00145001A52C, task 01, subtask 006. ETL project engineer was Lawrence A. Gambino, Chief, Advanced Technology Division, Computer Sciences Laboratory.

TABLE OF CONTENTS

Table of Contents (Continued)

ADVANCED METHODS FOR THE CALIBRATION OF METRIC CAMERAS

By

Duane C. Brown

1. INTRODUCTION

It is generally appreciated that calibration is most meaningful and effective when it is performed on a system in its operating environment. Despite the acknowledged soundness of this principle, the calibration of aerial mapping cameras has almost universally been relegated to the laboratory. Laboratory methods were long ago found to be inadequate for the stringent calibration required for ballistic cameras and have been supplanted by more powerful, and more comprehensive methods of stellar calibration. The outstanding success of stellar calibration with ballistic cameras, some of which employ the same type of lenses as certain aerial cameras, has naturally led to suggestions that the stellar technique also be applied to aerial mapping cameras. This has been done experimentally to a limited extent. However, despite its potential advantages, the stellar method does indeed share with laboratory methods the shortcoming of failing to simulate the typical operational utilization and environment of mapping cameras. It follows that for the stellar method to become fully acceptable for calibration of mapping cameras, it must be shown to yield results equivalent to those obtainable from definitive operational calibrations.

In mid 1966, D. Brown Associates, Inc. (DBA) received a contract from the Army's Engineering Test Laboratories (ETL) to implement an unsolicited DBA proposal to develop an advanced procedure for the definitive metric calibration of photogrammetric cameras in their operating environment. Although also applicable to stellar calibrations, the proposed technique,

called SMAC (Simultaneous Multiframe Analytical Calibration), was especially directed at the problem of calibrating aerial cameras from photography taken over a targeted calibration range. Here it was recognized that in many situations, any one frame would be unlikely to contain enough target images to permit a definitive calibration. Even with highly dense control, it was appreciated that such factors as residual uncompensated film deformation and refractive effects of air turbulence or shock waves could conceivably compromise the results from a single frame. Accordingly, it was considered to be desirable to be able to merge observations from a large number of frames in order to arrive at a comprehensive result. Inasmuch as each frame would have a unique set of elements of exterior orientation (corresponding to the instantaneous position and angular orientation of the cameras), such an approach, if rigorously applied, would entail the introduction of six fresh unknowns for each frame carried in the reduction. Seemingly, then, the reduction for a moderately large number of frames could well become computationally prohibitive. The SMAC reduction overcomes such difficulties by exploiting certain patterned characteristics of the general system of normal equations to produce a practical and fully rigorous solution to the problem no matter how many frames are carried in the reduction. By virtue of this, the computational requirements of a SMAC reduction increase only linearly with the number of frames exercised rather than as the cube of the number as in a 'brute force' reduction. The number of frames that can be accommodated in a simultaneous adjustment is therefore without set limit.

In this report we shall outline the development of the SMAC reduction and shall present the results of its application to the calibration of the Air Force KC-6A aerial mapping camera. We shall also discuss results of other specific applications and shall indicate how the method can be applied to laboratory calibrations. As we shall see, exceptionally accurate and meaningful calibrations are made possible by the application of SMAC to sets of photographs taken over an aerial calibration range. Such calibrations can be particularly useful as standards for evaluating the adequacy of laboratory and stellar methods of calibration.

2. THEORETICAL DEVELOPMENT

2.1 Symmetric Radial Distortion

The SMAC method of calibration is a direct and natural outgrowth of our earlier work (Brown, 1956, 1957, 1958, 1964, 1965; Brown, Davis, Johnson, 1964). In Brown (1956) the stellar method of calibration of symmetric radial distortion was placed on a rigorous footing through the extension of the basic plate reduction developed by Schmid (1953). This extension exploited the result from optical ray tracing that the radial distortion δ_r of a perfectly centered lens can be expressed as an odd powered series of the form

$$\delta_r = K_1 r^3 + K_2 r^5 + K_3 r^7 + \dots \tag{1}$$

in which

$r = (x^2 + y^2)^{\frac{1}{2}}$ = radial distance

x, y = coordinates of image referred to principal point as origin.

By virtue of the fact that the x, y components of distortion can be expressed as

$$\delta_x = \frac{x}{r} \delta_r$$

$$\delta_y = \frac{y}{r} \delta_r \tag{2}$$

it was shown that coefficients of distortion (K_1, K_2, K_3, ...) could be introduced directly into the projective equations and that these parameters could be sharply recovered simultaneously with the elements of orientation in a rigorous least squares adjustment. This reduction marked the beginning of the strictly analytical approach to camera calibration. To be sure, stellar techniques had previously been used for camera calibration, but they were dichotomous in character. That is, the elements of orientation were determined from an initial reduction involving a carefully balanced selection of control, but otherwise ignoring the existence of

radial distortion. From the resulting residual vectors, the distortion function was then established by graphical means based on a plot of the radial components of the residuals versus radial distance.

The method developed in Brown (1956) immediately became standard for Air Force ballistic cameras. Although the method constituted a significant advance, it was found with some cameras to be impossible to achieve an rms error of plate residuals of much better than four microns when stars throughout the entire plate format were carried in the reduction. By contrast, when stars were limited to areas of about one third the diameter of the format, no difficulty was encountered in achieving rms errors within the 2 to 3 micron range considered to characterize random plate measuring errors. This clearly meant that for such cameras a significant unmodelled systematic error was affecting the results. Although the source of the systematic error was not known at the time (plate measuring comparators were suspected, but were later vindicated), adverse effects were minimized in trajectory reductions by the expedient of performing independent plate reductions for two or three slightly overlapping regions covering the trajectory on each plate.

2.2 Decentering Distortion

It was not until 1962 that the underlying difficulty was resolved in an investigation reported in Brown (1964) and later extended in Brown (1965). The unmodelled systematic error was identified as decentering distortion, i.e., the distortion resulting from the imperfect centration of lens elements. This type of distortion had been considered earlier in terms of the thin prism model as described in both the second and third editions of the Manual of Photogrammetry. However, it was not possible to reconcile the observed systematic components of residuals from plate reductions with this model. The reason was uncovered in Brown (1964) by means of analytical ray tracing through a thin prism situated in front of a hypothetically perfect lens. This revealed the exact analytical expression for the thin prism model and showed that the generally adopted description of the thin prism effect was incomplete. The full statement of the model was found to demand an asymmetric radial component in addition to the

previously accepted tangential component. As thus revised, the thin prism model was found to be consistent with observed residuals when effects of projective compensations were duly taken into account.

In Brown (1965), the thin prism model was compared with a mo derived by Conrady (1917). Although the Conrady model was derived by means of direct analytical ray tracing through a decentered lens (rather than from arguments of analogical equivalence underlying the thin prism model), it had been neglected by the photogrammetric community. The thin prism and Conrady models were found to be in agreement with regard to the magnitude of the tangential component of decentering distortion, but the radial components of the two models were found to differ by a factor of three. It was shown that this discrepancy could be resolved by a projective transformation insofar as first order effects were concerned. However, the projective equivalence of the two models was found no longer to hold when higher order effects were of significance. Accordingly, the thin prism model was supplanted in Brown's plate reduction by an extended form of the more widely applicable model of Conrady.

In terms of radial and tangential components, Conrady's model assumes the form

$$\begin{aligned} \Delta r &= 3 P_r \sin(\varphi - \varphi_o) \\ \Delta t &= P_r \cos(\varphi - \varphi_o) \end{aligned} \tag{3}$$

in which

$P_r = J_1 r^2 + J_2 r^4 + J_3 r^6 + \ldots$ = profile function of tangential distortion

φ = angle between positive x axis and radius vector to point x,y = arc sin (x/r) = arc cos (y/r)

φ_o = angle between positive x axis and axis of maximum tangential distortion.

In the thin prism model, the factor of three in the expression for Δr is replaced by unity. In both models, the quantities requiring determination in the process of calibration are the phase angle φ_o and the coefficients of the profile function $J_1, J_2, \ldots$. In Brown (1965) it is shown that Conrady's model can be expressed in terms of x and y components as

$$\Delta x = [P_1(r^2 + 2x^2) + 2P_2 xy][1 + P_3 r^2 + \dots]$$

(4)

$$\Delta y = [2P_1 xy + P_2(r^2 + 2y^2)][1 + P_3 r^2 + \dots]$$

in which the new coefficients P_1, P_2, P_3 are defined by

$$\begin{aligned} P_1 &= -J_1 \sin\phi_o \\ P_2 &= J_1 \cos\phi_o \\ P_3 &= J_2/J_1 \\ P_4 &= J_3/J_1 \\ &\vdots \end{aligned} \qquad (5)$$

This formulation has the advantage of being a linear expression in the leading coefficients P_1, P_2 when the higher order coefficients P_3, P_4 are zero.

When decentering exists, the principal point of autocollimation does not coincide with the principal point of photogrammetry. With mapping lenses this separation is likely to amount to only a few tens of microns and is of no metric consequence. With objectives having very long focal lengths (such as those of astronomical telescopes) the separation could amount to several millimeters and thus assume a degree of significance. The means for handling this situation is discussed in Brown (1965).

When the model for decentering distortion was incorporated into the plate reduction, it became possible with good consistency to achieve rms errors within the desired two to three micron range without resorting to piecewise reductions.

2.3 Single Frame Calibration

2.3.1 Introduction

We shall define a frame to consist of an exposure or a series of exposures for which the position and orientation of the camera may be considered to be invariant. In this context,

a stellar plate containing several different exposures may be regarded as consisting of either

(a) a single frame if the orientation is considered to remain unchanged throughout the series of exposures;

or

(b) several frames if the orientation is considered to change (however slightly) from one exposure (or group of exposures) to the next.

In the case of aerial photographs, each exposure would ordinarily constitute an independent frame.

In this section we shall formulate the plate reduction for a single frame under the assumption that the photographed control (whether stellar or ground control) is flawless. Such a reduction is a special case of the advanced plate reduction formulated in Brown (1964). As we shall presently see, the single frame reduction generates the basic building blocks needed in the Simultaneous Multiframe Analytical Calibration SMAC.

2.3.2 Observational Equations

The projective equations resulting from an undistorted central projection may be written as (Brown, 1957)

$$x - x_p = c\,\frac{A\lambda + B\mu + C\nu}{D\lambda + E\mu + F\nu}$$

(6)

$$y - y_p = c\,\frac{A'\lambda + B'\mu + C'\nu}{D\lambda + E\mu + F\nu}$$

in which

x_p, y_p, c = elements of interior orientation,

$\begin{bmatrix} A & B & C \\ A' & B' & C' \\ D & E & F \end{bmatrix}$ = orientation matrix, elements of which are functions of three independent angles α, ω, κ referred to arbitrary X, Y, Z frame in object space,

λ, μ, ν = X, Y, Z direction cosines of ray joining corresponding image and object points.

When points in object space are at a sensibly finite distance, the direction cosines may be expressed as

$$\begin{aligned} \lambda &= (X - X^c)/R \\ \mu &= (Y - Y^c)/R \\ \nu &= (Z - Z^c)/R \end{aligned} \tag{7}$$

in which X, Y, Z and X^c, Y^c, Z^c are object space coordinates of the point and the center of projection, respectively, and R is the distance between these points, i.e.,

$$R = [(X - X^c)^2 + (Y - Y^c)^2 + (Z - Z^c)^2]^{\frac{1}{2}}. \tag{8}$$

When stellar or other strictly directional control is employed, the direction cosines may be expressed as

$$\begin{aligned} \lambda &= \sin \alpha^* \cos \omega^* \\ \mu &= \cos \alpha^* \cos \omega^* \\ \nu &= \sin \omega^* \end{aligned} \tag{9}$$

in which the angles α^*, ω^* are measured in the same sense as the pair of angles α, ω defining the direction of the camera axis.

We shall assume that the direction cosines λ, μ, ν have been corrected for atmospheric refraction by means of standard formulas. If we then let x^o, y^o denote the observed plate coordinates, the left hand sides of the projective equations (6) can be replaced by

$$\begin{aligned} x - x_p &= \bar{x} + v_x + \bar{x}(K_1 r^2 + K_2 r^4 + K_3 r^6 + \ldots) \\ &\quad + [P_1(r^2 + 2\bar{x}^2) + 2P_2 \bar{x}\bar{y}][1 + P_3 r^2 + P_4 r^4 + \ldots] \\ y - y_p &= \bar{y} + v_y + \bar{y}(K_1 r^2 + K_2 r^4 + K_3 r^6 + \ldots) \\ &\quad + [2P_1 \bar{x}\bar{y} + P_2(r^2 + 2\bar{y}^2)][1 + P_3 r^2 + P_4 r^4 + \ldots] \end{aligned} \tag{10}$$

in which v_x and v_y are plate measuring residuals and

$$\left.\begin{aligned} \bar{x} &= x^o - x_p \\ \bar{y} &= y^o - y_p \end{aligned}\right\} = \text{observed plate coordinates referred to principal point.}$$

$$r = (\bar{x}^2 + \bar{y}^2)^{\frac{1}{2}}$$

When these relations are substituted into (6), the projective equations explicitly involve the coefficients of radial and decentering distortion. It is to be noted that in formulating equation (10) we implicitly regard the optical axis and principal axis as being coincident. This formulation can introduce no error of metric consequence with conventional metric cameras focussed at or near infinity, for here the optical axis and principal axis must, in fact, nearly coincide if acceptably sharp imagery is to be maintained throughout the format. A more complicated formulation accounting for the variation of distortion with object distance would be needed for close-in terrestrial photogrammetry. A still more complicated formulation would be needed when the Scheimpflug condition is exercised in terrestrial photogrammetry to maintain perfect focus throughout a selected plane in object space that is not perpendicular to the optical axis. Although the present treatment will be limited to cameras focussed at or near infinity, it is capable of being extended to embrace specialized applications to terrestrial photogrammetry.

We shall use the term projective parameters to denote collectively the nine elements of orientation (x_p, y_p, c, α, ω, κ, X^c, Y^c, Z^c) and the coefficients of radial and decentering distortion (K_1, K_2, ..., P_1, P_2, ...). We shall also distinguish between 'interior' projective parameters consisting of x_p, y_p, c, K_1, K_2, ..., P_1, P_2, ..., and 'exterior' projective parameters consisting of α, ω, κ, X^c, Y^c, Z^c. Anticipating later results, we find it convenient to introduce the symbol $\dot{u}_i$ to denote the i^{th} interior projective parameter and the symbol $\ddot{u}_j$ to denote the j^{th} exterior projective parameter. Specifically,

$$
\begin{array}{lll}
\dot{u}_1 = x_p & \dot{u}_4 = K_1 & \dot{u}_7 = P_1 \\
\dot{u}_2 = y_p & \dot{u}_5 = K_2 & \dot{u}_8 = P_2 \\
\dot{u}_3 = c & \dot{u}_6 = K_3 & \dot{u}_9 = P_3
\end{array} \tag{12}
$$

and

$$
\begin{array}{ll}
\ddot{u}_1 = \alpha & \ddot{u}_4 = X^c \\
\ddot{u}_2 = \omega & \ddot{u}_5 = Y^c \\
\ddot{u}_3 = \kappa & \ddot{u}_6 = Z^c \quad .
\end{array} \tag{13}
$$

In (12) we take note of practical experience involving the calibration of a wide variety of lenses which indicates that no more than three coefficients are likely to be required for either

radial or decentering distortion (indeed, with but few exceptions, two coefficients have been found to suffice for decentering distortion and one or two coefficients have been found to suffice for radial distortion).

With the above symbolism, the projective equations may be expressed functionally as

$$
\begin{aligned}
f_1 &= f_1 (x^\circ + v_x, y^\circ + v_y; \dot{u}_1, \dot{u}_2, \ldots, \dot{u}_9; \ddot{u}_1, \ddot{u}_2, \ldots, \ddot{u}_6) = 0 , \\
f_2 &= f_2 (x^\circ + v_x, y^\circ + v_y; \dot{u}_1, \dot{u}_2, \ldots, u_9; \ddot{u}_1, \ddot{u}_2, \ldots, \ddot{u}_6) = 0 .
\end{aligned} \tag{14}
$$

We shall now proceed as if all parameters were unknown and had to be recovered from plate measurements of images of photographed control points. Accordingly, we follow the usual procedure of operating on observational equations that have been linearized about initial approximations by means of Taylor's series. Thus, in (14) we replace the $\dot{u}$'s and $\ddot{u}$'s by the expressions

$$
\begin{aligned}
\dot{u}_i &= \dot{u}_i^{\circ\circ} + \delta \dot{u}_i , \quad i = 1,2, \ldots, 9 , \\
\ddot{u}_j &= \ddot{u}_j^{\circ\circ} + \delta \ddot{u}_j , \quad j = 1,2, \ldots, 6 ,
\end{aligned} \tag{15}
$$

in which the $\dot{u}^{\circ\circ}$ and $\ddot{u}^{\circ\circ}$ denote approximations and the $\delta \dot{u}$ and $\delta \ddot{u}$ are associated corrections. When equations (15) are substituted into (14) and the resulting expressions are linearized, we obtain the following result

$$
\begin{aligned}
&a_1 v_x + a_2 v_y + \dot{b}_1 \delta \dot{u}_1 + \dot{b}_2 \delta \dot{u}_2 + \ldots + \dot{b}_9 \delta \dot{u}_9 \\
&\qquad + \ddot{b}_1 \delta \ddot{u}_1 + \ddot{b}_2 \delta \ddot{u}_2 + \ldots + \ddot{b}_6 \delta \ddot{u}_6 = f_1^\circ \\
&a_1' v_x + a_2' v_y + \dot{b}_1' \delta \dot{u}_1 + \dot{b}_2' \delta \dot{u}_2 + \ldots + \dot{b}_9' \delta \dot{u}_9 \\
&\qquad + \ddot{b}_1' \delta \ddot{u}_1 + \ddot{b}_2' \delta \ddot{u}_2 + \ldots + \ddot{b}_6' \delta \ddot{u}_6 = f_2^\circ .
\end{aligned} \tag{16}
$$

At this point, we introduce the subscript i to distinguish the equations arising from the measurements of the i th image. The pair of observational equations (16) can then be represented in matrix form as

$$(17)\quad A_1 v_1 + \dot{B}_1 \dot{\delta} + \ddot{B}_1 \ddot{\delta} = \epsilon_1$$

in which

$$v_1 = (v_x\ v_y)_1^T$$

$$(18)\quad \dot{\delta} = (\delta\dot{u}_1\ \delta\dot{u}_2\ \ldots\ \delta\dot{u}_9)^T$$

$$\ddot{\delta} = (\delta\ddot{u}_1\ \delta\ddot{u}_2\ \ldots\ \delta\ddot{u}_6)^T$$

and

$$A_1 = \begin{bmatrix} a_1 & a_2 \\ a_1' & a_2' \end{bmatrix}_1 = \frac{\partial (f_1^0,\ f_2^0)_1}{\partial (x^0,\ y^0)_1},$$

$$\dot{B}_1 = \begin{bmatrix} \dot{b}_1 & \dot{b}_2 & \ldots & \dot{b}_9 \\ \dot{b}_1' & \dot{b}_2' & \ldots & \dot{b}_9' \end{bmatrix}_1 = \frac{\partial (f_1^0,\ f_2^0)_1}{\partial (\dot{u}_1^{00},\ \dot{u}_2^{00},\ \ldots,\ \dot{u}_9^{00})},$$

$$(19)$$

$$\ddot{B}_1 = \begin{bmatrix} \ddot{b}_1 & \ddot{b}_2 & \ldots & \ddot{b}_6 \\ \ddot{b}_1' & \ddot{b}_2' & \ldots & \ddot{b}_6' \end{bmatrix}_1 = \frac{\partial (f_1^0,\ f_2^0)_1}{\partial (\ddot{u}_1^{00},\ \ddot{u}_2^{00},\ \ldots,\ \ddot{u}_6^{00})},$$

$$\epsilon_1 = \begin{bmatrix} -f_1^0 \\ -f_2^0 \end{bmatrix}_1 = \begin{bmatrix} -f_1\ (x^0,\ y^0,\ \dot{u}_1^{00},\ \dot{u}_2^{00},\ \ldots,\ \dot{u}_9^{00};\ \ddot{u}_1^{00},\ \ddot{u}_2^{00},\ \ldots,\ \ddot{u}_6^{00}) \\ -f_2\ (x^0,\ y^0,\ \dot{u}_1^{00},\ \dot{u}_2^{00},\ \ldots,\ \dot{u}_9^{00};\ \ddot{u}_1^{00},\ \ddot{u}_2^{00},\ \ldots,\ \ddot{u}_6^{00}) \end{bmatrix}_1.$$

in these equations the following notation for the generalized Jacobian has been adopted:

$$(20)\quad \frac{\partial (p_1, p_2, \ldots, p_m)}{\partial (q_1, q_2, \ldots, q_n)} = \begin{bmatrix} \frac{\partial p_1}{\partial q_1} & \frac{\partial p_1}{\partial q_2} & \ldots & \frac{\partial p_1}{\partial q_n} \\ \frac{\partial p_2}{\partial q_1} & \frac{\partial p_2}{\partial q_2} & \ldots & \frac{\partial p_2}{\partial q_n} \\ \vdots & \vdots & & \vdots \\ \frac{\partial p_m}{\partial q_1} & \frac{\partial p_m}{\partial q_2} & \ldots & \frac{\partial p_m}{\partial q_n} \end{bmatrix}.$$

Explicit expressions for the elements of the matrices defined in (19) are provided in Appendix A. There it is shown that the coefficient matrix A_i of the residual vector becomes equal to the unit matrix when negligible first order terms are dropped. Accordingly, the entire set of linearized observational equations arising from all n measured control points may be merged into the single matrix equation

$$(21) \quad v + \dot{B}\,\dot{\delta} + \ddot{B}\,\ddot{\delta} = \epsilon$$

in which

$$(22) \quad \underset{(2n,1)}{v} = \begin{bmatrix} v_1 \\ v_2 \\ \cdot \\ \cdot \\ \cdot \\ v_n \end{bmatrix}, \quad \underset{(2n,9)}{\dot{B}} = \begin{bmatrix} \dot{B}_1 \\ \dot{B}_2 \\ \cdot \\ \cdot \\ \cdot \\ \dot{B}_n \end{bmatrix}, \quad \underset{(2n,6)}{\ddot{B}} = \begin{bmatrix} \ddot{B}_1 \\ \ddot{B}_2 \\ \cdot \\ \cdot \\ \cdot \\ \ddot{B}_n \end{bmatrix}, \quad \underset{(2n,1)}{\epsilon} = \begin{bmatrix} \epsilon_1 \\ \epsilon_2 \\ \cdot \\ \cdot \\ \cdot \\ \epsilon_n \end{bmatrix}.$$

We shall assume that the covariance matrix Λ of the observational vector is of the form

$$(23) \quad \underset{(2n,2n)}{\Lambda} = \operatorname{diag}\left(\underset{(2,2)}{\Lambda_1}, \underset{(2,2)}{\Lambda_2}, \cdots, \underset{(2,2)}{\Lambda_n} \right),$$

in which

$$(24) \quad \underset{(2,2)}{\Lambda_i} = \begin{bmatrix} \sigma_{x_i}^2 & \sigma_{x_i y_i} \\ \sigma_{x_i y_i} & \sigma_{y_i}^2 \end{bmatrix}.$$

Thus, Λ is a block diagonal matrix of 2×2 matrices which need not necessarily be diagonal, a fact that admits consideration of plate coordinates that have been derived from more primary measurements (e.g., measurements made on a polar coordinate comparator).

2.3.3. Introduction of A Priori Constraints on Projective Paramters

Thus far, we have regarded the projective parameters as being completely unknown. For greater generality and flexibility we shall now abandon this assumption and assume that each parameter is subject to a priori constraints. Accordingly, we introduce the 'supplementary' sets of observational equations

$$(25)\qquad \begin{aligned} \dot{u}_i^\circ + \dot{v}_i &= \dot{u}_i \qquad (i = 1,2,\ldots,9) \\ \ddot{u}_j^\circ + \ddot{v}_j &= \ddot{u}_j \qquad (j = 1,2,\ldots,6) \end{aligned}$$

The quantities $\dot{u}_i$ and $\ddot{u}_j$ in (25) can be replaced by expressions given in (15) to produce the alternative set of supplementary observational equations:

$$(26)\qquad \begin{aligned} \dot{v}_i &= \delta\dot{u}_i = \dot{\epsilon}_j \quad , \qquad (i = 1,2,\ldots,9) \\ \ddot{v}_j &= \delta\ddot{u}_j = \ddot{\epsilon}_j \quad , \qquad (j = 1,2,\ldots,6) \end{aligned}$$

in which

$$(27)\qquad \begin{aligned} \dot{\epsilon}_i &= \ddot{u}_i^{\circ\circ} - \dot{u}_i^\circ \quad , \\ \ddot{\epsilon}_j &= \ddot{u}_j^{\bullet\circ} - \ddot{u}_j^\circ \quad . \end{aligned}$$

These may be represented in matrix form as

$$(28)\qquad \begin{aligned} \underset{(9,1)}{\dot{v}} - \underset{(9,1)}{\dot{\delta}} &= \underset{(9,1)}{\dot{\epsilon}} \quad , \\ \underset{(6,1)}{\ddot{v}} - \underset{(6,1)}{\ddot{\delta}} &= \underset{(6,1)}{\ddot{\epsilon}} \quad , \end{aligned}$$

in which

$$(29)\qquad \dot{v} = \begin{bmatrix} \dot{v}_1 \\ \dot{v}_2 \\ \cdot \\ \cdot \\ \cdot \\ \dot{v}_9 \end{bmatrix} , \quad \dot{\epsilon} = \begin{bmatrix} \dot{\epsilon}_1 \\ \dot{\epsilon}_2 \\ \cdot \\ \cdot \\ \cdot \\ \dot{\epsilon}_9 \end{bmatrix} , \quad \ddot{v} = \begin{bmatrix} \ddot{v}_1 \\ \ddot{v}_2 \\ \cdot \\ \cdot \\ \cdot \\ \ddot{v}_6 \end{bmatrix} , \quad \ddot{\epsilon} = \begin{bmatrix} \ddot{\epsilon}_1 \\ \ddot{\epsilon}_2 \\ \cdot \\ \cdot \\ \cdot \\ \ddot{\epsilon}_6 \end{bmatrix} .$$

We shall let $\dot{\Lambda}$ (a 9 x 9 matrix) and $\ddot{\Lambda}$ (a 6 x 6 matrix) denote the specified covariance matrices of the observational vectors $\dot{u}^\circ$ and $\ddot{u}^\circ$, respectively. Later, we shall discuss various applications of these covariance matrices.

2.3.4 Formation of Normal Equations

The observational equations defined by (21) and (28) can be merged into the composite equation

$$(30)\quad \begin{bmatrix} v \\ \dot{v} \\ \ddot{v} \end{bmatrix} + \begin{bmatrix} \dot{B} & \ddot{B} \\ -I & 0 \\ 0 & -I \end{bmatrix} \begin{bmatrix} \dot{\delta} \\ \ddot{\delta} \end{bmatrix} = \begin{bmatrix} \epsilon \\ \dot{\epsilon} \\ \ddot{\epsilon} \end{bmatrix}$$

which, with obvious notation, can be expressed compactly as

$$(31)\quad \ddot{v} + \bar{B}\,\delta = \bar{\epsilon} \ .$$

The composite covariance matrix associated with $\bar{v}$ is of the form

$$(32)\quad \underset{(2n+15,\,2n+15)}{\Lambda} = \begin{bmatrix} \underset{(2n,2n)}{\Lambda} & 0 & 0 \\ 0 & \underset{(9,9)}{\dot{\Lambda}} & 0 \\ 0 & 0 & \underset{(6,6)}{\ddot{\Lambda}} \end{bmatrix} .$$

The normal equations arising from the least squares adjustment of the observations governed by (31) and (32) are of the form

$$(33)\quad \underset{(15,15)}{N}\ \underset{(15,1)}{\delta} = \underset{(15,1)}{c} \ ,$$

in which

$$(34)\quad \begin{aligned} N &= \bar{B}^T\ \bar{\Lambda}^{-1}\ \bar{B} \ , \\ c &= \bar{B}^T\ \bar{\Lambda}^{-1}\ \bar{\epsilon} \ . \end{aligned}$$

By virtue of the structure of $\bar{B}$, δ, Λ and $\bar{\epsilon}$, the normal equations can be expressed in the more expanded form

$$(35)\quad \begin{bmatrix} \dot{N} + \dot{W} & \bar{N} \\ \bar{N}^T & \ddot{N} + \ddot{W} \end{bmatrix} \begin{bmatrix} \dot{\delta} \\ \ddot{\delta} \end{bmatrix} = \begin{bmatrix} \dot{c} - \dot{W}\dot{\epsilon} \\ \ddot{c} - \ddot{W}\ddot{\epsilon} \end{bmatrix}$$

in which

$$(36)\quad \begin{aligned} \dot{N} &= \dot{B}^T W \dot{B} \quad , \quad \dot{c} = \dot{B}^T W \epsilon \quad , \\ \bar{N} &= \dot{B}^T W \ddot{B} \quad , \quad \ddot{c} = \ddot{B}^T W \epsilon \quad , \\ \ddot{N} &= \ddot{B}^T W \ddot{B} \end{aligned}$$

wherein

$$(37)\quad W = \Lambda^{-1} \, , \; \dot{W} = \dot{\Lambda}^{-1} \, , \; \ddot{W} = \ddot{\Lambda}^{-1} \, .$$

By virtue of the block diagonality of Λ, the expressions for $\dot{N}$, $\bar{N}$, $\ddot{N}$, $\dot{c}$, $\ddot{c}$ can be expressed as sums

$$(38)\quad \begin{aligned} \dot{N} &= \sum_{i=1}^{n} N_i \quad , \quad \dot{c} = \sum_{i=1}^{n} \dot{c}_i \quad , \\ \bar{N} &= \sum_{i=1}^{n} \bar{N}_i \quad , \quad \ddot{c} = \sum_{i=1}^{n} \ddot{c}_i \quad , \\ \ddot{N} &= \sum_{i=1}^{n} \ddot{N}_i \quad , \end{aligned}$$

in which

$$(39)\quad \begin{aligned} \dot{N}_i &= \dot{B}_i^T W_i \dot{B}_i \quad , \; \dot{c}_i = \dot{B}_i^T W_i \epsilon_i \quad , \\ \bar{N}_i &= \dot{B}_i^T W_i \ddot{B}_i \quad , \; \ddot{c}_i = \ddot{B}_i^T W_i \epsilon_i \quad , \\ \ddot{N}_i &= \ddot{B}_i^T W_i \ddot{B}_i \quad , \end{aligned}$$

where

(40) $W_i = \Lambda_i^{-1}$.

It should be appreciated that the above development of the normal equations is strictly derivational. The computational flow itself is actually quite short and consists of the following major steps:

(1) By means of formulas given in Appendix A, the basic matrices $\dot{B}_i$, $\ddot{B}_i$ and ϵ_i are evaluated from the following given data:

(a) The observed plate coordinates x_i°, y_i° ;

(b) The direction cosines λ_i , μ_i , ν_i (in the case of stellar control) or the X_i , Y_i , Z_i coordinates of the ith control point;

(c) The approximations $\dot{u}_j^{oo}$, $\ddot{u}_j^{oo}$ of the projective parameters.

(2) In terms of the computed $\dot{B}_i$, $\ddot{B}_i$, ϵ_i together with the given Λ_i , eqs. (39) are evaluated to generate $\dot{N}_i$, $\overline{N}_i$, $\ddot{N}_i$ $\dot{c}_i$, $\ddot{c}_i$.

(3) As each $\dot{N}_i$, $\overline{N}_i$, $\ddot{N}_i$, $\dot{c}_i$, $\ddot{c}_i$ is formed, it is added to the sum of its predecessors, thereby ultimately generating the $\dot{N}$, $\overline{N}$, $\ddot{N}$, $\dot{c}$, $\ddot{c}$ indicated in equation (38).

(4) From the given a priori values $\dot{u}_j^\circ$, $\ddot{u}_j^\circ$ and the associated covariance matrices $\dot{\Lambda}$ and $\ddot{\Lambda}$, the terms $\dot{W}$, $\dot{\hat{W}}$, $\ddot{W}$, $\dot{\epsilon}$ and $\ddot{W}\ddot{\epsilon}$ are evaluated in accordance with equations (27), (29), and (37).

(5) From the results of steps (3) and (4), the normal equations (35) are formed.

2.3.5 Computation of Residuals

Once the normal equations have been formed, they may be solved for the vectors $\dot{\delta}$, $\ddot{\delta}$ which provide corrections to the initial approximations. The improved approximations would then be used to initiate an iterative process which would continue until the revised corrections become negligibly small. Upon convergence (which is normally obtained in three iterations), the plate residuals for the i^{th} point may be computed from

$$(41) \qquad \underset{(2,1)}{v_i} = \underset{(2,1)}{\epsilon_i}$$

in which the discrepancy vector ϵ_i is based on the final set of projective parameters. Similarly, the residuals of the a priori values of the projective parameters may be computed from

$$(42) \qquad \begin{aligned} \dot{v} &= \dot{\epsilon} \\ \ddot{v} &= \ddot{\epsilon} \end{aligned}$$

in which the elements of $\dot{\epsilon}$ and $\ddot{\epsilon}$ are generated from equations (27) with the final set of projective parameters being used for $\dot{u}_i^{oo}$ and $\ddot{u}_j^{oo}$. The quadratic form of the composite residual vector is

$$(43) \qquad q = \dot{v}^T \dot{W} \dot{v} + \ddot{v}^T \ddot{W} \ddot{v} + \sum_{i=1}^{n} (v_i^T W_i v_i) .$$

The statistical degrees of freedom associated with q may be taken as $2n - k$, where k denotes the number of projective parameters for which no effective a priori constraints are exercised.

2.3.6 Practical Exercise of A Priori Constraints

Not only do the covariance matrices $\dot{\Lambda}$ and $\ddot{\Lambda}$ provide proper weighting of actual a priori values of projective parameters, but they also can be exploited for other purposes. With regard to any given projective parameter, three situations arise:

(1) The parameter is actually known in advance to a worthwhile degree of accuracy; here, the pertinent elements covariance matrix would realistically reflect ones knowledge of the parameter.

(2) The parameter is not known in advance to a worthwhile degree of accuracy; here, the pertinent variance would be deliberately inflated by several orders of magnitude over what is considered to be a reasonable measure of the uncertainty of the adopted initial approximation. This allows the parameter virtually unrestricted freedom to adjust.

(3) The parameter is not to be exercised in the adjustment (most commonly, the case with higher order coefficients of radial and decentering distortion); here the pertinent variance would be set equal to a value effectively equal to zero. An appropriate value would be one several orders of magnitude smaller than the variance to be expected for the recovery of the parameter if it were free to adjust.

By thus using the covariance matrix of the projective parameters to exercise general control over the adjustment, one not only avoids the need for programming a variety of special options but one also gains added simplicity by avoiding the redimensioning of operational matrices.

A specific application of the process of exercising a priori constraints to effect parametric control involves the solution for decentering distortion. When the higher order coefficient P_3 is equal to zero, the expressions in the projective equations accounting for decentering distortion become linear in the leading coefficients P_1 and P_2. This means that one can adopt values of zero as initial approximations for P_1 and P_2. However, by doing this, one causes the entire set of coefficients corresponding to P_3 in the $\dot{B}$ matrix to be zero, thereby rendering the normal equations indeterminate. The remedy consists of using a priori constraints to suppress P_3 to zero in the initial iterations. Once stable, nonzero approximations have been obtained for P_1, P_2, the constraints on P_3 can be relaxed in subsequent interations to permit recovery of this parameter together with final refinement of P_1 and P_2.

Another application of the special exercise of a priori constraints is of particular value in the calibration of cameras having narrow angular fields. Here, the projective effects of a small translation δx_p, δy_p of the plate are very nearly equivalent to the projective effects effects of a small, suitably directed rotation of the camera. This coupling of translation and rotation can sometimes lead to a sufficiently ill-conditioned system of normal equations to prevent convergence of the iterative process. The problem is compounded when decentering distortion is being recovered, for decentering coefficients also interact to a moderate degree with x_p, y_p. The remedy consists of subjecting x_p, y_p in the initial reduction to fairly tight a priori constraints (e.g., a few hundred microns) and of relaxing such constraints by stages in subsequent iterations until they ultimately become inconsequential.

2.3.7 Error Propagation

The covariance matrix of the adjusted projective parameters is provided by the inverse of N, the coefficient matrix of the normal equations. If n^{ij} denotes the element in the i^{th} row and j^{th} column of N^{-1}, it follows from the ordering of the parameters that the standard deviations of the adjusted elements of interior orientation are given by

$$\begin{aligned} \sigma_{x_p} &= (n^{11})^{\frac{1}{2}} \\ \sigma_{y_p} &= (n^{22})^{\frac{1}{2}} \\ \sigma_c &= (n^{33})^{\frac{1}{2}} \end{aligned} \tag{44}$$

The variances of the radial and decentering parameters are provided by elements n^{44} through n^{99}. However, these are of little interest in themselves. Rather, what is of interest is the uncertainty of the calibrated distortion functions throughout the format.

In the case of symmetric radial distortion, the propagation of errors into the distortion function is readily accomplished. Inasmuch as the covariance matrix of the coefficients of radial distortion is

$$\Omega_k = \begin{bmatrix} n^{44} & n^{45} & n^{46} \\ n^{45} & n^{55} & n^{56} \\ n^{46} & n^{56} & n^{66} \end{bmatrix} \tag{45}$$

and the distortion function is defined by

$$\delta_r = K_1 r^3 + K_2 r^5 + K_3 r^7 + \ldots, \tag{46}$$

it follows from the theory of error propagation that the standard deviation of δ_r for an arbitrary radial distance is given by

$$\sigma_{\delta_r} = (u_k \Omega_k u_k^T) \tag{47}$$

in which

$$(48) \qquad u_k = \frac{\partial(\delta r)}{\partial(K_1, K_2, K_3)} = (r^3\ r^5\ r^7).$$

By means of this result one can generate confidence intervals (or error bounds) associated with the calibrated distortion curve.

In the case of decentering distortion the error propagation is somewhat more involved since the end results are most conveniently expressed in terms of the tangential profile function P_r and its associated phase angle ϕ_o. By virtue of (5) we have

$$(49) \qquad \begin{aligned} J_1 &= (P_1^2 + P_2^2)^{\frac{1}{2}} \\ J_2 &= -(P_1^2 + P_2^2)^{\frac{1}{2}} P_3 \\ \phi_0 &= -\arctan(P_1/P_2) \end{aligned}$$

Inasmuch as the covariance matrix of the adjusted decentering parameters P_1, P_2, P_3 is given by

$$(50) \qquad \Omega_p = \begin{bmatrix} n^{77} & n^{78} & n^{79} \\ n^{78} & n^{88} & n^{89} \\ n^{79} & n^{89} & n^{99} \end{bmatrix}$$

It follows that the covariance matrix of the derived parameters J_1, J_2, ϕ_o is given by

$$(51) \qquad \Omega_o = (u_p\ \Omega_p\ u_p)^{\frac{1}{2}}$$

in which

$$(52) \qquad u_p = \frac{\partial(J_1, J_2, \phi_o)}{\partial(P_1, P_2, P_3)} = (P_1^2 + P_2^2)^{-\frac{1}{2}} \begin{bmatrix} P_1 & P_2 & 0 \\ -P_1 P_3 & -P_2 P_3 & -(P_1^2 + P_2^2) \\ \cos\phi_o & \sin\phi_o & 0 \end{bmatrix} .$$

inasmuch as the profile function is defined by

$$(53) \qquad P_r = J_1 r^2 + J_2 r^4 + \ldots ,$$

the covariance matrix of the profile function and the phase angle is given by

$$(54) \qquad \begin{bmatrix} \sigma_{P_r}^2 & \sigma_{P_r \phi_o} \\ \sigma_{P_r \phi_o} & \sigma_{\phi_o}^2 \end{bmatrix} = U_o \, \Omega_o \, U_o^T ,$$

in which

$$(55) \qquad U_o = \frac{\partial(P_r, \phi_o)}{\partial(J_1, J_2, \phi_o)} = \begin{bmatrix} r^2 & r^4 & 0 \\ 0 & 0 & 1 \end{bmatrix} .$$

By virtue of this result, error bounds can be established for the representation of decentering distortion in terms of tangential profile and phase angle.

In the error propagations for both radial and decentering distortion we ignored the fact that the coordinates x_p, y_p of the principal point are implicit in the radial distances r (since the radial distances are referred to the calibrated principal point). It turns out, however, that the errors in the x_p, y_p have only a second order effect on the above error propagations and thus need not be considered.

The radial distortion function δ_r generated by the adjustment corresponds to the calibrated principal distance c. As is shown in Brown (1956) this function can be transformed into a projectively equivalent distortion function δ_r' associated with an arbitrary specified principal distance $c + \Delta c$. The transformation is expressed by

$$(56) \qquad \delta_r' = (1 + \frac{\Delta c}{c}) \, \delta_r + \frac{\Delta c}{c} \, r ,$$

which leads to the alternative version of the distortion function

$$(57) \quad \delta_r' = K_0' r + K_1' r^3 + K_2' r^5 + K_3' r^7 + \ldots$$

in which

$$(58) \quad K_0' = \Delta c/c, \quad K_1' = (1+\Delta c/c) K_1, \quad K_2' = (1+\Delta c/c) K_2, \quad \text{etc.}$$

One can use this result to force the transformed distortion function to assume the value of zero at a specified radial distance r_o. Thus, if δ_{r_o} denotes the value of δ_r at $r = r_o$, it follows from (56) that the choice

$$(59) \quad \Delta c = -\left(\frac{c}{r_o + \delta_{r_o}}\right) \delta_{r_o},$$

renders δ_r' equal to zero at $r = r_o$.

Alternatively, Δc can be chosen so that the mean value of the distortion function out to a specified radial distance r_o is zero. This results in the choice

$$(60) \quad \Delta c = -\frac{w c}{w + \frac{1}{2} r_o^2}$$

in which

$$(61) \quad w = \int_o^{r_o} \delta_r \, dr = \frac{r_o^4}{2}\left(\frac{K_1}{2} + \frac{K_2}{3} r_o^2 + \frac{K_3}{4} r_o^4 + \ldots\right).$$

Still another choice consists of transforming the distortion function to minimize the rms value of distortion out to a specified radial distance r_o. This is accomplished by choosing Δc as

$$(62) \quad \Delta c = -\frac{(s+w)\, c}{2s + w + r_o^2}$$

in which w is as above and

$$(63) \quad s = \int_o^{r_o} r \delta_r \, dr = r_o^5 \left(\frac{K_1}{5} + \frac{K_2}{7} r_o^2 + \frac{K_3}{9} r_o^4 + \ldots\right).$$

The final transformation to be considered is one in which the largest positive and negative values of distortion out to specified radial distance r_o are forced to have the same absolute value. Here, the appropriate Δc is most readily established by a two stage process. The first stage consists of choosing an initial value Δc_o in accordance with either (60) or (62). One then determines the slope m of the straight line that passes through the origin and is such that the largest positive and negative departures of the transformed distortion function from the line are of equal magnitude. This determination can be made either graphically (with the aid of a transparent ruler) or numerically (by a trial and error process). In either case, the final value of Δc is given by

$$\Delta c = \Delta c_o - m\,(c + \Delta c_o)\ . \tag{63}$$

All of the above transformations yield projectively equivalent results. When $\Delta c/c$ is small (as is generally the case), the error in the calibrated value of c has no sensible effect on the transformation and may be safely ignored. Also when $\Delta c/c$ is small, the standard deviation given by (47) may be used in conjunction with the transformed distortion function.

A decided advantage of the analytical approach to camera calibration is that the error propagation associated with the end results can be readily computed. By contrast, conventional laboratory methods do not lend themselves to precise statements concerning the accuracies of the results.

2.4 Simultaneous Multiframe Analytical Calibration (SMAC).

2.4.1 Introduction

The results of the preceding section are not new. Rather, they constitute a detailed review of our earlier theory. The development has been specifically constructed to facilitate the derivation of the SMAC calibration. Before proceeding, we would emphasize that the theory applies both to a stellar calibration and to an aerial calibration (i.e., a calibration using aerial photographs taken over a suitable testing range). In the stellar calibration, the

coordinates X^c, Y^c, Z^c of the camera are inherently unrecoverable (and hence are suppressed) inasmuch as all control points are sensibly at infinity. In the aerial calibration, they are carried as unknowns subject possibly to a priori constraints (as when the precise position of the aircraft is established by a tracking system). While the elements of interior orientation (x_p, y_p, c) can be recovered in a stellar calibration, they may not be recoverable in an aerial calibration. This stems from the fact that when all control points are nearly coplanar, a small translation (δX^c, δY^c, δZ^c) in object space is projectively equivalent to a small translation (δx_p, δy_p, δc) in image space. It follows that the recovery of x_p, y_p, c in an aerial calibration requires either a strongly three dimensional distribution of control or else precise external tracking of the aircraft. This matter will be discussed more fully later. It should be kept in mind throughout the development to follow that in extending the single frame calibration to the SMAC calibration, we shall preserve the dual applicability of the reduction to stellar and aerial photographs.

2.4.2 Formation of the General Normal Equations

We now consider the general situation in which an indefinitely large number of frames of photographed control are to be employed for camera calibration. We assume that a common set of interior projective parameters applies to all frames and that (possibly) a different set of exterior projective parameters applies to each frame. To begin, we shall assume that only three frames are involved in the reduction. Then ignoring momentarily the a priori constraints on the interior projective parameters, we obtain the following three sets of normal equations for the independent single frame reductions:

$$\text{(64a)} \qquad \begin{bmatrix} \dot{N}_1 & \bar{N}_1 \\ \bar{N}_1^T & \ddot{N}_1 + \ddot{W}_1 \end{bmatrix} \begin{bmatrix} \dot{\delta} \\ \ddot{\delta}_1 \end{bmatrix} = \begin{bmatrix} \dot{c}_1 \\ \ddot{c}_1 - \ddot{W}_1 \ddot{\epsilon}_1 \end{bmatrix} ,$$

$$\text{(64b)} \qquad \begin{bmatrix} \dot{N}_2 & \bar{N}_2 \\ \bar{N}_2^T & \ddot{N}_2 + \ddot{W}_2 \end{bmatrix} \begin{bmatrix} \dot{\delta} \\ \ddot{\delta}_2 \end{bmatrix} = \begin{bmatrix} \dot{c}_2 \\ \ddot{c}_2 - \ddot{W}_2 \dot{\epsilon}_2 \end{bmatrix} ,$$

$$\text{(64c)} \qquad \begin{bmatrix} \dot{N}_3 & \bar{N}_3 \\ \bar{N}_3^T & \ddot{N}_3 + \ddot{W}_3 \end{bmatrix} \begin{bmatrix} \dot{\delta} \\ \ddot{\delta}_3 \end{bmatrix} = \begin{bmatrix} \dot{c}_3 \\ \ddot{c}_3 - \ddot{W}_3 \ddot{\epsilon}_3 \end{bmatrix} .$$

If the only available information were to consist of the a priori constraints on the interior projective parameters, the following system of normal equations would apply

$$(65) \quad \dot{W}\,\dot{\delta} = -\dot{W}\,\dot{\epsilon} \ .$$

Now it has been shown (Brown, 1957) that systems of normal equations formed from consistently weighted, independent observations and operating on a common parametric vector are additive: that is, they can be summed to form the system of normal equations that would have arisen from the adjustment of the combined observational vectors. This additive property of independent systems of normal equations cannot be applied directly to the normal equations written above because each operates on a different vector. This difficulty is easily overcome by a process of zero augmentation to force each system to operate on the total parametric vector to be recovered. Accordingly, equations (64) and (65) may be rewritten as

$$(66a) \quad \begin{bmatrix} \dot{N}_1 & \bar{N}_1 & 0 & 0 \\ \bar{N}_1^T & \ddot{N}_1 + \ddot{W}_1 & 0 & 0 \\ 0 & 0 & 0 & 0 \\ 0 & 0 & 0 & 0 \end{bmatrix} \begin{bmatrix} \dot{\delta} \\ \ddot{\delta}_1 \\ \ddot{\delta}_2 \\ \ddot{\delta}_3 \end{bmatrix} = \begin{bmatrix} \dot{c}_1 \\ \ddot{c}_1 - \ddot{W}_1\,\ddot{\epsilon}_1 \\ 0 \\ 0 \end{bmatrix}$$

$$(66b) \quad \begin{bmatrix} \dot{N}_2 & 0 & \bar{N}_2 & 0 \\ 0 & 0 & 0 & 0 \\ \bar{N}_2^T & 0 & \ddot{N}_2 + \ddot{W}_2 & 0 \\ 0 & 0 & 0 & 0 \end{bmatrix} \begin{bmatrix} \dot{\delta} \\ \ddot{\delta}_1 \\ \ddot{\delta}_2 \\ \ddot{\delta}_3 \end{bmatrix} = \begin{bmatrix} \dot{c}_2 \\ 0 \\ \ddot{c}_2 - \ddot{W}_2\,\ddot{\epsilon}_2 \\ 0 \end{bmatrix}$$

$$(66c)\quad \begin{bmatrix} \dot{N}_3 & 0 & 0 & \bar{N}_3 \\ 0 & 0 & 0 & 0 \\ 0 & 0 & 0 & 0 \\ \bar{N}_3^T & 0 & 0 & \ddot{N}_3 + \ddot{W}_3 \end{bmatrix} \begin{bmatrix} \dot{\delta} \\ \ddot{\delta}_1 \\ \ddot{\delta}_2 \\ \ddot{\delta}_3 \end{bmatrix} = \begin{bmatrix} \dot{c}_3 \\ 0 \\ 0 \\ \ddot{c}_3 - \ddot{W}_3\ \ddot{\epsilon}_3 \end{bmatrix}$$

$$(67)\quad \begin{bmatrix} \dot{W} & 0 & 0 & 0 \\ 0 & 0 & 0 & 0 \\ 0 & 0 & 0 & 0 \\ 0 & 0 & 0 & 0 \end{bmatrix} \begin{bmatrix} \dot{\delta} \\ \ddot{\delta}_1 \\ \ddot{\delta}_2 \\ \ddot{\delta}_3 \end{bmatrix} = \begin{bmatrix} -\dot{W}\dot{\epsilon} \\ 0 \\ 0 \\ 0 \end{bmatrix} .$$

Thus augmented, each system of normal equations now operates on the same parametric vector. Inasmuch as each is formed from an independent set of observations, we are thus in a position to apply the additive property of independent sets of normal equations to obtain the following result:

$$(68)\quad \left[\begin{array}{c|ccc} \dot{N} + \dot{W} & \bar{N}_1 & \bar{N}_2 & \bar{N}_3 \\ \hline \bar{N}_1^T & \ddot{N}_1 + \ddot{W}_1 & 0 & 0 \\ \bar{N}_2^T & 0 & \ddot{N}_2 + \ddot{W}_2 & 0 \\ \bar{N}_3^T & 0 & 0 & \ddot{N}_3 + \ddot{W}_3 \end{array}\right] \left[\begin{array}{c} \dot{\delta} \\ \hline \ddot{\delta}_1 \\ \ddot{\delta}_2 \\ \ddot{\delta}_3 \end{array}\right] = \left[\begin{array}{c} \dot{c} - \dot{W}\ \dot{\epsilon} \\ \hline \ddot{c}_1 - \ddot{W}_1\ \ddot{\epsilon}_1 \\ \ddot{c}_2 - \ddot{W}_2\ \ddot{\epsilon}_2 \\ \ddot{c}_3 - \ddot{W}_3\ \ddot{\epsilon}_3 \end{array}\right]$$

in which $\dot{N}$ and $\dot{c}$ are defined by

$$(69)\quad \begin{aligned} \dot{N} &= \dot{N}_1 + \dot{N}_2 + \dot{N}_3 , \\ \dot{c} &= \dot{c}_1 + \dot{c}_2 + \dot{c}_3 . \end{aligned}$$

This system represents the normal equations resulting from a calibration based on the simultaneous adjustment of plate coordinates from three arbitrary frames.

The extension of the above development to an arbitrarily large number of frames m is immediate. The resulting system of normal equations is

$$(70)\quad \begin{bmatrix} \dot{N}+\dot{W} & \dot{N}_1 & \bar{N}_2 & \cdots & \bar{N}_m \\ \bar{N}_1^T & \ddot{N}_1+\ddot{W}_1 & 0 & \cdots & 0 \\ \bar{N}_2^T & 0 & \ddot{N}_2+\ddot{W}_2 & \cdots & 0 \\ \vdots & \vdots & \vdots & & \vdots \\ \bar{N}_m^T & 0 & 0 & \cdots & \ddot{N}_m+\ddot{W}_m \end{bmatrix} \begin{bmatrix} \dot{\delta} \\ \ddot{\delta}_1 \\ \ddot{\delta}_2 \\ \vdots \\ \delta_m \end{bmatrix} = \begin{bmatrix} \dot{c}-\dot{W}\,\dot{\epsilon} \\ \ddot{c}_1-\ddot{W}_1\,\ddot{\epsilon}_1 \\ \ddot{c}_2-\ddot{W}_2\,\ddot{\epsilon}_2 \\ \vdots \\ \ddot{c}_m-\ddot{W}_m\,\ddot{\epsilon}_m \end{bmatrix}$$

where now

$$(71)\quad \begin{aligned} \dot{N} &= \dot{N}_1+\dot{N}_2+\cdots+\dot{N}_m \\ \dot{c} &= \dot{c}_1+\dot{c}_2+\cdots+\dot{c}_m \end{aligned}$$

The above derivation of the normal equations is designed to emphasize the close relationship that exists between the basic single frame reduction and the composite multiframe reduction. An alternative derivation closely paralleling the procedure developed in Brown (1958) is given in Gambino (1967).

2.4.3 Solution of the Normal Equations

The above system of normal equations is of order 6m + 9 (for the general case) and thus increases linearly with the number of frames m. When m is small, one can solve the system directly without difficulty. Our concern, however, is with the general case in which m is without set limit. Here, a conventional direct solution becomes impractical after a certain point inasmuch as the number of computations is proportional to $(6m + 9)^3$. Fortunately, the system of normal equations (68) has the same general structure as the system that we had developed in Brown 1958 for the rigorous adjustment of a general photogrammetric net. There we showed that the partial block diagonality of the coefficient matrix could be exploited to produce an efficient solution in which computations increased only linearly with the number of unknown $\ddot{\delta}_j$ vectors. Inasmuch as the derivation of the solution is given in the above reference and is further elaborated in Brown, Davis, Johnson 1964, we shall not repeat the derivation here. Instead, we shall merely adapt results pertinent to the problem at hand.

Although the general normal equations for the SMAC calibration are given by (70), one would not actually set up this system in the course of the reduction. Rather, one would generate the reduced system of normal equations resulting from the elimination of the $\ddot{\delta}_j$'s from the general system. This entails the following steps. Starting with the first frame ($j = 1$), one generates the coefficient matrix and constant column for the single frame calibration according to the development of the preceding section. This provides the primary matrices: $\dot{N}_j$, $\bar{N}_j$, $\ddot{N}_j + \ddot{W}_j$, $\dot{c}_j$ and $\ddot{c}_j - \ddot{W}_j \ddot{\epsilon}_j$. In terms of these, one computes the following set of auxiliary matrices

$$(72) \qquad \underset{(6,9)}{Q_j} = (\underset{(6,6)}{\ddot{N}_j + \ddot{W}_j})^{-1} \underset{(6,9)}{\bar{N}_j^T}$$

$$(73) \qquad \underset{(9,9)}{R_j} = \underset{(9,6)}{N_j} \underset{(6,9)}{Q_j}$$

$$(74) \qquad \underset{(9,9)}{S_j} = \underset{(9,9)}{\dot{N}_j} - \underset{(9,9)}{R_j}$$

$$(75) \qquad \underset{(9,1)}{\bar{c}_j} = \underset{(9,1)}{\dot{c}_j} - \underset{(9,6)}{Q_j^T} (\underset{(6,1)}{\ddot{c}_j - \ddot{W}_j \ddot{\epsilon}_j})$$

As S_j and $\bar{c}_j$ are formed for the j^{th} frame, they are added to the sums of their predecessors. After all m frames have thus been processed, this produces the quantities:

$$(76) \qquad \begin{aligned} S &= S_1 + S_2 + \ldots + S_n \,, \\ \bar{c} &= \bar{c}_1 + \bar{c}_2 + \ldots + \bar{c}_n \,. \end{aligned}$$

The reduced system of normal equations, a 9 x 9 system involving only the interior projective parameters, is then

$$(77) \qquad (S + \dot{W})\dot{\delta} = \bar{c} - \dot{W}\dot{\epsilon} \,.$$

The solution is given by

$$(78) \qquad \dot{\delta} = \dot{M}(\bar{c} - \dot{W}\dot{\epsilon})$$

in which

$$(79) \qquad \dot{M} = (S + \dot{W})^{-1} \,.$$

Once the vector of interior projective parameters has thus been obtained, each vector of exterior projective parameters can be computed in turn from

$$(80) \qquad \ddot{\delta}_j = (\dot{N}_j + \ddot{W}_j)^{-1}(\ddot{c}_j - \ddot{W}_j\,\ddot{\epsilon}_j) - Q_j\,\dot{\delta}, \quad (j = 1, 2, \ldots, m).$$

The values obtained from (78) and (80) are added to the original approximations to obtain improved approximations. These are then used to initiate an iterative process that is cycled to convergence. Computation of observational residuals follows the procedure of Section 2.3.5.

2.4.4 Error Propagation

The matrix $\dot{M}$ represents the covariance matrix of the interior projective parameters. Accordingly, with suitable reinterpretation, the results of Section 2.3.7 for error propagation associated with a single frame calibration can be applied to the SMAC calibration.

The covariance matrix of the adjusted values of the exterior projective parameters for the j^{th} frame is given by

$$(81) \qquad \underset{(6,6)}{\ddot{M}_j} = \underset{(6,6)}{(\ddot{N}_j + \ddot{W}_j)^{-1}} + \underset{(6,9)}{Q_j} \underset{(9,9)}{M_j} \underset{(9,6)}{Q_j^T}.$$

The first term on the right represents the covariance matrix for the limiting case in which the interior projective parameters are perfectly known, and the second term accounts for the dilution of limiting accuracies attributable to errors in the adjusted values of the interior projective parameters. The contribution of the second term automatically becomes suppressed into relative insignificance when the SMAC reduction involves a moderate number of frames each containing a moderate number of control points.

2.4.5 General Remarks

The interior projective parameters resulting from a SMAC calibration may be considered as the best possible compromise for the set of frames carried in the reduction. This means that errors, both random and systematic, arising from a variety of sources to be mentioned below are in large measure averaged out insofar as their effects on the interior projective parameters are concerned. In considering the results of a SMAC calibration, it is convenient to classify systematic errors into the following two categories:

(1) transient systematic errors,
(2) persistent systematic errors.

Transient systematic errors are those errors that are systematic on a given frame but are essentially independent from frame to frame. Persistent systematic errors are those that tend to remain highly correlated from frame to frame.

In an aerial SMAC calibration one finds it easy to postulate a large number of possible sources of transient systematic error (particularly, if quantitative estimates are not demanded).

A list might include:

(a) variations in thickness of film-emulsion combination;

(b) nonuniform dimensional instability of film;

(c) broad refractive anomalies induced by atmospheric turbulence;

(d) random local failure of film to conform precisely to platen;

(e) angular motion of camera during exposure;

(f) variations in orientation of window and shockwave relative to camera because of variations in aircraft attitude;

(g) dynamic deformations of camera induced by aircraft accelerations or by corrective accelerations by camera mount;

(h) deformations attributable to thermal imbalances;

(i) time varying component of systematic errors in comparator used to measure film;

(j) variations in personal equation of measuring personnel during course of measuring (e.g., fatigue factor).

No doubt, other potential contributors to transient systematic error could be added to the list. The point is that while the total effect of such errors may assume significance on a given frame, the effect will tend to be independent from frame to frame. Because the combination of a moderate number of individually inconsequential, second order systematic effects can amount to a definitely significant first order effect, there is little merit, in our view, in employing in an aerial SMAC calibration more than 50 or so well-distributed images on any single frame. In many instances, the reduction of 500 images on a single frame would produce only a slight actual improvement over the results obtainable from the reduction of 50 images. This is because errors in plate coordinates are not strictly independent, as one would like to believe, but rather are correlated by virtue of residual systematic effects. Accordingly, it follows that redundancy is effective only up to a certain point on a single frame and that further improvement from redundancy must be wrought from exploitation of random frame-to-frame variations of otherwise systematic effects.

For this reason, a SMAC reduction of, say, 20 frames having an average of 25 control points per frame is vastly to be preferred over a reduction involving a total of 500 points on a single frame.

Unlike the effects of transient systematic errors, the effects of persistent systematic errors do not average out in a SMAC reduction. Sources of such error in an aerial calibration include:

(a) departure of the platen from a true plane;

(b) tilt of the platen at instant of exposure (partially attributable to (a));

(c) prism effect of aircraft window;

(d) curvature of aircraft window induced by pressure and temperature differentials between inside and outside of aircraft;

(e) refractive effects of shock waves of aircraft;

(f) persistent, uncompensated component of film deformation;

(g) image aberrations, other than true optical distortion, that affect measured coordinates (e.g., in photographic measurements, coma superimposes on classical radial distortion a component that is dependent both on radial distance and on mean image diameter);

(h) systematic errors in reseau coordinates employed to compensate for film deformation;

(i) systematic deficiencies in image motion compensation (IMC) system;

(j) errors in the given survey of ground control;

(k) uncompensated systematic errors of comparator used to measure plates.

Persistent systematic errors may be partially absorbed by the calibrated projective parameters. Thus a platen that happens to be essentially spherically concave or convex would introduce an effect that would be completely absorbed by the calibrated coefficients of radial distortion. A similar remark applies to the effect of the spherical component of the aircraft window. For flights at a given altitude and velocity in a given aircraft, the various layers bounded by shock waves act to a first approximation as very weak prisms and hence produce effects that can largely be absorbed by the calibrated parameters of decentering distortion. A similar remark applies to the prism effect of the aircraft window. A slight tilt in the camera platen at the instant of exposure would be projectively compensated by a shift in the coordinates x_p, y_p of the principal point. In a camera exercising image motion compensation, such a shift would

also compensate for systematic failure of the fiducials to flash at the precise center of exposure (for a given V/H ratio).

That portion of persistent systematic errors that is not accommodated by projective parameters would be reflected (along with random errors and transient systematic errors) in the final set of least squares residuals resulting from the SMAC calibration. The residual vectors from all frames plotted against x,y plate coordinates on a common graph can be examined for possible uncompensated systematic effects. From numerical and statistical analysis of such residuals, one can derive either error contour maps or functional representations of residual systematic errors. These can subsequently be used, if due precautions are taken, to supplement the calibrated exterior projective parameters in the correction of operational data. A practical example of this approach will be given later.

From the foregoing considerations, it is clear that a SMAC calibration constitutes, not merely a lens calibration, but a total metric calibration of the entire photogrammetric system under operational conditions. To the extent that all pertinent elements of the system approximate in routine operations those applying to the photography used in the SMAC calibration, the compensation for persistent systematic error afforded by the calibrated parameters together with error functions derived from residuals is altogether desirable. On the other hand, such compensation would be partially or totally unsound in instances where key contributors to systematic error have characteristics differing significantly from those prevailing in the SMAC photography. For this reason, attempts should be made to isolate, insofar as possible, the contributions of those sources of systematic error that are likely to vary from one operation to the next. This matter will be discussed more fully later.

3. APPLICATIONS

3.1 Introduction

Having developed the theoretical basis for SMAC, we shall now direct our attention to a number of specific applications of the method. These have been selected to illustrate the power, flexibility and universality of the approach. Most of the applications are illustrated with actual

results, some of which may be of considerable significance to the future of the art of camera calibration. In certain instances, comparisons are made between SMAC results and results produced by conventional laboratory methods. Comparisons are also made between stellar SMAC and aerial SMAC calibrations of the same camera. The application of SMAC to laboratory calibrations is discussed and is demonstrated by SMAC calibrations of Lunar Orbiter cameras. Consideration is also given to applications of SMAC to the calibration of ballistic cameras and to the analysis of their physical stability.

3.2 Calibration of KC-6A Aerial Cameras

3.2.1 Design and Execution of Aircraft Tests

The KC-6A Camera is the most recent and most advanced of the aerial mapping cameras developed by the U. S. Air Force. It employs the 150 mm f/5.0 Geocon IV lens designed by Dr. James Baker. The lens has a resolution of 45 lines/millimeter AWAR on Plus X film and a resolution of not less than 25 lines/millimeter anywhere within a 9x9 inch format. The camera incorporates image motion compensation (IMC), automatic exposure control and a platen reseau that contains a set of 25 points evenly spaced at 2 inch intervals and a set of 12 edge points associated with the fixed fiducials. It also incorporates an optical linkage to the vertical gyro of the Hypernas II Inertial Navigator. This permits the precise determination of the direction of the camera axis with respect to the local vertical. Further details concerning the KC-6A Camera are given by Livingstone (1966).

A major motivation for the development of SMAC was its application to the flight testing of the KC-6A as part of the USQ-28 geodetic mapping and surveying system. In view of the extensive development and demanding requirements of the KC-6A, the decision was made by the U. S. Army and Air Force to implement a test designed by DBA to perform a definitive calibration of the camera in its operational environment. A desired by-product of the calibration was to consist of the determination of the precise angular elements of orientation of a series of exposures for the purpose of evaluating the accuracies of the verticality system.

The testing program was based on flights over the McLure Photogrammetric Test Range, a targeted range established in Ohio by the US Coast and Geodetic Survey. Inasmuch as one of the objectives of the test was to perform an operational calibration of elements of interior orientation, it was necessary to provide extremely accurate independent determinations of exposure stations. Because only stellar-oriented ballistic cameras could provide the needed accuracies, this meant that the flight testing had to be conducted at night. This in turn meant that the portion of the range to be used had to be converted temporarily into a night photogrammetric range through the installation suitable light sources over selected targets. The layout of the range, the intended flight paths and the locations of ballistic camera tracking stations are shown in Figure 1.

In the designed test, four flight paths cross the center of the range from the following directions:

Path 1: south to north,
Path 2: east to west,
Path 3: north to south,
Path 4: west to east.

At intervals of approximately two thousand feet throughout each crossing, synchronized photographs are taken of the range by the pair of KC-6A Cameras carried in the USQ-28 RC-135 aircraft. At the center of each exposure, a small strobe unit (positioned close to the prime camera) flashes. The five most nearly central flashes on each flight path are recorded against the stellar background by at least two of three ballistic cameras located at known stations on the range (see Figure 1). Aircraft velocity is approximately 600 feet per second and aircraft altitude is approximately 12,500 feet above mean terrain.

The test program was successfully executed in March 1967. The actual test conformed closely to the design. Army personnel made arrangements with local power companies to provide an electrical outlet at each of the 51 selected targets and at each of the three ballistic camera stations. The incomplete symmetry in the pattern of selected targets (Figure 1) is attributable to unavailability of power in some areas and to absence of targets in others. Light sources consisted of 500 watt quartz iodide lamps having an output of 10,000 lumens and measuring 1/2 inch

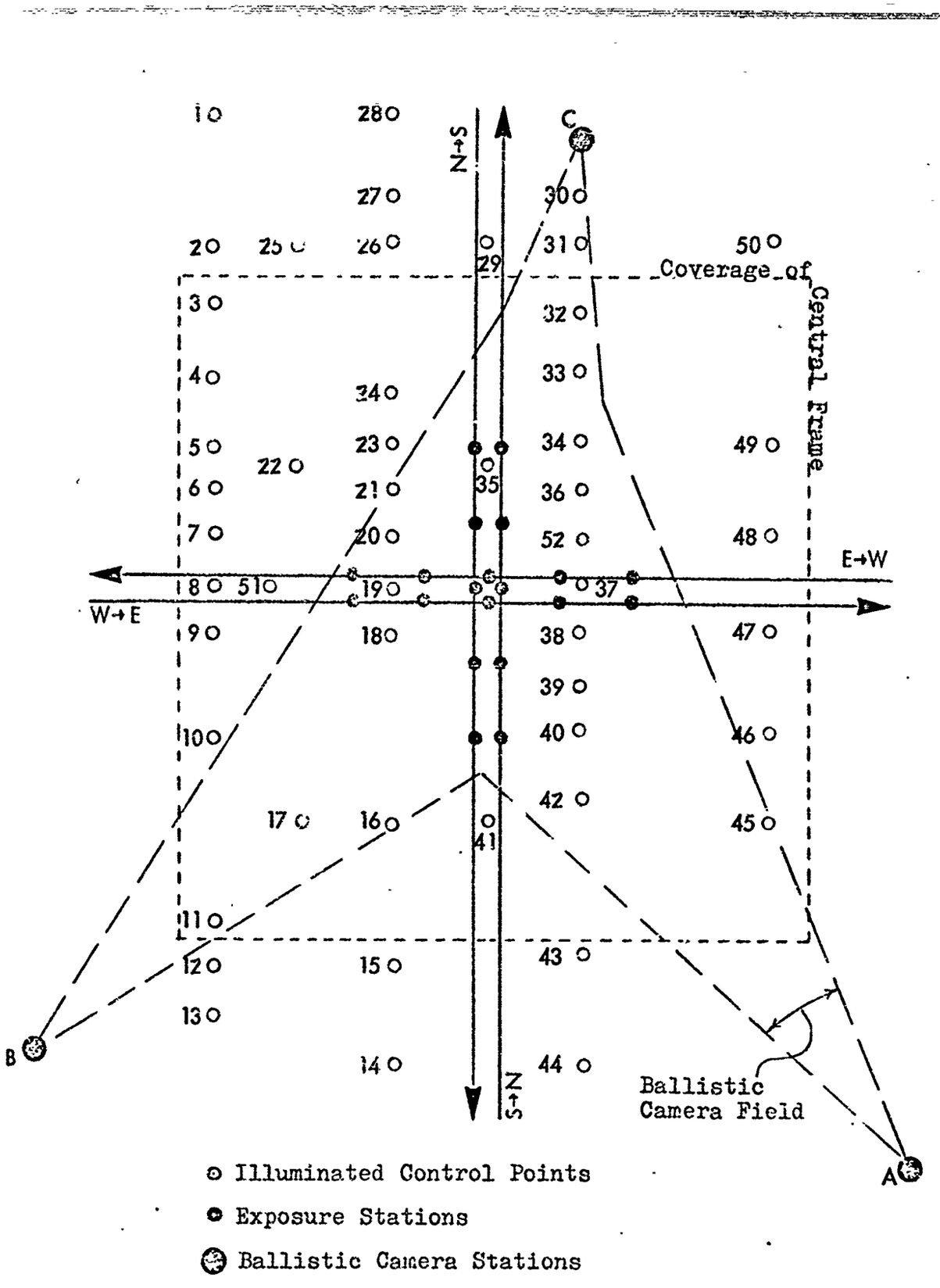

Figure 1. Design of flight test over McLure Photogrammetric Test Range (converted temporarily to night range).

in diameter by 3½ inches in length. This type of lamp had been selected from a variety of potential light sources on the basis of preliminary aircraft tests. Each lamp, mounted on a small shot bag as a base, was carefully positioned over the center of each target.

A small strobe lamp was installed in one of the three camera windows at precisely known offsets from the primary and secondary cameras. (Offsets were 41 inches from the primary camera and 71 inches from the secondary camera.) The lamp was synchronized to flash at the center of each shutter opening.

Ballistic camera support for the tests was provided by DBA personnel operating three 600 mm f/3.5 ballistic cameras leased from Space Systems Laboratories. The camera shutters were driven by DBA Digital Programmer Clocks synchronized with WWV to within one millisecond. Kodak microflat plates coated with 103F emulsion were employed for the photography.

Successful tests were conducted on the nights of March 24 and 29. Of the four orthogonal passes for each night, three turned out to lie within one half mile of the designated lines and one turned out to be almost a mile off. Because of such difficulties of navigation, only eleven of the twenty exposure stations for each night were actually triangulated by ballistic cameras. This, however, did not seriously compromise the reduction, inasmuch as triangulation of but a single exposure station would theoretically have been sufficient for the recovery of the elements of interior orientation.

Altogether, three KC-6A's provided photography over the improvised night photogrammetric test range. On the first test, cameras 005 and 006 were flown and on the second, cameras 006 and 008 were flown. Thus, camera 006 participated in both tests. In the first test, 006 occupied the primary mount (i.e., at the station providing the Hypernas indication of verticality), and in the second test, it occupied the secondary mount. Unfortunately, the Hypernas verticality subsystem did not function properly on either of the two tests. Accordingly, the desired evaluation of the accuracy of the verticality subsystem could not be accomplished. Except for this, the flight test program was a complete success.

3.2.2 Preliminary Corrections

DBA had full responsibility for the data reduction of ballistic camera plates and aerial photographs. All measurements were made on a fully calibrated Mann 422G Comparator owned by DBA. The ballistic camera reductions turned out to be routine with rms closures of triangulation of 2 to 3 seconds of arc being attained. Such closures, propagated into triangulated coordinates of flashes, lead to one sigma accuracies not exceeding 0.2 feet in X, Y, or Z. This positional accuracy is equivalent to better than 1:60,000 of the flying height or to better than 2.5 microns on a given aerial photograph. Inasmuch as eleven of each group of twenty exposure stations were triangulated, the net effect of errors of ballistic camera triangulation on the determination of x_p, y_p, c can be expected to be well under one micron.

Before the SMAC reductions could be performed, a number of small preliminary corrections had to be applied to the data. Aside from comparator corrections, these consisted of:

(a) offset corrections ΔX^c, ΔY^c, ΔZ^c to the triangulated positions of the flashes to establish the coordinates of the exposure stations of the aerial cameras,

(b) corrections to plate coordinates to account for effects of atmospheric refraction,

(c) corrections to plate coordinates to account for effects of refraction of aircraft window,

(d) corrections to plate coordinates to account for effects of film deformation by means of measurements made of reseau images.

Inasmuch as the flash lamp was located directly behind the primary and secondary cameras, the direction cosines of the straight line joining the two cameras and the flash lamp are defined by

$$\lambda = \sin H \cos \delta$$
$$\mu = \cos H \cos \delta$$
$$\nu = \sin \delta$$

in which H is aircraft heading measured clockwise from north (the adopted direction of the positive Y axis in a plane tangent to the spheroid at the center of the range) and δ is the pitch angle of the aircraft (positive when nose is up). Precise values of H and δ are provided by the

navigation system. The offset corrections to be added to the triangulated coordinates of a flash are given by

$$\Delta X = D\lambda$$
$$\Delta Y = D\mu$$
$$\Delta Z = D\nu$$

in which D = 3.63 ft. for the primary camera and D = 5.88 ft. for the secondary camera. The error in these corrections is unlikely to exceed ± 0.1 feet.

It is readily shown by ray tracing based on a flat earth model that the corrections to be applied or added to the plate coordinates of a vertical photograph of flat terrain to account for the combined effects of atmospheric refraction and 'window' refraction are given by the expressions

$$\delta x = Gx$$
$$\delta y = Gy$$

in which

$$G = (\mu_o - \mu)\left(1 + \frac{x^2 + y^2}{c^2}\right)$$

wherein

c = principal distance of camera,
x, y = plate coordinates referred to principal point,
μ_o = index of refraction of light at ground level,
μ = index of refraction at camera.

The value of μ is computed from the formula

$$(\mu - 1)\, 10^6 = \left(77.34 + \frac{0.44}{\lambda^2}\right)\frac{P}{T+273},$$

in which

P = pressure in millibars,
T = temperature in degrees Centigrade,
λ = wave length of light in microns (approximately 0.55 microns for the middle of the visible range).

When the camera is in a pressurized compartment (as in the USQ-28 System), the index μ applies to the compartment and not to the atmosphere immediately outside the aircraft. It follows that when air density in the camera compartment is equal to that at ground level, $\mu = \mu_o$ and the result is that atmospheric refraction and window refraction perfectly cancel each other. We point this out to emphasize the consequences of the camera window in a pressurized aircraft. Other treatments of refraction that we have encountered (e.g., those in the Manual of Photogrammetry) fail to distinguish between the refractive effects of pressurized and unpressurized camera compartments.

The last of the preliminary corrections, the reseau corrections for film deformation, were applied to each frame selected to be measured for the SMAC reduction. The entire set of 37 reseau images was measured on each selected frame along with images of fiducials and control points. Corrections for film deformation employed the models:

$$\Delta x = x_r - x = a_o + a_1 x + a_2 y + a_3 x^2 + a_4 xy + a_5 y^2 + a_6 x^3 + a_7 x^2 y + a_8 x y^2 + a_9 y^3$$

$$\Delta y = y_r - y = b_o + b_1 x + b_2 y + b_3 x^2 + b_4 xy + b_5 y^2 + b_6 x^3 + b_7 x^2 y + b_8 x y^2 + b_9 y^3$$

in which

Δx, Δy = corrections to be added to measured coordinates x, y;
x_r , y_r = reseau coordinates;
a_i , b_i = coefficients determined from least squares fit to discrepancies between pre-established coordinates and measured coordinates of reseau images.

Several trials of the fitting process were made to determine the set of coefficients providing a compact model, i.e., one containing no inessential coefficients. In both the Δx and Δy models, it was found that the coefficients of x^3 and y^3 could be consistently dropped without adversely affecting the quadratic form of the residuals. All other coefficients were found to contribute significantly to the fit. Accordingly, in the final reseau reductions only 8 of the 10 coefficients in each model were exercised.

Initial fits of the models for deformation yielded rms errors on the order of 5 to 6 microns for each frame. In the light of our previous experience, this was not considered to be satisfactory. Upon examining the residuals, we found that a few points had large residuals (over 10 microns) of nearly constant magnitude on frame after frame. When these points were dropped from the reduction, rms errors were reduced to about half their previous values. This suggests that either the pre-calibrated values for the coordinates of these particular points were of marginal accuracy or else that the individual projection units for these points had become slightly misaligned after calibration.

In Table 1 we have listed the standard deviations of the reseau fit for each of the twenty frames reduced from camera 006 on each of the two flights. All 37 reseau images were used, with the coordinates of the poor reseau points being replaced by adjusted values. On Test No. 1 the fit of the model was excellent with typical rms errors being 2.0 microns in x and 2.4 microns in y. Somewhat poorer fits were generally obtained on Test No. 2, the typical rms errors being 2.3 microns in x and 3.6 microns in y. Inasmuch as the y axis runs laterally across the film, the greater rms error in y in both tests is probably attributable to the occasionally severe lateral deformation occurring near the edges of the film. This is borne out by the finding that the largest y residuals tend consistently to correspond to points closest to the edges of the film. Residuals in x, on the other hand, display no such tendency. When the fitting is limited to the 25 interior reseau points (spaced at 2 inch intervals) results on the poorer frames (e.g. frames 53, 153, in Table 1) become significantly improved (to about the 2 micron level). In applications to routine aerotriangulation, it would probably be best to exercise only the interior reseau points in the correction for film deformation (here, correction of the fiducials for deformation is of no practical consequence, for the recovered horizontal coordinates of the exposure station provide effective projective compensation for small errors in the adopted coordinates of the principal point). In the application to SMAC, on the other hand, the fiducials should define a consistent frame center so that the calibrated coordinates of the principal point are referred to a common origin. It was for this reason that we employed the entire set of reseau images on each frame in establishing the coefficients of the model for film deformation.

TABLE 1. Results of Fitting of Models for Film Deformation of Frames from Camera 00

TEST NO. 1, 24 March 1967			TEST NO. 2, 29 March 1967		
Frame No.	σ_x (Microns)	σ_y (Microns)	Frame No.	σ_x (Microns)	σ_y (Microns)
194	1.7	2.0	118	1.6	2.5
195	1.2	2.3	119	1.4	4.3
196	1.9	2.1	120	1.8	4.1
197	1.7	2.1	121	2.2	1.9
198	1.5	2.1	122	1.7	3.8
222	1.3	2.0	153	3.9	6.3
223	1.5	2.5	154	1.8	2.1
224	1.9	2.4	155	2.4	2.6
225	2.7	2.1	156	2.2	2.6
226	1.9	1.9	157	1.7	1.9
282	1.7	2.2	51	2.3	4.0
283	2.2	2.2	52	2.0	2.7
284	1.6	2.1	53	3.2	7.6
285	3.8	4.5	54	2.0	3.1
286	1.9	2.6	55	2.5	3.8
310	2.7	2.3	86	2.2	3.0
311	2.4	2.1	87	1.9	3.4
312	1.4	2.1	88	2.0	2.9
313	2.2	2.2	90	2.1	2.3
314	1.8	2.7	91	1.7	2.8
Grand RMS	2.0	2.4	Grand RMS	2.3	3.6

3.2.3 Results of Aerial SMAC Calibration of Camera 006

The primary calibration to be performed from the data gathered on the McLure test was that for Camera 006. Although, Cameras 005 and 008 were also flown, they were under engineering evaluation, whereas Camera 006 had been officially delivered to the Air Force. Accordingly, our major concentration of effort was on 006 and it is the results for this camera that we shall discuss in greatest detail.

The five most central frames on each of the four passes from the two tests were selected for measurement. All target images (typically about 30 per frame), all 37 reseau images, and the images of the primary and secondary fiducials were measured on each frame, double settings being made on each point. The quality of all images was excellent. In particular, images of the targets throughout the format were decidedly better than any stellar images that we had examined on plates taken by commercial mapping cameras.

Each of the two sets of twenty frames was subjected to an independent SMAC reduction in order to ascertain the consistency of the results from one flight to another. Totals of 574 images and 640 images were measured on the first and second sets of frames, respectively. Trial runs established that two coefficients of radial distortion (K_1, K_2) and two coefficients of decentering distortion (P_1, P_2) provided an adequate model (exercise of higher order coefficients produced essentially no reduction in the quadratic form of the residuals). Ballistic camera positions, corrected for offset between flashing light and camera, were exercised as apriori constraints in the SMAC reduction on the eleven frames in each set that were successfully observed. Although propagation of closures of ballistic camera triangulation indicated one sigma accuracies of better than 0.2 feet in X, Y, and Z, the a priori constraints actually used in the SMAC reduction were relaxed by a factor of 5. This was done to avoid the possibility of overconstraining in view of the consideration that errors in the given survey of ballistic camera stations could conceivably introduce a bias of as much as 0.5 feet into the triangulations of the flashes.

The distortion functions resulting from the two independent aerial SMAC reductions are plotted in Figure 2 and are tabulated in Table 2 (one sigma error bounds are indicated in both presentations). The calibrated values of the interior projective parameters are also tabulated in Table 2. The rms error of the plate measuring residuals turned out to be 3.3 microns for the first set of frames and 3.7 microns for the second. The somewhat poorer result for the second set is probably attributable in part to the somewhat poorer corrections obtained for film deformation (review Table 1). The error bounds in Figure 2 and the standard deviations given in Table 2 are based on the rms errors of the residuals from the respective adjustments (i.e., 3.3 and 3.7 microns).

We see from the plotted and tabulated results that the two calibrations are mutually consistent considering their standard deviations. The rms disrecpancy between the two radial distortion functions is under one micron, and the maximum discrepancy of 1.8 microns (at r=120 mm) is not out of line with the sigmas of the two curves. Decentering distortion from both calibrations is unusually low, amounting to only 1.4 and 2.3 microns, respectively, at the extremeties of the format. Although the phase angles ϕ_o from the two calibrations differ significantly from each other, this is of no practical consequence inasmuch as both decentering profiles are so close to zero.

Distortion curves generated by the aerial SMAC calibrations of Cameras 005 and 008 are presented in Appendix B.

3.2.4 Discussion of Observed Shift of Principal Point

An unexpected finding concerns the magnitude of the coordinates of the principal point (Table 2). Both calibrations agree to within uncertainties of a few microns that x_p is well over 200 microns and y_p is about 100 microns. However, these values are inconsistent with the laboratory calibration and with the stellar calibration, both of which are much closer to zero (these will be taken up later). The aerial SMAC calibrations for Cameras 005 and 008 also recovered large values for x_p, y_p (namely, x_p = .167 mm, y_p = .045 mm for 005, and x_p = .175 mm, y_p = -.052 mm for 008). Naturally, we sought an explanation for such large discrepancies in x_p, y_p. Several hypothetical explanations were given consideration, namely,

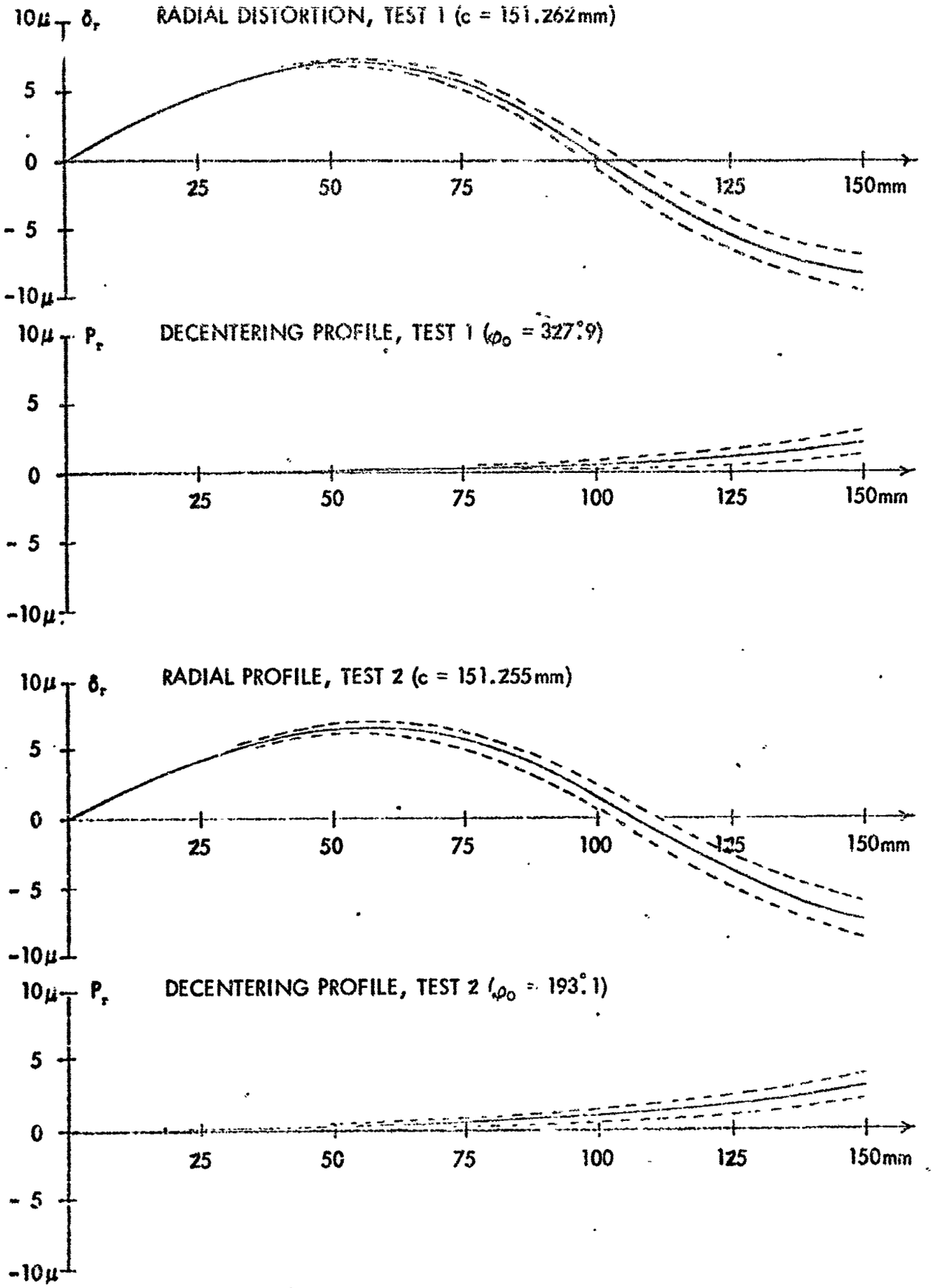

Figure 2. Radial distortion curves and decentering profiles resulting from Aerial SMAC calibrations of Camera 006 for two independent flight tests (accompanied by one sigma error bounds).

TABLE 2. Summary of Results of Aerial SMAC Calibrations of Camera 006

TEST NO. 1		TEST NO. 2	
Parameter	Value	Parameter	Value
x_p (mm)	.231±.003	x_p (mm)	.222±.004
y_p (mm)	.104±.003	y_p (mm)	.099±.004
c (mm)	151.231±.002	c (mm)	151.227±.002
K_1 (mm/mm^3)	$(-.274\pm.015)\times 10^{-7}$	K_1 (mm/mm^3)	$(-.214\pm.015)\times 10^{-7}$
K_2 (mm/mm^5)	$(.730\pm.065)\times 10^{-12}$	K_2 (mm/mm^5)	$(.509\pm.068)\times 10^{-12}$
J_1 (mm/mm^2)	$(.706\pm.356)\times 10^{-7}$	J_1 (mm/mm^2)	$(1.192\pm.363)\times 10^{-7}$
Φ_o (deg)	327.9±28.4	Φ_o (deg)	193.1±16.4

POINTS ON RADIAL AND DECENTERING DISTORTION CURVES

TEST NO. 1			TEST NO. 2		
r (mm)	δ_r [(a)] (Microns)	P_r (Microns)	r (mm)	δ_r [(b)] (Microns)	P_r (Microns)
0	0	0	0	0	0
20	3.9±0.01	0.03±0.01	20	3.4±0.01	0.05±0.01
40	6.6±0.09	0.11±0.06	40	5.9±0.09	0.19±0.06
60	7.0±0.27	0.25±0.13	60	6.6±0.27	0.43±0.13
80	4.9±0.55	0.45±0.23	80	5.1±0.56	0.76±0.23
100	0.5±0.85	0.71±0.36	100	1.7±0.87	1.19±0.36
120	-4.5±1.07	1.02±0.51	120	-2.7±1.08	1.72±0.52
140	-7.2±1.17	1.39±0.70	140	-6.2±1.18	2.34±0.71

(a) referred to value of c of 151.262mm

(b) referred to value of c of 151.255mm

1. Refractive effects of the shockwave of the aircraft;
2. Prism effect of the camera window;
3. Biases in ballistic camera triangulations;
4. Incorrectly applied offset corrections between triangulated flashes and cameras;
5. Timing bias in occurrence of flash relative to exposure of frame;
6. Tilts in the platen during IMC operation.

Analysis eliminated the first four of these hypothesis. The first hypothesis was eliminated by three considerations: (a) 'worst case' ray tracing through a prismatic analog of a shock wave indicated an effect more than an order of magnitude smaller than that observed; (b) the effect, furthermore, would cause a displacement in x_p opposite in direction to that observed; (c) lateral symmetry of the shock wave would preclude any effect on y_p.

Prism effect of the window attributable to lack of parallelism of front and rear surfaces would have to be equivalent to a wedge angle of about 0°1 in order to account for a 200 micron displacement of principal point. This would be about 150 times greater than specifications for the window. Moreover, prism effect would not explain the observed values of y_p which are opposite sign for cameras 005 and 008 relative to 006.

Inasmuch as the flying height is about 12,000 feet above ground level, a bias in the triangulated coordinates of the flashes of 12000 x (0.2/150) = 16 feet would be needed to explain a shift of 200 microns in the principal point. This is almost one hundred times greater than the standard deviations of the triangulated coordinates and corresponds to an error of about 0.5 mm on the ballistic camera plate. Above and beyond this, because of the design of the flight test, a bias in ballistic camera triangulation, if constant for all flight paths, would have no ultimate effect on the determination of the principal point. Thus a constant bias of say 16 feet in Y (north) would produce a bias of plus 200 microns in x_p in the separate reduction of photos taken on the south to north flight and a bias of minus 200 microns in x_p in the separate reduction of photos taken on the north to south flight. Similarly, it would produce biases of plus and minus 200 microns in

y_p on the separate reductions of west to east and east to west flights, respectively. Accordingly, when all four legs are reduced simultaneously, the effects of a constant bias of triangulation mutually cancel one another insofar as the net displacement of the principal point is concerned. This, in fact, was a guiding consideration in the design of the flight test.

Assuming the triangulated positions of the flashes to be correct, we find that the misapplication of offset corrections could only partially explain the observed discrepancies. If the corrections were not applied at all, the bias to be expected in x_p would amount to plus 43 microns when the prime station is occupied and to plus 75 microns when the alternate station is occupied. If they were applied with the wrong sign, the biases would be doubled in magnitude and changed in sign (i.e., they would become minus 86 and minus 150 microns, respectively). It follows that the observed values of x_p of over plus 200 microns with the camera in both primary and alternate positions cannot be explained in terms of any likely blunder in application offset corrections. Moreover, a thorough investigation of the matter showed that the corrections were indeed correctly applied.

The flashing light is supposed to be synchronized to flash with the exposure of the primary fiducials which in turn is supposed to occur at the center of exposure of each frame. Let us postulate that the primary fiducials were properly synchronized with the exposures but that the flashing light was not properly synchronized with the primary fiducials. To analyze this situation let us assume perfectly vertical photography at a constant altitude H above a flat earth. Then we can write the projective equations in the simplified form

$$\begin{aligned} x - x_p &= \frac{c}{H}\left[(X - X^c)\cos\kappa + (Y - Y^c)\sin\kappa\right] \\ y - y_p &= \frac{c}{H}\left[-(X - X^c)\sin\kappa + (Y - Y^c)\cos\kappa\right] \end{aligned} \tag{86}$$

in which κ denotes the swing angle. If these are viewed as observational equations for the recovery of x_p and y_p, we see that errors δX^c, δY^c in the coordinates of the exposure station will result in errors in x_p and y_p of

$$\delta x_p = \frac{c}{H}\left[(\cos\kappa)\,\delta X^c + (\sin\kappa)\,\delta Y^c\right],$$

(87)

$$\delta y_p = \frac{c}{H}\left[-(\sin\kappa)\,\delta X^c + (\cos\kappa)\,\delta Y^c\right].$$

If we now assume that errors in δX^c, δY^c are attributable to a timing offset δt between the exposures of the frames and the flashing of the strobe, we have

$$\delta X^c = \dot{X}\,\delta t$$

(88)

$$\delta Y^c = \dot{Y}\,\delta t$$

in which

$$\delta t = t - t_o = (\text{time of flash}) - (\text{time of frame exposure}).$$

If we further assume the total velocity V of the aircraft is constant and that the positive x axis of the plate is always aligned with the direction of flight, the $\dot{X}$, $\dot{Y}$ components of velocity become simply:

$$\dot{X} = V\cos\kappa\,,$$

(89)

$$\dot{Y} = V\sin\kappa\,.$$

Substitution of (89) into (88), followed by substitution of the resulting expressions into (87) yields the results

$$\delta x_p = \frac{c\,V}{H}\,\delta t\,,$$

(90)

$$\delta y_p = 0\,.$$

These expressions are independent of the direction of flight. It follows that the exercise of direct and reverse flight paths does not automatically cause the effects of a constant bias in synchronization to cancel out as is the case with a constant bias in position. It is clear that such cancellation could have been achieved from direct and reverse flight paths if the camera were rotated 180° in swing angle between direct and reverse paths (on the other hand, such a procedure would undo the

the automatic cancellation of the effects of constant bias in triangulation). Inasmuch as $c \approx 150$ mm, $H \approx 12{,}000$ ft., $V \approx 600$ ft./sec. for the McLure tests, it follows from (90) that to account for an error of $\delta x_p = 0.2$ mm, an error of synchronization of $\delta t = .028$ sec. is needed. When image motion compensation (IMC) is operative, as it was in the McLure tests, an error of synchronization projectively equivalent to that just considered is one in which the flashing light is perfectly synchronized with the exposure, but the primary fiducials are exposed .028 sec. too late. A third possibility is for the flashing light to be perfectly synchronized with the primary fiducials, which, in turn, are not perfectly synchronized perfectly with the exposure of the frame. In this situation, the expression for δx_p would become

$$(91) \qquad \delta x_p = 2 \frac{c V}{H} \delta t,$$

and an error of $\delta t = .014$ sec. would be sufficient to explain a 200 micron shift in x_p.

From the information available to us, we are unable to rule out any of the three possibilities just cited, namely:

1. primary fiducials perfectly synchronized with exposure of frame, but strobe flash occurring about 28 milliseconds too late;
2. strobe flash perfectly synchronized with exposure of frame, but primary fiducials exposed about 28 milliseconds too late;
3. strobe flash and exposure of primary fiducials perfectly synchronized, but occurring 14 milliseconds after exposure of frame.

While each of these could explain a 200 micron shift in x_p, we have no way of verifying which, if any, is correct. We do, however, have solid evidence that something is amiss in the timing of events. By measuring the distances between the primary and secondary fiducials on each frame and comparing them with their calibrated values (no IMC), we were able to ascertain the precise amount of film movement occurring between their respective exposures. This averaged 93 microns on the first flight test and 87 microns on the second. Specifications for the camera call for the following sequence of events:

1. well prior to initiation of the shutter pulse, the platen is brought up to full speed in accordance with the V/H input;

2. at the initiation of the shutter pulse, the secondary fiducials are exposed and the shutter begins to open;

3. precisely 5 milliseconds later at the center of the exposure (which has a constant duration of 10 milliseconds) the primary fiducials are exposed;

4. 5 milliseconds after this, the shutter is fully closed.

In the McLure tests, the IMC rate ideally should have been about c (V/H) ≈7.1 millimeters/second. Accordingly, the amount of film movement in the 5 milliseconds between exposure of secondary and primary fiducials should have been about 36 microns. As has already been pointed out, it was in fact 87 and 93 microns, on the average, for the two tests. This suggests that either the IMC rate was in error by a factor of about 2.5 or else the interval between exposures of secondary and primary fiducials was about 2.5 times longer than the 5 milliseconds specified. Inasmuch as the images of the ground lights were perfectly round and not the least elongated, we may conclude that the IMC rate was not at fault and that the time interval between exposures of secondary and primary fiducials therefore must have been about 13 milliseconds. The finding that the actual interval between one pair of events is definitely incorrect, lends support to the hypothesis that a deficiency in synchronization is a likely explanation for the observed displacement of the principal point in x_p. Recall that a delay of 14 milliseconds in the exposure of the primary fiducials relative to the exposure of the frame would explain a 200 micron shift in x_p if the flashing light were truly synchronized with the primary fiducial (as it is supposed to be). In view of the similar interval (13 milliseconds) between exposure of secondary and primary fiducials, a natural conjecture is that it was the exposure of the secondary fiducials that actually coincided with the center of the frame exposure. Whether or not this is the case, it is clear that a thorough investigation should be made into the timing and synchronization of events occurring throughout the exposure cycle of the KC-6A*.

---

* After the above was written an oscilloscope test performed on Camera 006 by the 1370 Photo Squadron showed that the flashing light actually occurred between 25 and 30 milliseconds after the midpoint of the exposure. Thus the first hypothesis forwarded above is now confirmed.

An error in synchronization does not serve to explain the observed displacement of about 100 microns in y_p. If the platen should somehow become tilted laterally by about 2 minutes of arc during the IMC movement, such a displacement in y_p would occur. The effects of such a tilt on focus would, at worst, be only barely noticeable. If, for instance, the edge of the frame were 75 microns from the plane of best focus, the resulting 'circle of confusion' of an image patch near the edge would have a diameter of only 15 microns (for the camera aperture at f/5). This would not perceptibly degrade the images of the ground targets, for these are about 50 microns in diameter. For this reason, examination of image quality does not provide a means for either confirming or denying the existence of a tilt of the platen as small as two minutes of arc. Although we are unable at this time to suggest any other plausible explanation for the displacement in y_p, this naturally does not rule out the existence of alternative explanations.

Considering the possible implication of IMC in the shift of the principal point, we would urge that in any future aerial SMAC calibrations of the KC-6A, the basic flight test pattern be flown both with and without the operation of IMC. This would settle many matters that are now subject to conjecture.

Just what is the precise photogrammetric significance of the elements of interior orientation? In view of our findings concerning the principal point, consideration of this matter is clearly in order. In conventional aerotriangulation over flat terrain rather large errors in x_p, y_p and c are readily tolerated inasmuch as almost perfect projective compensation is provided by the recovered coordinates X^c, Y^c, Z^c of the exposure station. Here, the central problem reduces to one of interpolation within a framework of known control points to establish the coordinates of other points of interest. Thus the process, being essentially interpolative in character, is not normally compromised by projective tradeoffs of errors in x_p, y_p and c insofar as the desired end results are concerned. However, this comfortable situation no longer applies as soon as the photogrammetric process becomes extrapolative, as is the case in operations exercising the full capability of the USQ-28 System. Here, external sensors (Shiran, Hypernas, Terrain Profile Recorder) provide sharp constraints on elements of exterior orientation. Theoretically, this permits one to perform aerotriangulation without recourse to

ground control. However, since tight constraints on elements of exterior orientation sharply limits the effectiveness of projective compensation for defects in elements of interior orientation, it follows that far higher accuracies are required of elements of interior orientation when such constraints are brought to bear. While errors of 100 or 200 microns in x_p, y_p, c are of no practical consequence in conventional aerotriangulation, such errors would be intolerable when accurate external sensors are exercised. Full realization of the potential of the USQ-28 System demands that errors in x_p, y_p and c be suppressed to under 10 microns. Hence, our concern with the results of aerial SMAC with regard to the principal point; the 200 micron shift in x_p would, if real and unaccounted for, introduce an error in planimetry of H/750.

Another situation in which errors in elements of interior orientation have a first order effect merits discussion. This is in photogrammetric resection wherein the objective is the accurate recovery of the coordinates X^c, Y^c, Z^c of the exposure station. This approach has been used, for example, for the evaluation of tracking accuracies of Hiran and Shiran from photography taken over the Phoenix Test Range. For H = 30,000 feet, an error of 200 microns in principal point would introduce an error of H/750 = 40 feet in the horizontal position of the camera as obtained by resection. Such an error would clearly invalidate the evaluation of any accurate tracking system. It is to be emphasized that whenever the coordinates X^c, Y^c, Z^c recovered from a photogrammetric reduction are to be interpreted as having physical significance, the errors in x_p, y_p, c assume paramount importance. This fact seems not to have been given due consideration in certain flight testing programs which may have been significantly compromised as a result.

3.2.5 Analysis of Residuals

We have yet to consider in detail the observational residuals obtained from the SMAC reductions. These should ideally be completely random and should have a standard deviation consistent with the 2 to 3 microns typical of the reseau reduction. As we have seen, the standard deviations of the residuals from the two reductions turned out to be 3.3 and 3.7 microns, respectively, or somewhat higher than desirable. This suggests the presence of some degree of unmodeled systematic error. To aid in the examination of the residuals,

we have provided in Figures 3 and 4 graphs of the residual vectors from the two SMAC reductions. In these figures, all residuals from the 20 frames carried in each SMAC reduction are plotted on a common graph against the plate coordinates of the images. The resulting high density of residuals helps to isolate any localized systematic tendencies.

We see from Figures 3 and 4 that definite systematic patterns do exist, particularly near the lower left hand and upper right hand corners as well as near the right hand edge between y = 20 and y = 70 millimeters. A fairly good correlation is seen to exist between the more pronounced systematic tendencies in both figures. Indeed, when both figures are superimposed, as is done in Figure 5, systematic patterns become even more clearly defined.

In examining the tabulations of residuals, we noticed that the residuals for certain control points appeared to be consistently larger than average in magnitude and to be systematic in direction within a given run. To illustrate this, we have listed in Table 3 the residuals for point no. 39 for all frames on both tests. It is clear from the table that the residuals from the two tests are strongly correlated. The pattern of the residuals corresponds closely to that to be expected from an error in the survey of the control point. Thus significant negative errors in the given X (east) and Y (north) coordinates of a target would tend to generate positive x residuals and positive y residuals on west to east runs; positive y residuals and negative x residuals on south to north runs; negative x residuals and negative y residuals on east to west runs; and negative y residuals and positive x residuals on north to south runs. This is indeed the general tendency of the residuals in Table 3, with the effects of a possible error in X predominating.

In view of the fact that residuals from several other control points also indicated the presence of significant survey error, we decided to examine more closely the matter of survey accuracies. From ETL contacts with USCGS we had been informed that the McLure survey was considered to be a third order survey exercising second order procedures. Although this was deemed to be decidedly marginal for the SMAC calibrations, we reasoned that ultimate effects of survey errors on interior projective parameters would be largely averaged out by virtue of the orthogonal pattern of direct and reverse flights. Inasmuch as the basic SMAC

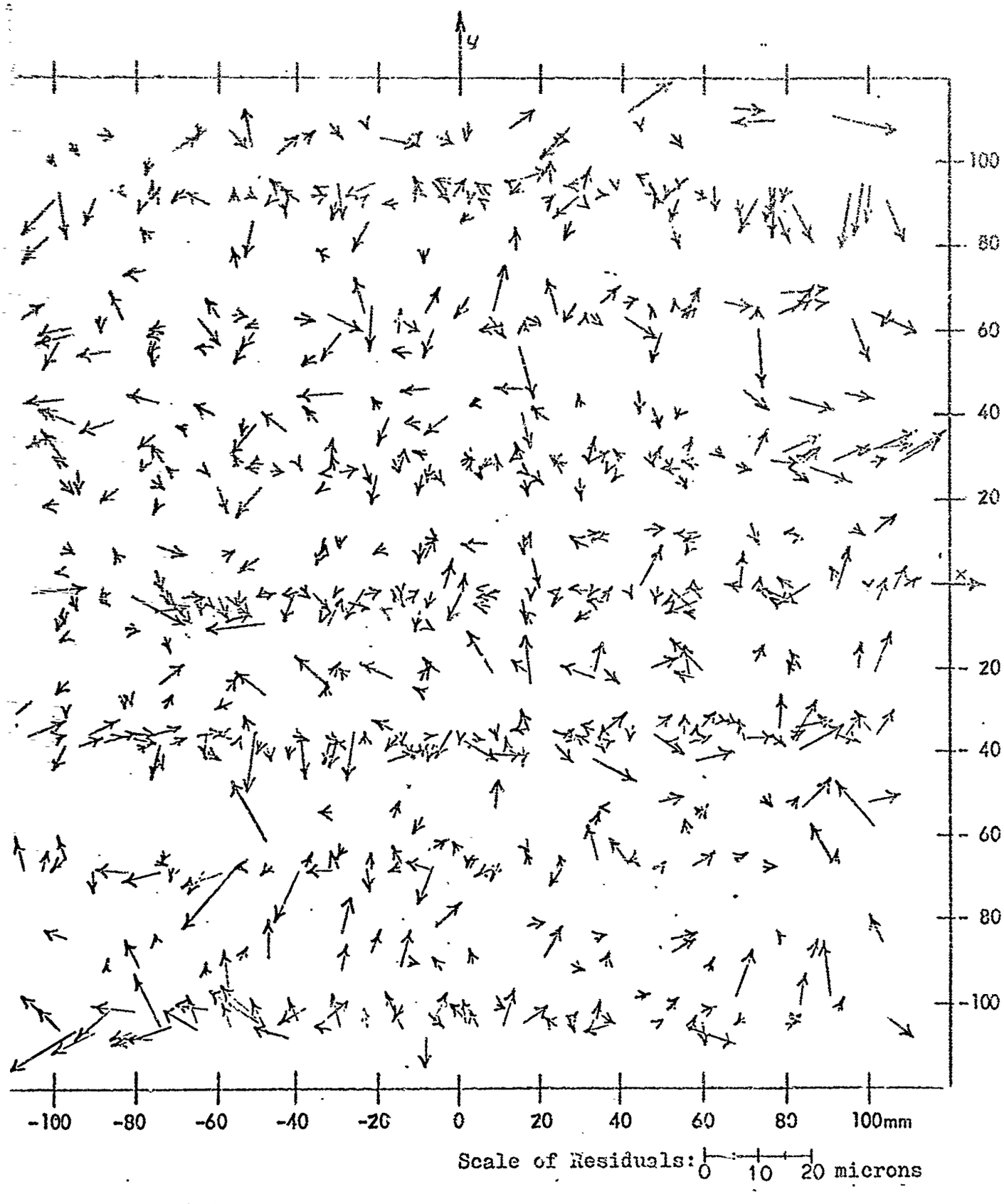

Figure 3. Composite plot of residual vectors from 20 frames carried in Aerial SMAC calibration of Camera 006, Flight Test No. 1 (rms value of residuals = 3.3 microns).

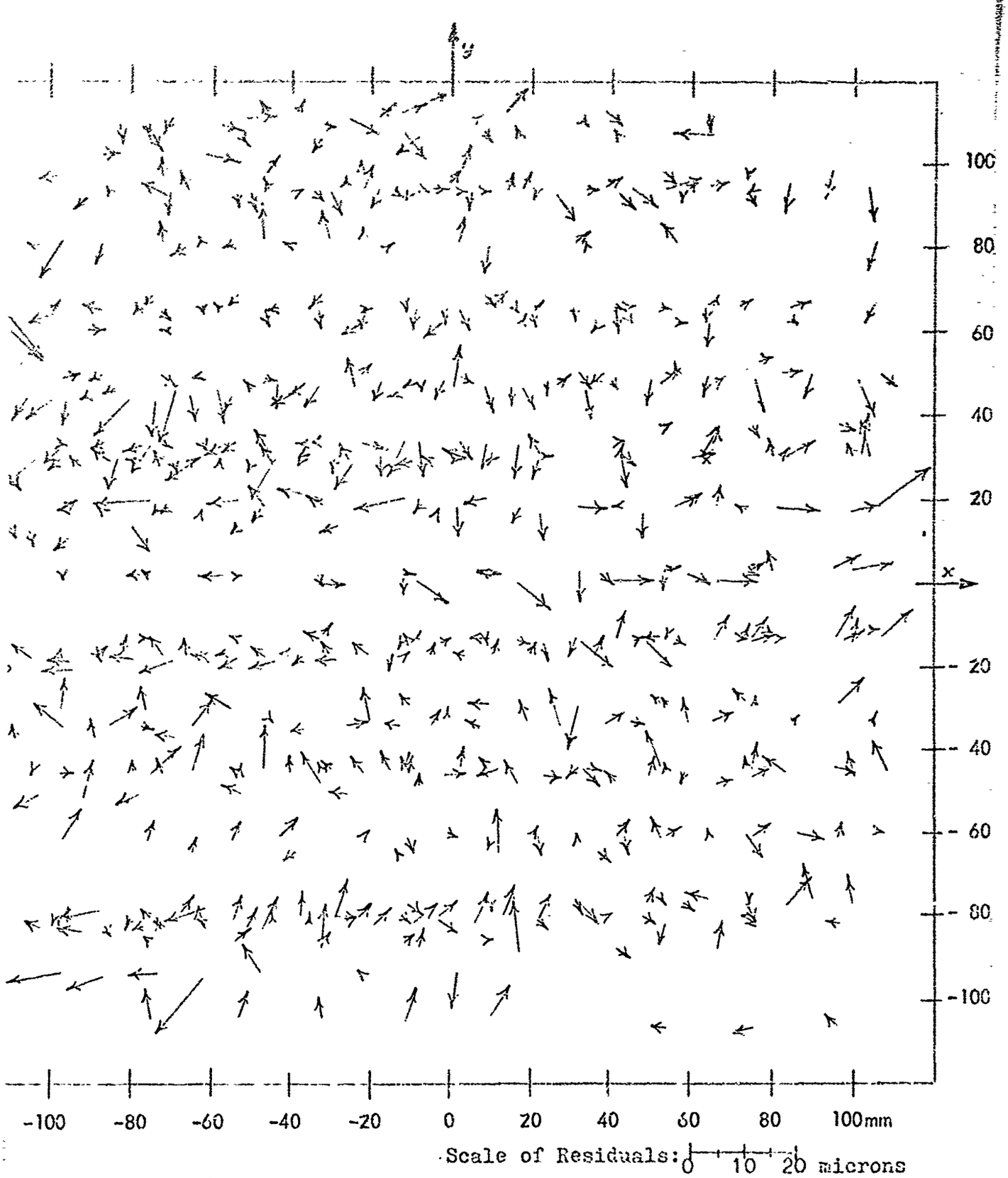

Figure 4. Composite plot of residual vectors from 20 frames carried in Aerial SMAC calibration of Camera 006. Flight Test No. 2 (rms value of residuals =3.7 microns).

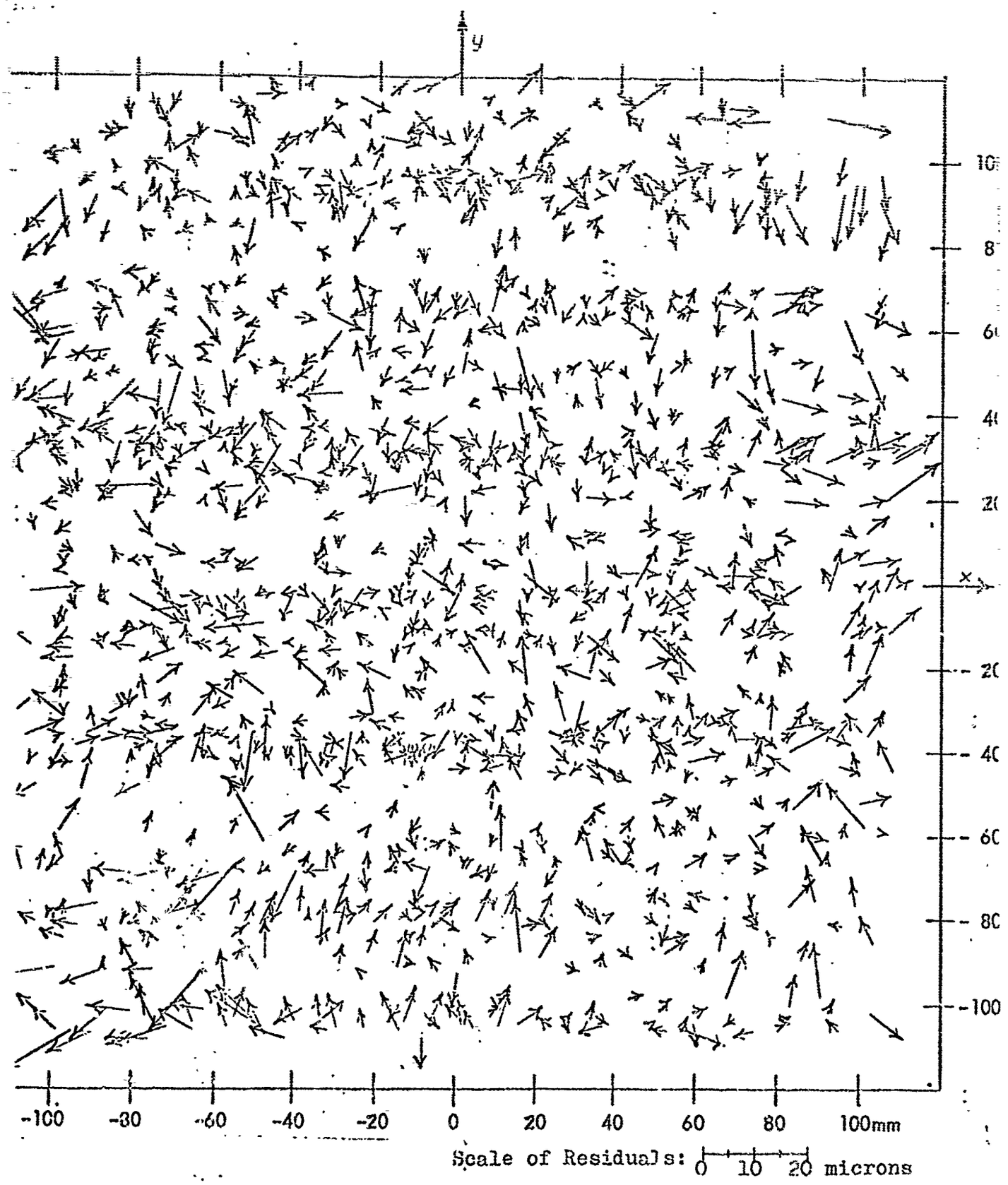

Figure 5. Combined plot of residual vectors in Figures 3 and 4.

TABLE 3. Plate residuals for Control Point No. 39 on each frame from separate SMAC reductions of two flight tests (a) with original survey and (b) after adjustment of survey (numbers in parenthesis)

Run	TEST 1			TEST 2		
	Frame	v_x (Microns)	v_y (Microns)	Frame	v_x (Microns)	v_y (Microns)
W→E	194	3.9(2.2)	3.2(-4.0)	51	2.8(0.3)	8.5(-2.0)
	195	2.7(1.4)	2.1(-5.0)	52	1.4(-0.7)	7.6(1.2)
	196	1.5(0.6)	7.9(0.7)	53	5.6(4.0)	8.5(2.0)
	197	- 0.6(-1.0)	5.5(-1.7)	54	-1.3(-2.6)	6.2(-0.2)
	198	0.9(-0.9)	0.6(-6.5)	55	1.5(0.6)	5.7(-0.7)
N→S	222	- 5.4(-0.8)	-0.8(-2.1)	86	-5.4(0.8)	0.5(-1.2)
	223	-11.1(-4.5)	-1.9(-3.2)	87	-6.5(0.0)	- 0.5(0.0)
	224	- 8.9(-2.1)	2.1(0.8)	88	-8.4(-1.5)	- 0.5(-2.2)
	225	- 6.2(1.0)	-0.6(-1.9)	90	-6.2(1.4)	1.6(0.0)
	226	-11.9(-4.3)	-0.5(-1.8)	91	-7.5(0.6)	- 0.9(-2.5)
E→W	282	- 4.2(-2.9)	-5.6(0.3)	118	-3.4(-2.4)	- 5.6(1.4)
	283	- 4.8(-3.0)	-7.8(-1.9)	119	-1.7(-0.3)	- 9.9(-2.8)
	284	- 6.5(-4.4)	-4.3(1.6)	120	-2.0(-0.2)	-11.5(-4.4)
	285	- 2.0(0.3)	-6.2(-0.3)	121	-1.0(1.0)	- 6.1(1.1)
	286	- 6.4(-3.8)	-5.2(0.0)	122	-2.5(0.0)	- 4.6(2.5)
S→N	310	8.2(0.8)	-0.2(0.8)	153	8.7(0.8)	4.1(5.6)
	311	7.4(0.4)	0.2(-0.4)	154	7.0(-0.4)	1.2(2.7)
	312	6.7(0.0)	-5.2(-4.2)	155	7.9(0.9)	- 4.6(-3.1)
	313	6.9(0.7)	-4.5(-3.4)	156	6.7(0.1)	- 0.4(1.0)
	314	4.8(-1.4)	-0.7(0.4)	157	6.5(-0.3)	- 2.7(2.4)

Grand RMS for point 39 before adjustment of survey: 5.4 microns
Grand RMS for point 39 after adjustment of survey: 2.2 microns

reduction does not consider survey errors, it follows that their influence will be reflected, as we have seen, in the plate measuring residuals. Inasmuch as this influence does indeed assume significance in the residuals for several points, we decided to adjust the survey to minimize its effects. This would most properly be done through a rigorous extension of SMAC to consider errors in the given control, as is discussed in a later section. Since such an approach would be beyond the scope of the present undertaking, we adopted a compromise along the following lines. The projective parameters recovered from the SMAC reductions were considered to be flawless for each frame. The coordinates of all control points were then regarded as unknown and the coordinates of a given control point were established by spatial triangulation of rays from all frames containing the point. As many as 40 rays were involved in the triangulation of the more central points, inasmuch as these were recorded on all 40 frames. The corrections to the survey resulting from this process are listed in Table 4 along with their standard deviations.

The rms values of the corrections for those points appearing on least 20 frames turn out to be 0.20 ft. in X, .17 ft. in Y, and 0.22 ft. in Z, respectively. Accordingly, these values were adopted as being characteristic of the given survey. The revised corrections listed in the final three columns of Table 4 are derived from the weighted averages of the original values and the corresponding values resulting from the adjustment. Thus $\delta X, \delta Y, \delta Z$ are given by

$$\delta X = \frac{(.20)^2}{(.20)^2 + \sigma_x^2} \Delta X$$

$$\delta Y = \frac{(.17)^2}{(.17)^2 + \sigma_y^2} \Delta Y \qquad (93)$$

$$\delta Z = \frac{(.22)^2}{(.22)^2 + \sigma_z^2} \Delta Z$$

in which σ_x, σ_y, σ_z are the sigmas listed in Table 4. By virtue of the weighting, the revised corrections for those points that are poorly determined in adjustment become close to zero, whereas the revised corrections for those points that are strongly determined become only slightly altered.

TABLE 4. Corrections to Survey of McLure Range Derived from Aerial SMAC Residuals

Pt. No.	No. Frames	Original Corrections to Survey from Aerotriang.			Standard Deviations of Original Corrections			Revised Corrections from Weighted Averages		
		ΔX (Ft)	ΔY (Ft)	ΔZ (Ft)	$\sigma_{\Delta x}$ (Ft)	$\sigma_{\Delta y}$ (Ft)	$\sigma_{\Delta z}$ (Ft)	δX (Ft)	δY (Ft)	δZ (Ft)
1	2	0.66	0.35	0.52	1.40	1.25	2.32	0.01	0.00	0.00
2	9	0.33	-0.15	0.58	0.29	0.23	0.46	0.11	-0.04	0.11
3	14	0.22	-0.10	0.48	0.21	0.19	0.35	0.10	-0.04	0.14
4	20	-0.25	0.31	-0.23	0.13	0.15	0.26	-0.18	0.15	-0.10
5	21	-0.20	-0.03	-0.15	0.10	0.14	0 25	-0.16	-0.02	-0.07
6	22	-0.22	0.11	-0.21	0.08	0.13	0.22	-0.19	0.06	-0.11
7	22	-0.17	-0.02	0.05	0.06	0.13	0.22	-0.15	-0.01	0.03
8	21	-0.19	-0.07	-0.07	0.05	0.13	0.22	-0.18	-0.04	-0.04
9	23	-0.07	-0.13	0.18	0.05	0.12	0.21	-0.06	-0.08	0.10
10	21	-0.17	-0.35	0.56	0.08	0.14	0.24	-0.15	-0.19	0.26
11	10	-0.54	-0.67	0.91	0.25	0.25	0.45	-0.21	-0.18	0.18
12	7	0.22	0.37	-0.94	0.37	0.35	0.62	0.05	0.06	-0.11
13	2	0.92	1.04	-1.40	1.03	1.07	2.00	0.03	0.02	-0.02
14	2	0.02	-0.01	-0.28	1.24	0.25	2.00	0.00	0.00	0.00
15	10	0.41	0.02	-0.91	0.21	0.11	0.34	0.20	0.01	-0.28
16	34	0.02	-0.04	0.02	0.08	0.06	0.15	0.02	-0.03	0.01
17	27	-0.17	-0.08	0.26	0.09	0.09	0.18	-0.14	-0.06	0.16
18	40	0.03	0.04	-0.11	0.04	0.05	0.12	0.03	0.04	-0.08
19	40	0.04	0.15	0.11	0.04	0.05	0.12	0.04	0.14	0.08
20	40	0.14	0.15	0.16	0.04	0.05	0.12	0.13	0.14	0.12
21	40	-0.08	0.01	0.01	0.05	0.05	0.12	-0.08	0.01	0.01
22	30	0.09	-0.08	-0.29	0.07	0.08	0.17	0.08	-0.06	-0.18
23	39	0.05	-0.05	-0.30	0.06	0.05	0.13	0.05	-0.05	-0.22
24	38	0.12	-0.04	-0.21	0.07	0.06	0.13	0.11	-0.03	-0.16
25	14	-0.03	0.45	-0.09	0.18	0.12	0.28	-0.02	0.27	-0.04

TABLE 4 (Continued)

Pt. No.	No. Frames	Original Corrections to Survey from Aerotriang.			Standard Deviations of Original Corrections			Revised Corrections from Weighted Averages		
		ΔX (Ft)	ΔY (Ft)	ΔZ (Ft)	$\sigma_{\Delta x}$ (Ft)	$\sigma_{\Delta y}$ (Ft)	$\sigma_{\Delta z}$ (Ft)	δX (Ft)	δY (Ft)	δZ (Ft)
26	21	0.38	0.09	0.20	0.12	0.08	0.18	0.28	0.07	0.12
27	5	0.36	-0.16	-0.02	0.27	0.17	0.45	0.13	-0.07	0.00
28	4	0.42	-0.36	0.33	0.34	0.22	0.54	0.11	-0.11	0.05
29	20	-0.18	0.18	-0.09	0.13	0.06	0.19	-0.13	0.16	-0.05
30	7	0.15	-0.32	0.33	0.24	0.09	0.40	0.06	-0.24	0.08
31	21	-0.39	-0.15	-0.22	0.12	0.06	0.18	-0.29	-0.13	-0.13
32	27	-0.32	-0.25	-0.30	0.09	0.05	0.16	-0.27	-0.22	-0.20
33	36	-0.06	-0.17	-0.12	0.07	0.04	0.13	-0.05	-0.16	-0.09
34	20	-0.00	-0.06	-0.44	0.07	0.07	0.20	-0.00	-0.05	-0.25
35	38	-0.03	-0.14	-0.10	0.05	0.04	0.13	-0.03	-0.13	-0.07
36	39	-0.09	0.10	-0.20	0.05	0.04	0.12	-0.08	0.09	0.18
37	40	0.01	-0.27	-0.12	0.05	0.04	0.13	0.01	-0.25	0.16
38	40	-0.09	-0.24	0.00	0.08	0.04	0.15	-0.09	-0.22	-0.08
39	40	-0.08	0.52	-0.09	0.08	0.05	0.15	-0.08	0.48	-0.16
40	39	0.21	0.08	0.33	0.16	0.07	0.24	0.20	0.07	-0.09
41	33	0.13	0.01	0.00	0.08	0.04	0.15	0.11	0.01	0.00
42	33	0.23	-0.13	-0.09	0.08	0.05	0.15	0.20	-0.12	-0.06
43	16	0.10	-0.05	0.33	0.16	0.07	0.24	0.06	-0.04	0.15
44	1	-	-	-	-	-	-	0.00	0.00	0.00
45	22	-0.38	0.14	0.54	0.11	0.12	0.21	-0.29	0.08	0.29
46	30	-0.13	0.23	0.09	0.06	0.09	0.16	-0.12	0.17	0.06
47	33	0.12	0.14	-0.04	0.04	0.08	0.14	0.12	0.11	-0.03
48	28	-0.22	-0.04	-0.01	0.05	0.10	0.17	-0.21	-0.03	0.00
49	30	-0.14	-0.21	-0.06	0.06	0.09	0.16	-0.13	-0.15	-0.04
50	16	-0.06	0.32	-0.20	0.16	0.13	0.26	0.04	0.18	-0.08
51	25	0.02	-0.02	-0.34	0.05	0.10	0.20	0.02	-0.01	-0.19
52	20	0.06	-0.18	-0.27	0.05	0.07	0.20	0.06	-0.15	-0.15

It will be noted from Table 4 that the stronger triangulations produced proportional accuracies on the order of 1 part in 300,000 of the flying height in the horizontal coordinates X and Y and 1 part in 100,000 of the flying height in the vertical coordinate Z. Such a degree of accuracy is unprecidented in aerotriangulation, but then so also is the experiment itself. The results indicate that the unconventional 'cloverleaf' scheme of aerotriangulation can maintain first order accuracies in the process of densification of a sufficiently dense first order network.

When the revised survey was exercised in a repetition of the two SMAC calibrations, the resulting interior projective parameters were not sensibly altered from their former values. On the other hand, the combined set of measuring residuals from both tests was moderately improved, the rms error being reduced from 3.6 microns to 2.9 microns. As can be seen from the plotted results in Figure 6, the improvement is especially great over the central two thirds of the plate; here, the residuals are almost perfectly random. Nonetheless, systematic tendencies do persist near the edges of the format. Indeed, now that the effects of survey errors are diminished, persistent systematic components are somewhat more clearly defined than they were previously (Figure 5).

As an example of the improvement in the residuals wrought by the adjusted survey, we have also provided in Table 3 the plate residuals for Point No. 39 following the application of survey corrections in the revised SMAC reductions. The rms value of the original SMAC residuals for Point No. 39 is 5.4 microns; after the application of survey corrections the rms value is reduced to 2.2 microns.

3.2.6 Empirical Modeling of Residual Systematic Errors

While we were unable to isolate the causes of the observed residual systematic error, we did find that systematic components Δx, Δy of the residual vectors could be adequately represented by general fifth order polynomials of the form:

$$\Delta x = \sum_{i=0}^{5} \sum_{j=0}^{i} \alpha_{ij}\, x^{i-j}\, y^{j} \,, \qquad \Delta y = \sum_{i=0}^{5} \sum_{j=0}^{i} \beta_{ij}\, x^{i-j}\, y^{j} \,. \tag{94}$$

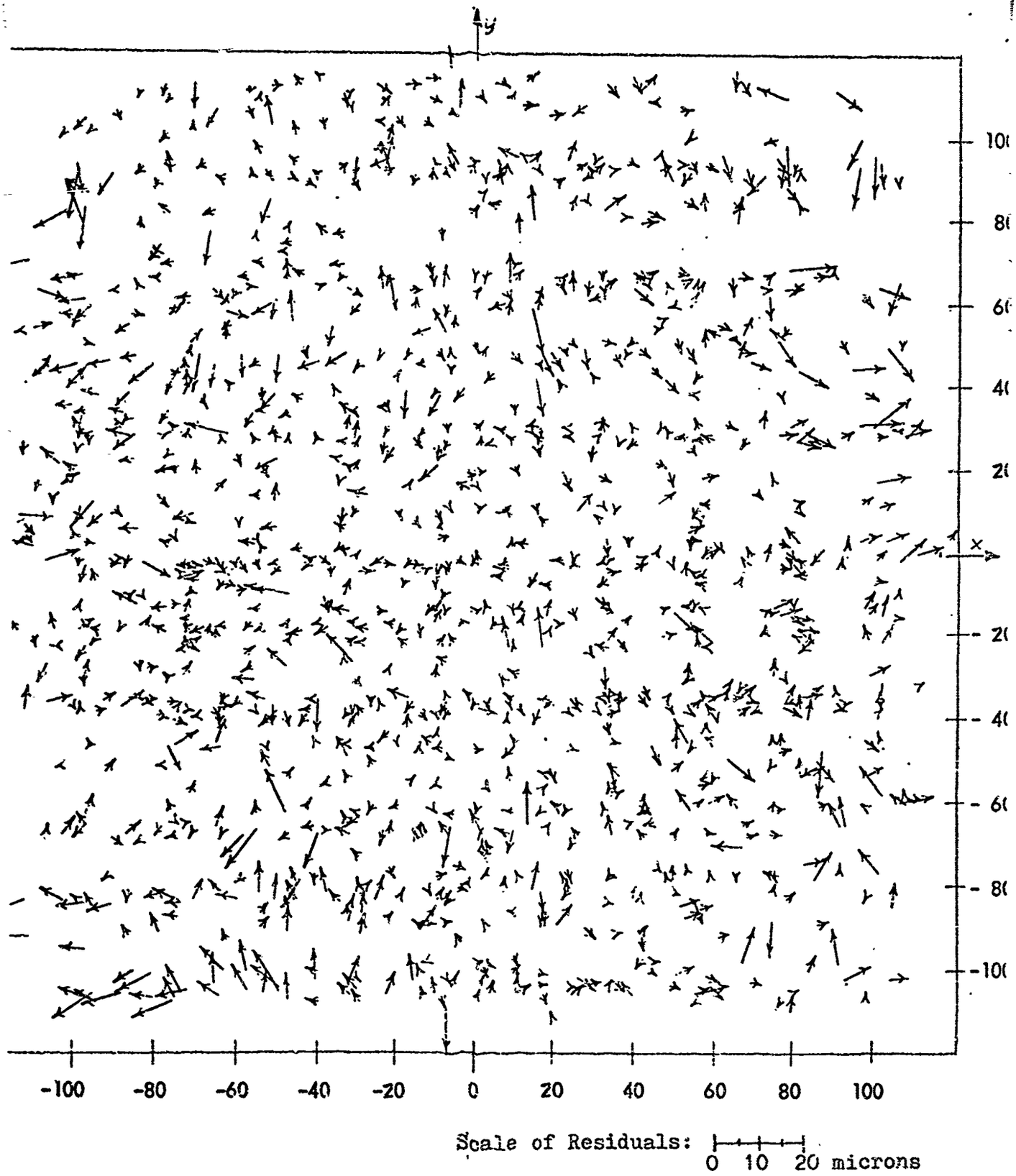

Figure 6. Revised version of Figure 5 after adjustment of McLure survey (rms value of residuals = 2.9 microns).

The coefficients of α_{ij} , β_{ij} of these error functions were established by means of a least squares fit to the residuals in Figure 6. The rms error of the revised residuals resulting from the fit turned out to be 2.3 microns, a substantial improvement over the 2.9 microns prior to the fit. Contour maps of the fitted error functions for Δx and Δy are shown in Figures 7 and 8. Ideally, the error functions could be regarded as empirically established corrections accounting for those systematic errors that are inadequately modeled in the SMAC calibration. However, before they can be applied with confidence as standard corrections, their general validity must be established in a variety of situations. It remains to be determined, for example, to what extent the error functions remain valid when such factors as the following are altered:

(a) flying altitude and velocity;
(b) calibrated coordinates of platen reseau;
(c) comparator used for measuring;
(d) exercise of image motion compensation;
(e) film magazine (and hence platen) used;
(f) photo processing of film.

Until such time as appropriate supplementary testing can be performed, the error functions derived from the SMAC residuals must be regarded as having no more than provisioned validity. The fact that their application does reduce the rms of the revised residuals to 2.3 microns in the present instance is clearly a strong inducement for a thorough investigation of the soundness of such empirically derived error functions. Thus, in conjunction with possible future testing programs, specific attention should be directed toward deliberate variation of those factors that could conceivably influence the results. By so doing, one would be better able to isolate specific causes of residual systematic error.

It should be appreciated that when only a modest number of control points appear on the typical frame, empirical modeling of residual systematic errors becomes practicable solely by virtue of the large sample of residuals that can nonetheless be generated by a SMAC reduction of a moderately large number of frames.

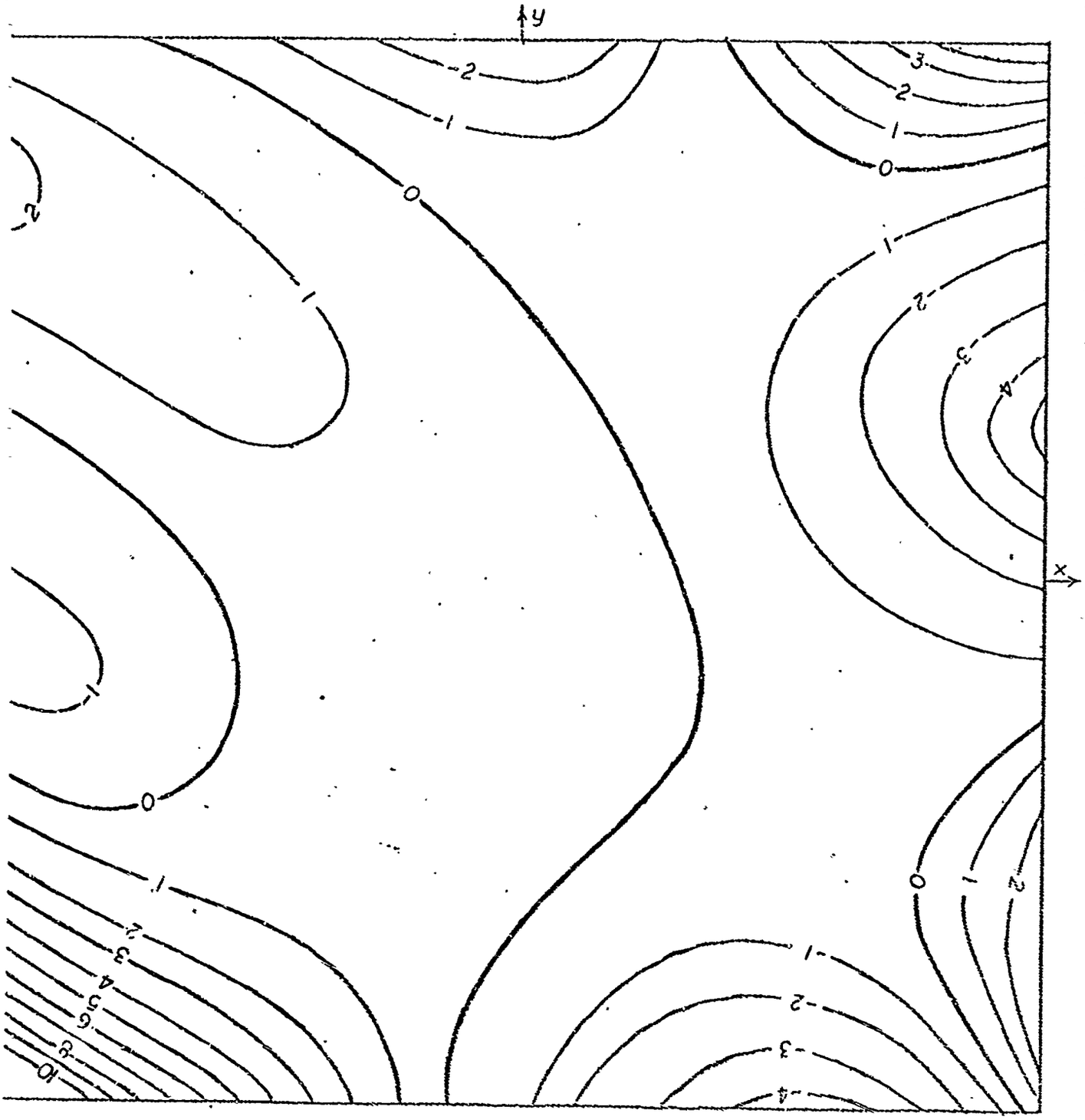

Figure 7. Isocontours of empirical corrections to x coordinates of frames exposed by Camera 006 (contour interval = 1 micron).

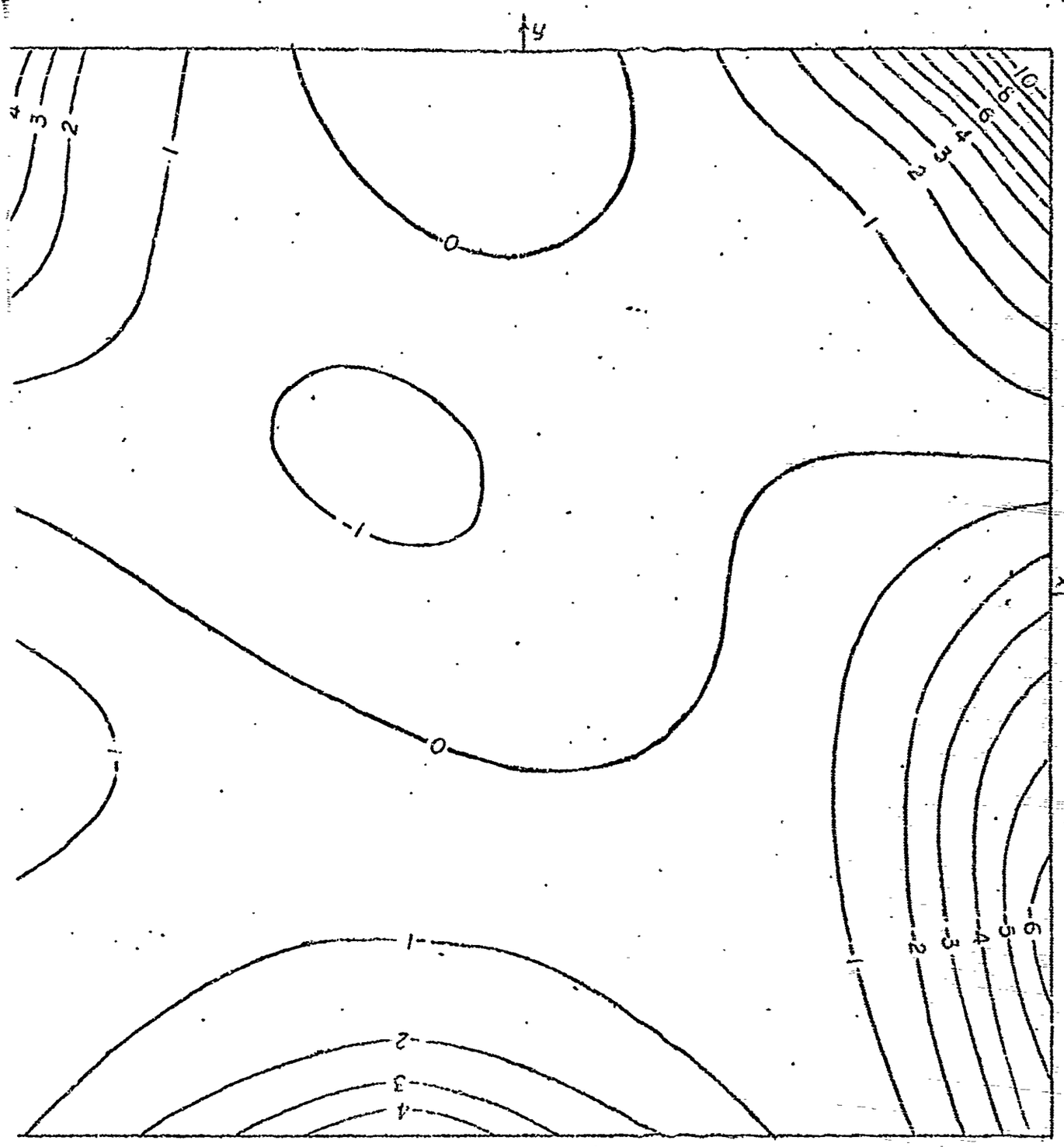

Figure 8. Isocontours of empirical corrections to y coordinates of frames exposed by Camera 006 (contour interval = 1 micron).

While we believe that the ultimate refinement of the process of camera calibration may well consist of the empirical modeling of the residual systematic errors remaining after the execution of a comprehensive SMAC reduction, this is hardly a matter for complacence. As long as significant residual systematic errors do persist, their source should be a matter of continuing concern, and one should not remain content until satisfactory physical explanations of such errors are established. Physical explanations can be expected to lead either to implementation of physical corrections, which is desirable when practicable, or to mathematical modeling of the physical process, which is far to be preferred over blind empirical modeling. At best, empirical modeling should be viewed as a crutch for ones ignorance, rather than as a panacea.

3.2.7 Empirical Determination of Weighting Functions of Plate Coordinates

It is generally appreciated that effective accuracies of plate coordinates vary with radial distance. Only a minor part of such variation can, in general, be attributed to shortcomings of the plate measuring comparator. On the other hand, much of it can presumably be attributed to the variations in image quality resulting from decreasing resolution of the lens with increasing radial distance. Other major contributions might well stem from departures from flatness of the photographic emulsion at the instant of exposure and from uncompensated deformation of the film.

Morén (1965) has reported an analysis of the pooled residuals obtained from a series of camera calibrations performed from photography of the Öland test field. The calibrations were accomplished by the grid method developed by Hallert (1954). Morén found that the dependence of the standard deviation of image coordinates on radial distance r is described by the formula:

$$(95) \quad \sigma = 2.1 + .053r + .00023r^2$$

in which σ is in microns and r is in millimeters Thus σ varies from about 2 microns in the center of the frame to about 10 microns at r = 100 mm, and to about 15 microns in the corners.

We considered it pertinent to our investigation to follow Morén's example by performing a similar analysis of the pooled SMAC residuals. Unlike Morén, we decided to perform separate analyses of the radial and tangential components of the residual vectors. Accordingly, we divided the format out to r = 120 mm into five circular zones of approximately equal area and then computed the rms errors of the radial and tangential components of the residuals in Figure 6 for each of the resulting zones. We also computed the coefficient of correlation of the radial and tangential components for each zone. The resulting values are listed in Table 5 and are plotted in Figure 9.

Table 5. Statistical Analysis of Residuals Plotted in Figure 6.

Interval	Mean Radius r	No. Residual Vectors	RMS of Radial Components: σ_r	RMS of Tangential Components: σ_t	*Correlation Coeff: ρ_{rt}
0 - 53mm	26.5mm	269	2.63μ	2.25μ	+.012
53 - 75	64.0	251	3.10	2.09	-.035
75 - 92	83.5	217	3.48	2.10	-.054
92 - 106	99.0	208	3.60	2.08	-.117
106 - 120	113.0	177	3.89	2.66	-.032
≧120	131.2	88	4.23	3.13	-.174

*None of the ρ_{rt} differs significantly from zero at the 95% level of confidence.

Interestingly enough, we find that the sigmas of the tangential components actually decrease slightly with radial distance out to r = 100mm. Moreover, they are significantly smaller throughout the format than the sigmas of the radial components. This suggests that departures from flatness of the surface of the emulsion may be of greater importance to our results than are variations in photographic resolution. We find the variation in the standard deviations of the image coordinates to be much less pronounced throughout the format than that experienced by Morén. This may be an indication of superior optical performance by the Geocon IV Lens. However, we suspect that Morén's results may reflect, to some extent, the influence of decentering distortion inasmuch as this was not explicitly accounted for in his calibrations.

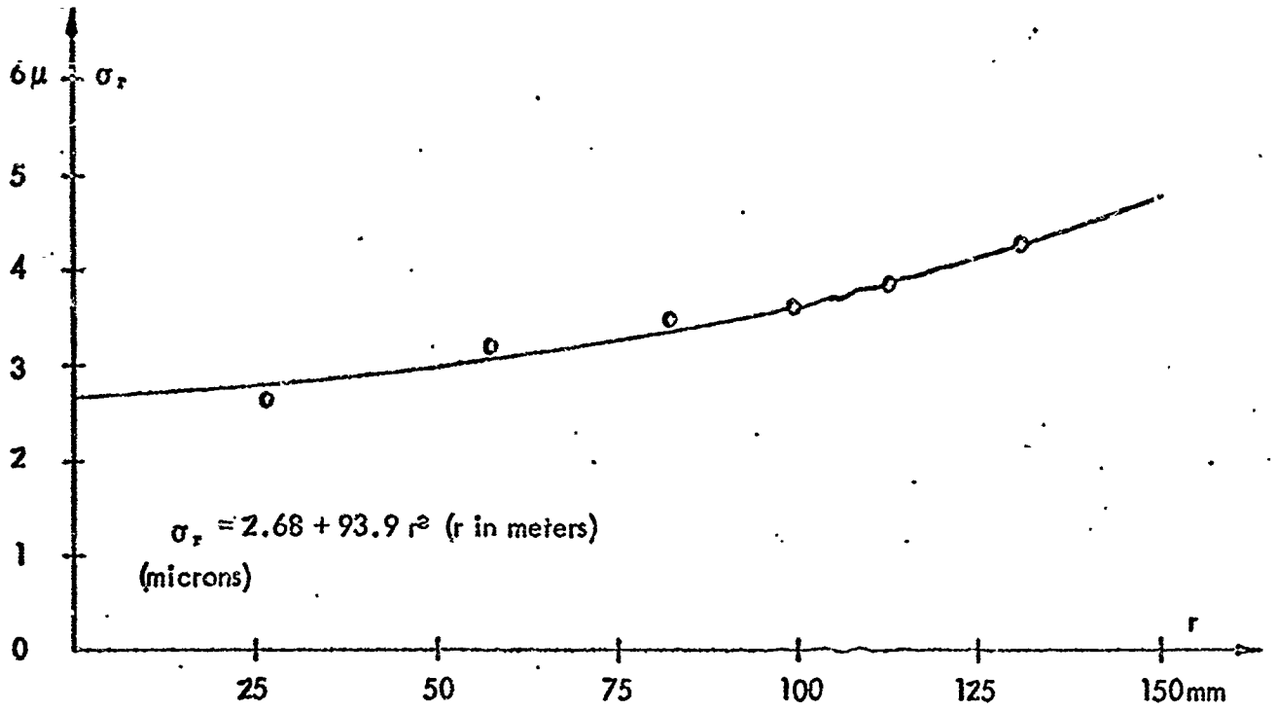

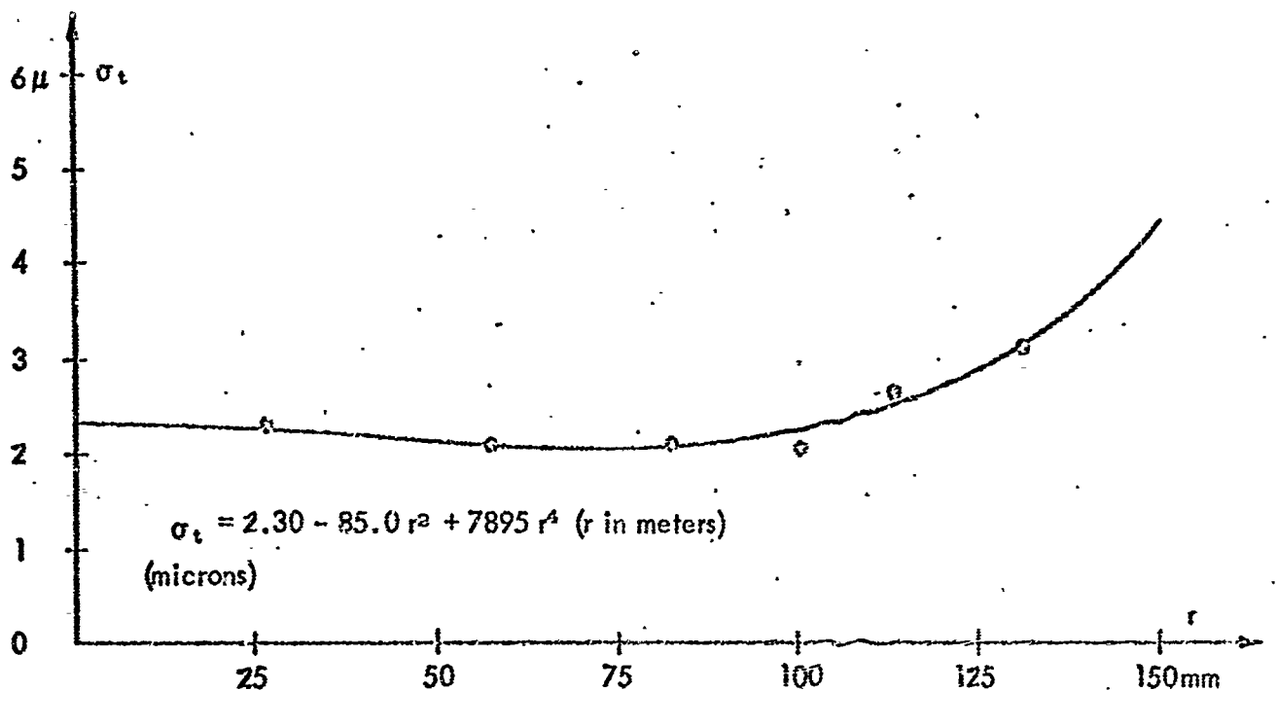

Figure 9. Radial and tangential weighting functions of KC-6A Camera No. 006 derived from Aerial SMAC residuals of Figure 6.

It will be noted that we chose to employ even powered polynomials to represent σ_r and σ_t in Figure 9. This is strictly a matter of preference stemming from intuitive optical considerations. Two terms of the expansion were found adequate to fit the observed values of σ_r whereas three were needed for σ_t.

Had we used the residuals remaining after the fit of the empirical functions Δx, Δy discussed in the preceding section, the resulting values of σ_r and σ_t would have exhibited even less variation than that encountered above. Indeed, should the empirical corrections prove to have general validity for the camera in question (KC-6A No. 006), one could safely regard the standard deviations of the image coordinates as being essentially invariant throughout the format. However, pending clarification of this matter, we consider it more prudent to adopt the results of Table 5 and Figure 9.

The practical application of the foregoing results to analytical aerotriangulation performed from photography taken by Camera 006 remains to be considered. Even though Table 5 indicates that radial and tangential components are essentially uncorrelated, this is not necessarily true of the x,y components. Inasmuch as components of error are related to radial and tangential components by

$$(96)\quad \begin{bmatrix} \Delta x \\ \Delta y \end{bmatrix} = \frac{1}{r} \begin{bmatrix} y & -x \\ x & y \end{bmatrix} \begin{bmatrix} \Delta r \\ \Delta t \end{bmatrix},$$

it follows that when Δr, Δt are uncorrelated

$$(97)\quad \begin{bmatrix} \sigma_x^2 & \sigma_{xy} \\ \sigma_{xy} & \sigma_y^2 \end{bmatrix} = \frac{1}{r^2} \begin{bmatrix} y & -x \\ x & y \end{bmatrix} \begin{bmatrix} \sigma_r^2 & 0 \\ 0 & \sigma_t^2 \end{bmatrix} \begin{bmatrix} y & x \\ -x & y \end{bmatrix}$$

$$= \frac{1}{r^2} \begin{bmatrix} y^2\sigma_r^2 + x^2\sigma_t^2 & -xy(\sigma_r^2 - \sigma_t^2) \\ -xy(\sigma_r^2 - \sigma_t^2) & x^2\sigma_r^2 + y^2\sigma_t^2 \end{bmatrix}.$$

For the special case in which $\sigma_r = \sigma_t = \sigma$, one has $\sigma_x = \sigma_y = \sigma$ and $\sigma_{xy} = 0$. In the general case in which $\sigma_r \neq \sigma_t$, $\sigma_{xy} = 0$ only when x or y is equal to zero. When $x = y$ the coefficients of correlation between x and y is given by $\rho_{xy} = (\sigma_r^2 - \sigma_t^2)/(\sigma_r^2 + \sigma_t^2)$.

Several of the values of σ_r and σ_t in Figure 9 lead to coefficients of correlation approaching 0.5. In view of this, it is clear that the adjustment of photogrammetric observations in the process of analytical aerotriangulation should admit the possibility of correlated x,y coordinates, as is done in our general theory (Brown, 1958; Brown, Davis, Johnson, 1964). The covariance matrices required for the adjustment can be computed by means of equation (97) in which σ_r and σ_t are defined by the polynomial expressions given in Figure 9.

The weighting functions generated from an analysis of SMAC residuals constitutes a most important by-product of the calibration of a given camera. We believe that in the future, the determination of such weighting functions should be required as one of the standard outputs of the process of calibration.

3.2.8 Stellar SMAC Calibration of KC-6A No. 006 and No. 008.

One of the objectives of the testing program was to compare the results obtained from an operational aerial calibration with those obtained from a stellar calibration. Because of delays encountered at Wright-Patterson Air Force Base in the design and fabrication of a suitable plate back for the camera, the stellar shots were not made until August 1967, or about five months after the completion of the aerial tests.

For the stellar photographs it was necessary to employ 12 by 12 inch plates in order to accommodate the three pads that define the focal plane of the camera. Kodak microflat plates (6 mm thick) coated with 103-F Spectroscopic emulsion were used for the photographic recording.

In conventional stellar calibrations of a camera, great pains must be taken to insure absolute stability of the camera throughout the period of recording. In addition, each exposure must be precisely timed in order to account for the rotation of the earth between exposures.

With cameras having the fairly small aperture typical of aerial mapping cameras, one usually has to make periodic exposures over a period of an hour or so in order to obtain the number (200-300) and distribution of stellar images needed for a comprehensive calibration. Unfortunately, ones success in maintaining stability and precise timing is not ordinarily known until after the reduction has been completed. When inconsistencies are then found to result from deficiencies in stability or timing, the test will usually have to be repeated. Because of such demanding requirements, conventional stellar calibration of mapping cameras has been too expensive for general application. Although expense was not a serious factor in the calibration of the KC-6A cameras, their limited availability made the execution of a conventional stellar calibration too risky to consider in view of the alternative afforded by a stellar SMAC calibration. Inasmuch as each stellar exposure can be regarded as a separate frame, a stellar SMAC calibration imposes no requirements for stability. Indeed, if desired, the camera could be deliberately reoriented between exposures. Likewise, stellar SMAC imposes no requirements for the precise timing of stellar exposures. This is because an error in the assigned time of an exposure is projectively equivalent to an error in the instantaneous right ascension of the camera axis. Accordingly, the angular elements of orientation for a given frame can fully accommodate timing errors. Indeed, were it not necessary to correct for the effects of atmospheric refraction, one could forego all need for timing of exposures. As it is, one must know the approximate zenith distance of each star at the instant of exposure in order to correct for refraction. Since an accuracy of 0?5 is altogether adequate for this purpose, it is more than sufficient if times of exposures are known to an accuracy of one minute. Accordingly, a good wristwatch is an adequate chronometer for a stellar SMAC calibration. Because timing requirements are so coarse, the special, electrically timed foreshutter needed in a conventional stellar calibration can be replaced in a SMAC calibration with a hand-operated piece of darkened cardboard. Because stability is of no concern, a SMAC calibration demands nothing in the way of special facilities such as massive concrete pedestals enclosed in observing domes. Thus, a stellar SMAC calibration not only has the advantage of rendering the results totally immune to deficiencies in stability and timing, but it also vastly expedites and simplifies the field operation.

Zenithal stellar plates were obtained from cameras 006 and 008. (Camera 005 was unavailable at the time.) Stellar exposures were made at ten minute intervals over a period of 50 minutes. About 80 star trails were selected for measurement on the plate from C06 and about 70 from 008. Up to 6 images were measured on each selected trail, leading to totals of 436 measured images for 006 and 385 measured images for 008. The calibrated values of the interior projective parameters resulting from the various SMAC reductions are given in Table 6 and the calibrated distortion functions are plotted in Figure 10. For future reference, Table 6 also includes corresponding results from a laboratory calibration performed by Fairchild.

In comparing the results of the stellar calibration for 006 with the results of the aerial calibration we find:

(1) the calibrated principal distance from stellar SMAC is about 30 microns shorter than that from aerial SMAC;

(2) x_p and y_p from stellar SMAC are much smaller than the values from aerial SMAC;

(3) the radial distortion curve from stellar SMAC is in excellent agreement with the mean of the two aerial SMAC curves;

(4) the profile function of decentering distortion is not in good agreement with the corresponding profile functions from aerial SMAC.

We believe that (1) can be considered a measure of the actual physical change resulting from the orientation of the camera which was pointed downward for the aerial SMAC exposure and upward for the stellar SMAC exposures. The sign of the difference between the principal distances agrees with what one would expect from the influence of gravity on the position of the lens relative to the focal plane.

The fact that x_p, y_p from stellar SMAC fails to confirm the large values resulting from aerial SMAC lends confirmation to the hypothesis that the latter are compromised (most likely) by errors of synchronization.

While the excellent agreement between the radial distortion curves is assuring, this is offset by the rather poor agreement between decentering profiles which is too great to be accidental. We suspect that an actual change in decentering of the lens elements may well have accompanied the opposing changes in orientation. If this should indeed prove to be the case, the validity of the stellar method for the calibration of mapping cameras would be significantly compromised.

TABLE 6. Elements of Interior Orientation of KC-6A Cameras Resulting from Different Calibrations

Type of Calibration	Parameter	CAMERA		
		005	006	008
Aerial SMAC (Test No. 1)	x_p (mm)	.167±.004	.231±.003	-
	y_p (mm)	-.045±.004	.104±.003	-
	c (mm)	152.539±.002	151.231±.002	-
Aerial SMAC (Test No. 2)	x_p (mm)	-	.222±.004	.175±.003
	y_p (mm)	-	.099±.004	-.052±.003
	c (mm)	-	151.227±.002	154.626±.002
Stellar SMAC	x_p (mm)	-	-.035±.002	-.033±.003
	y_p (mm)	-	-.017±.002	.000±.003
	c (mm)	-	151.200±.001	154.582±.002
*Laboratory (Fairchild multicollimator)	x_p (mm)	-.011	.015	-.009
	y_p (mm)	.020	-.013	.014
	c (mm)	152.565	151.220	154.626

*Standard deviations of laboratory results are not given in calibration certificate.

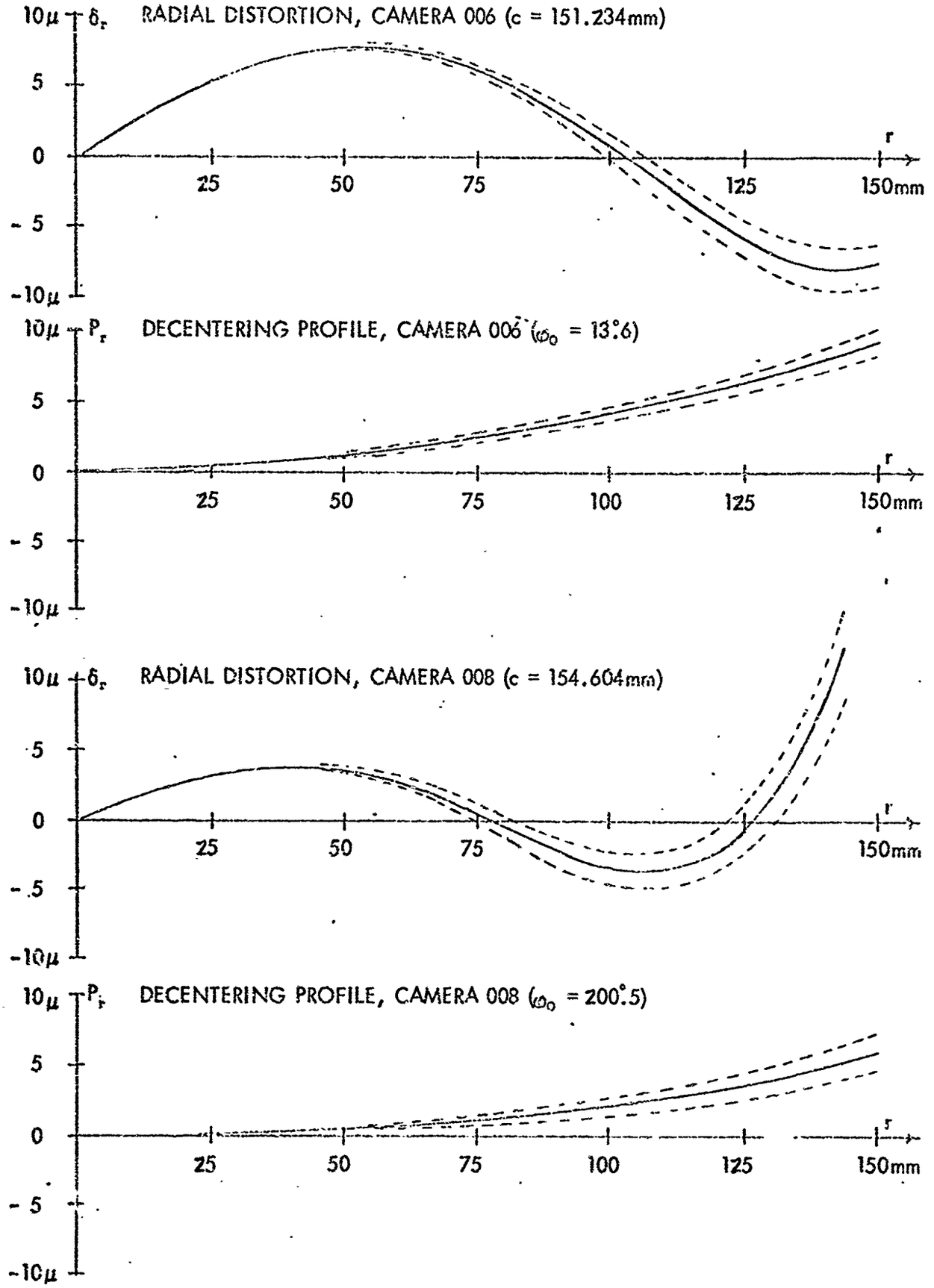

Figure 10. Radial distortion curves and decentering profiles resulting from Stellar SMAC calibrations of Cameras 006 and 008 (accompanied by one sigma error bounds).

A possible way around this difficulty would be to use an optically flat mirror or large pool of mercury to permit exposures about the zenith to be made with the camera pointed downwards. We would recommend that a future investigation be undertaken along such lines in order to establish the precise influence of the orientation of the camera on the interior projective parameters.

The agreement between the stellar SMAC calibration of radial distortion for 008 (Figure 10) and the aerial SMAC calibration (Appendix B) is not as good as that between the corresponding calibrations for 006. This could well be attributable to the effects of curvature of the surface of the photographic plate, a topic taken up below.

3.2.9 Analyses of Stellar SMAC Residuals

The residual vectors resulting from the stellar SMAC calibrations of cameras 006 and 008 are plotted in Figures 11 and 12. A grid having special vectors associated with each intersection has been superimposed on each figure. These are for future consideration and are to be ignored for the time being. In both figures, those images on common star trails are joined by straight lines.

Even a casual examination of the residual vectors in Figures 11 and 12 reveals the presence of pronounced systematic tendencies (especially so in Figure 12). The rms errors of the residual vectors of 3.5 and 4.4 microns respectively are unduly large for a stellar calibration. When the residual vectors are analyzed in terms of radial and tangential components, we find the radial components to have rms values of 3.0 and 4.0 microns, respectively, and the tangential components to have rms values of 1.8 and 1.9 microns. This immediately suggests that departures of the photographic surface from a true plane might be at the root of the difficulty. However, the specifications for Kodak microflat glass plates states: "the front surface of microflat glass, on which the emulsion is coated, does not depart by more than 0.00002 inch per linear inch from a true plane." This would permit a departure from flatness of, at most, about ± 3 microns across the diagonal of the 9 x 9 inch format, which is not nearly enough to account for the observed effect. In looking more deeply into the matter, it occurred to us that the above specification actually applies to uncoated plates. This consideration brought to our recollection an article in the Astronomical Journal on the subject of the effects on flatness of the photographic emulsion. Upon searching, we

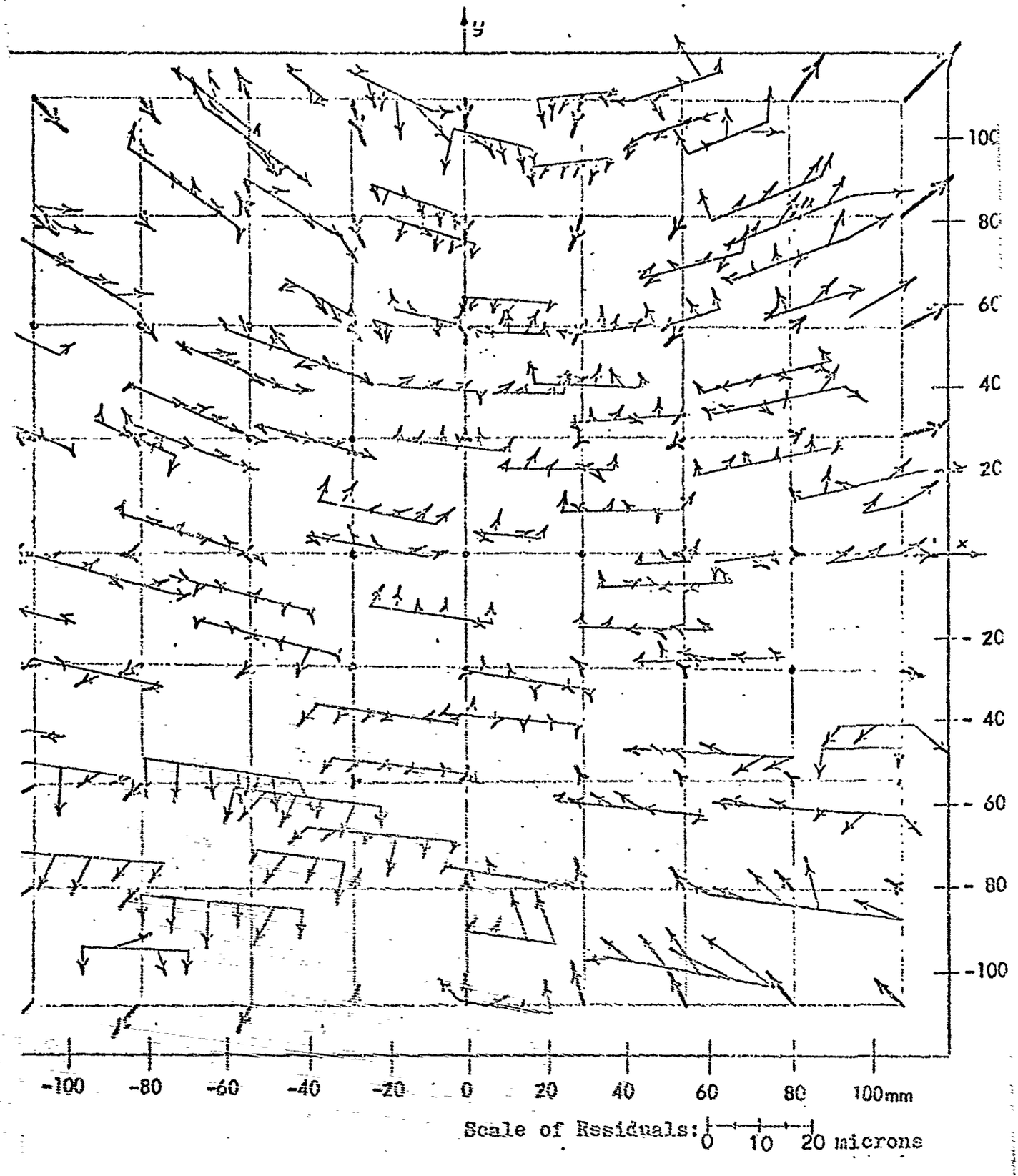

Figure 11. Residual vectors from Stellar SMAC calibration of Camera 006 (rms value of residuals = 3.5 microns).

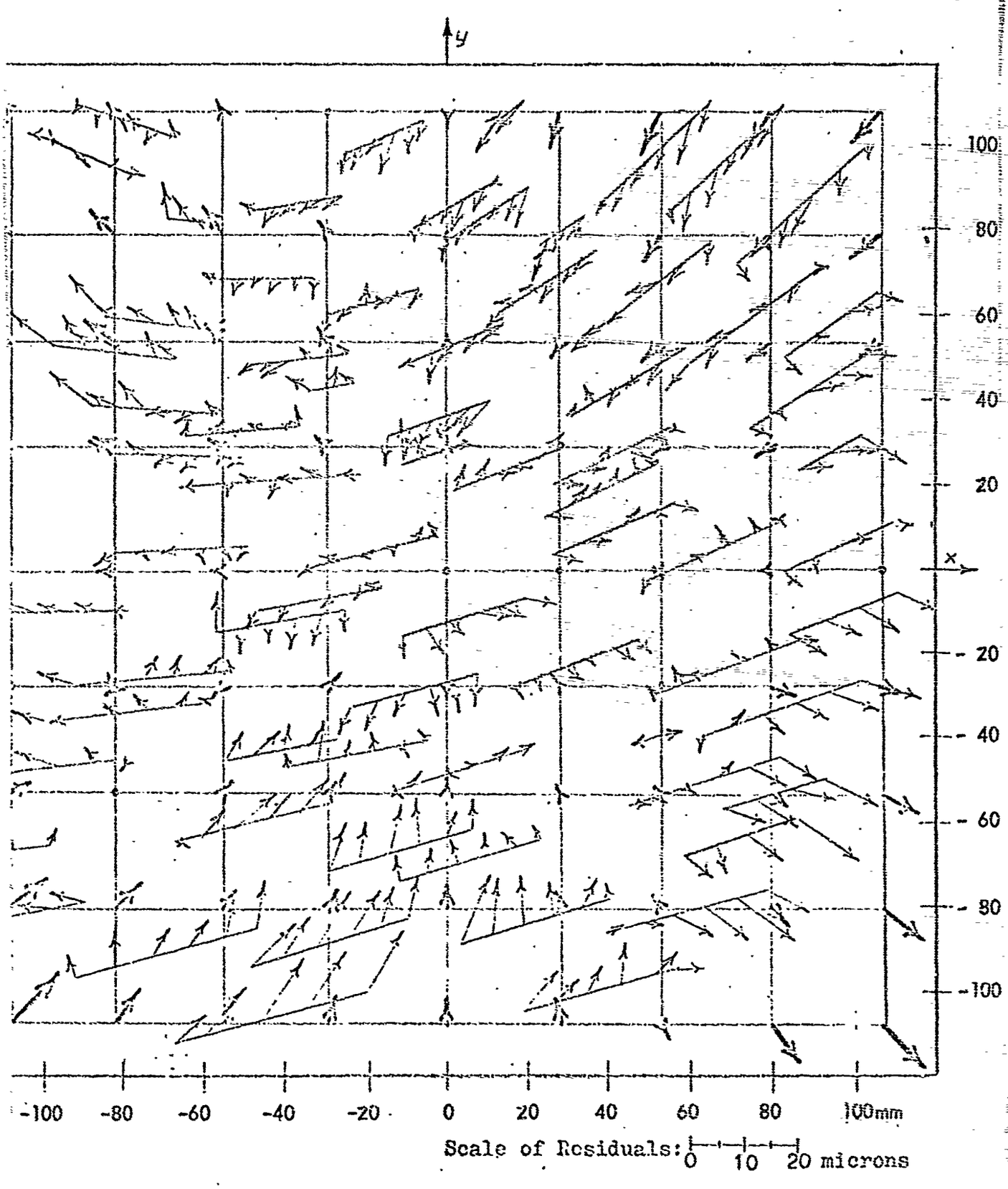

Figure 12. Residual vectors from Stellar SMAC calibration of Camera 008 (rms value of residuals = 4.6 microns).

found the desired article. It was in the 1942 Volume of the Journal and was entitled, "The Concavity of Photographic Plates", by Professor Frank Schlesinger of Yale University Observatory. Because of its pertinence and brevity, we quote it here in full:

> "The writer has several times stated that the shrinking of the gelatine in drying caused photographic plates to be concave on the coated side. Doubts of the correctness of this statement having been expressed, the matter now has been definitely tested by measuring the curvature of the identical plates before and after they had been coated. This was done by means of the simple spherometer described in the introduction to Volume 9 of the Yale Observatory Transactions. The plates, 76 in number, are of plate glass: they are 43 cm square by 5 or 6 mm thick. In every case they were found to be more concave on the coated side than they were before coating. The change varied from 0.004 mm to 0.110 mm, the average being 0.046 mm."
>
> "This concavity would give rise to an appreciable error in star positions near the edges of the plates if we did not flatten out the plates when they were being exposed."
>
> "While this experiment proves that the shrinking of the gelatine on plate-glass causes their concavity, the conclusion does not necessarily apply to ordinary glass. However, by measuring 14 such plates in the 16.5 by 2.15 cm size, about 1.6 mm thick, we found that they were concave on the coated side by an average of 0.023 mm. Allowing for the difference in size and thickness between the plate-glass and these plates, it looks as though the concavity in the latter case were likewise due to the contraction of the gelatine."
>
> "I am indebted to Mr. HOLLANDER for making the necessary measurement."

In view of Professor Schlesinger's findings, we deemed it advisable to investigate the matter of the flatness of the actual plates used in the stellar SMAC reductions. On the glass side of each plate, we established a grid array of 25 points evenly spaced over the 9 x 9 inch area corresponding to the photographic format. The plate was then placed, glass side down, on a Brown and Sharpe 24" x 30" granite surfcce plate accurate to ± 0.6 microns. A Brown and Sharpe dial indicator was employed to measure relative spot elevations of the points on the emulsion corresponding to the grid. The measurements were recorded to the nearest micron (or, more precisely, to the nearest .00005 incn), with double settings being made on each point, but not in succession.

The rms of the means of the settings was found to be 1.5 microns. A best fitting least squares plane was established from the measurements. The departures of the spot elevations from the best fitting plane were found to be entirely regular and were used to generate horizontal and vertical profiles which, in turn, were used to generate contour maps. The contour maps of the surfaces of the two plates relative to best fitting planes are presented in Figures 13a and 13b.

We note from the contour maps that the surfaces are not concave, as reported by Schlesinger, but rather are roughly saddle shaped. In addition, we see that the gradients of the surfaces in certain areas become up to ten times greater than that allowed by the specifications for micro flat glass. From this we may conclude that either the plates are significantly deformed by the stresses induced by the drying of the photographic emulsion, or else the thickness of the emulsion itself is far from uniform. To check the latter, we carefully scaped away a small patch of emulsion in the vicinity of each grid point and then took supplementary spot readings to ascertain the thickness of the emulsion. We found the variation in thickness to be negligible, thus confirming that it is the plate itself that is deformed.

Going a step further, we derived spot elevations Δz from the contour maps for 81 points evenly spaced over the format. For each point we then computed

$$\delta r = \frac{r}{c} \Delta z \tag{98}$$

in which r is the radial distance to the point and c is the focal length of the camera. The quantity δr defines the contribution to the radial residual to be expected from departure of the photographic surface from the best fitting plane. The resulting radial vectors at the grid intersections are superimposed on the residual plots of Figures 11 and 12. In Figure 11 the correlation between the radial vectors on the grid and the systematic components of the SMAC residuals is seen to be remarkably good and, in our view, is clearly too strong to be accidental. The correlation between the two sets of vectors in Figure 12, though not quite as pronounced as in Figure 11, is nonetheless strong.

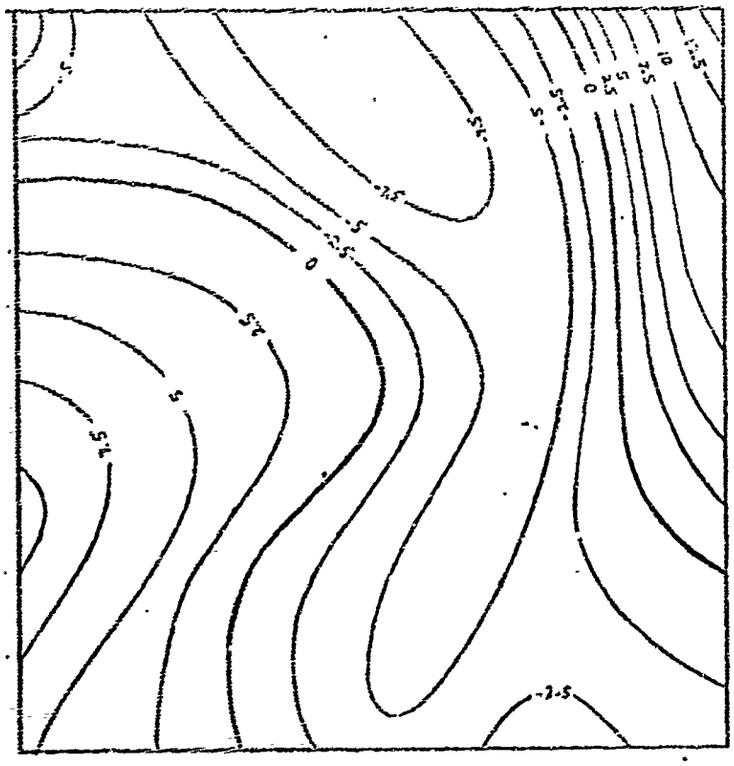

Figure 13a. Isocontours of plate used in Camera 006.

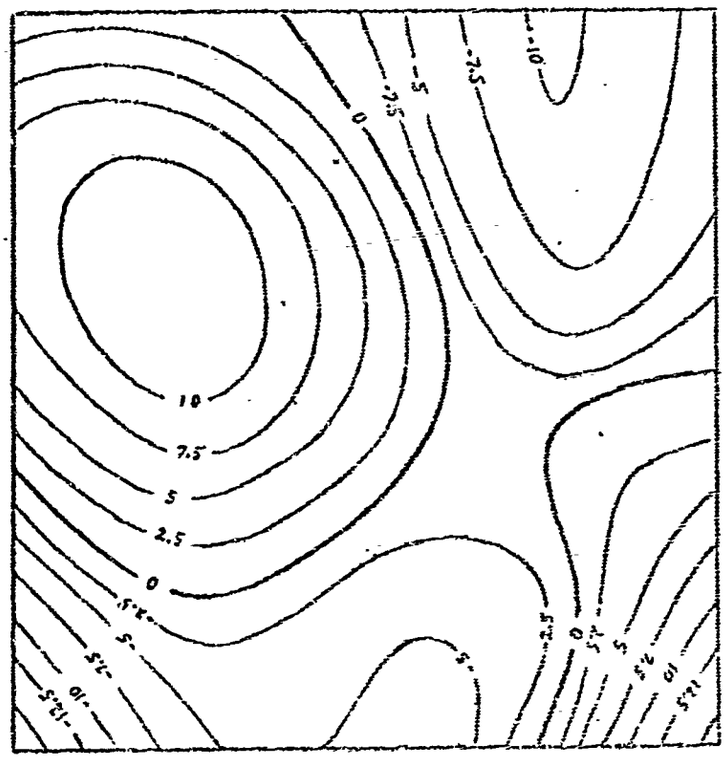

Figure 13b. Isocontours of plate used in Camera 008.

Figure 13. Isocontours of departures from flatness of surface of emulsion of plates used for Stellar SMAC calibrations of Cameras 006 and 008 (contour interval = 2.5 microns).

In both cases, but particularly in Figure 12, the correlation in direction is more pronounced than the correlation in magnitude. For the most part, the magnitudes of the grid residuals tend to be somewhat smaller than those of their counterparts from the SMAC reductions. This suggests that the deformation of the plate following photographic processing may actually be somewhat less severe than that of the undeveloped plate (quite possibly, stresses in the emulsion become partially relieved as a result of processing). We recommend that this matter be taken up in future investigations. With the aid of air gauging techniques it should be possible to work out a practical scheme for measuring the surface of undeveloped plates in total darkness.

Even though modern emulsions are likely to be appreciably thinner than those employed in Schlesinger's day, our results suggest that his findings continue to have pertinence. Even with 6mm thick plates, one is not assured that the flatness prior to coating will be maintained after coating. While the departures from flatness that we have observed are admittedly small by customary standards (rms values of 6.2 and 7.8 microns for the two plates measured), they are, as we have seen, enough to contaminate our results to a significant degree. A brute force solution to the problem would lie in the use of extra thick plates (perhaps a centimeter or more). Alternatively, satisfactory results might be obtainable if the plates were coated on both sides in order to balance the contractive stresses of the emulsion. Still another solution, although an operationally awkward one, would consist of employing a plate flattener prior to exposure, as was practiced by Schlesinger. Such a procedure has also been described by Carman (1968). Finally, if it were established that the free state figure of the plate is not significantly disturbed when it is pressed against the focal reference, one could measure the surface of the exposed plate before development to generate appropriate corrections to be applied prior to the adjustment. Once perfected, such a procedure would not necessarily be excessively burdensome.

For future investigations of the stellar SMAC calibration of wide angle mapping cameras we recommend that plates be abandoned altogether. Even if perfectly flat, they constitute an unnatural intrusion into the system. Better would be the use of thick based (preferably, 7mil) polyester film in conjunction with the actual magazine and platten associated with the camera.

If a total of 20 or more frames (in the usual sense of the word), each containing about 50 usable images, were measured, the final results would not be compromised by the vagaries of any one frame (a distinct drawback to conventional calibrations employing film). Exposures could be made with the camera pointed upward, as is customarily done in stellar calibrations, and with the camera pointed downward (using the mirror method alluded to earlier). Separate SMAC reductions performed on the two sets would establish, in a definitive manner, the influence of extremes of gravity on the metric properties of the camera. Fresh comparisons should also be made with aerial SMAC calibrations, preferably based on photography taken over the newly established Casa Grande Range. Finally, a future program should also consider SMAC calibrations based on the reduction of a moderate number of frames (again, at least 20) of a standard bank of collimators (the application of SMAC to laboratory calibrations will be taken up later). From the large sets of residuals generated by each of the various calibrations, empirical weighting functions could be generated and compared, as could empirical corrections for residual systematic errors. Such an exercise would determine the relative merits of the different approaches and would help to establish the confidence to be accorded the various empirical functions derived from the residuals. In Section 4 specific recommendations are made for future studies.

3.2.10 Comparisons with Laboratory Calibrations

All three cameras subjected to the Aerial SMAC calibration had previously been calibrated by Fairchild on a multicollimator bank. This provided an opportunity for further intercomparison of results from the different methods of calibration. In Figure 14 we have plotted the radial distortion curves produced by Fairchild and the corresponding curves resulting from Aerial SMAC calibrations. The signs of the original Fairchild curves have been reversed to make the corrections conform to our sign convention. Each Fairchild curve represents the average of the four curves generated by the four semi-diagonals of the format, and each curve is accompanied by an upper and lower envelope. The envelopes define boundaries that enclose all four individual distortion curves and thus provide a measure of dispersion.

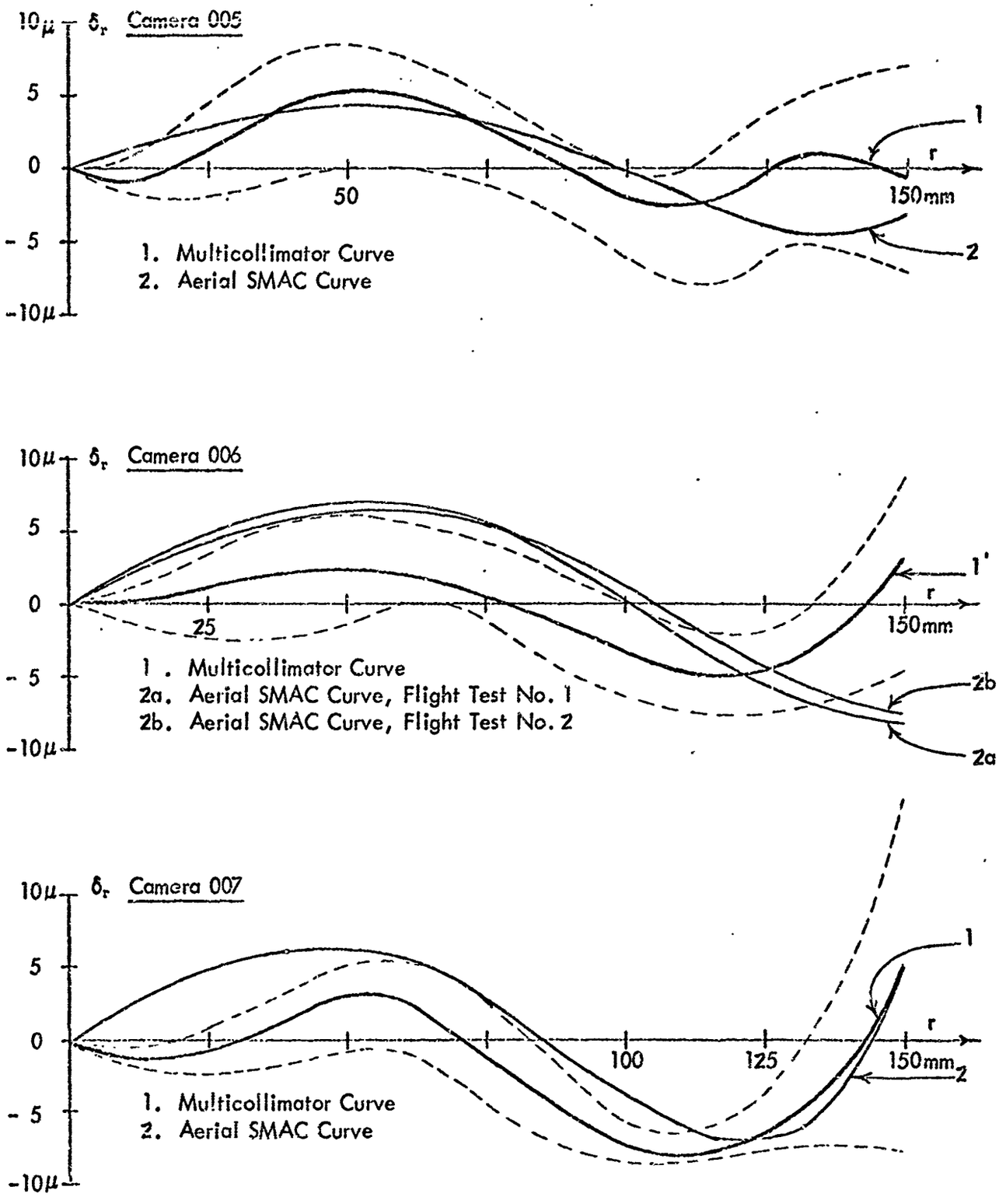

Figure 14. Comparison of Aerial SMAC radial distortion curves with Fairchild Multicollimator curves (broken curves represent envelopes enclosing individual multicollimator curves along different semi-diagonals).

The Aerial SMAC curve for camera 005 is in generally good agreement with the Fairchild curve and lies entirely within the Fairchild envelopes. The rms departure between the two curves is 2.4 microns, and maximum departure is about 5 microns.

The Aerial SMAC curves for cameras 006 and 008 lie, for the most part, outside the Fairchild envelopes. Their rms departures from the Fairchild curves are 4.6 and 3.3 microns, respectively, and their maximum departures are 10.5 and 5.5 microns. While such agreement is not especially good, neither is it particularly poor by normal standards of camera calibration. It is altogether likely that the Fairchild calibrations were compromised, as were our stellar calibrations, by unflatness of the photographic plates employed (the plates used by Fairchild were of the same type as those used in our stellar calibrations).

The values of the elements of interior orientation resulting from the various methods of calibration are listed in Table 6. If corrections for gravity of 30 microns are applied to the principal distances resulting from Stellar SMAC, the departures of the various calibrated principal distances for cameras 006 and 008 all become within 10 microns of the mean. The departures for camera 005 are within 13 microns of the mean. Such agreement is consistent with the accuracies generally attributed to laboratory calibrations.

For reasons discussed earlier, the results from Aerial SMAC for principal point are partially suspect and require investigation to establish their precise significance. The results from Stellar SMAC and Fairchild for principal point of cameras 006 and 008 agree to within 50 microns and 22 microns, respectively for x_p and to within 14 microns for y_p. Except for the 50 micron discrepancy, this agreement is within the range to be expected from the accuracies of the laboratory method. Here again, lack of flatness of the plates may have influenced the results.

3.2.11 General Conclusions Regarding KC-6A Calibrations

The application of SMAC to the calibration of KC-6A cameras has not only demonstrated the feasibility of the approach, but also has shown that SMAC can produce a total systems calibration to a degree previously unattainable. Indeed, it has become clear from our results that a more pragmatic view of calibration is in order. The interior projective parameters derived from

a moderate number of frames, are essentially unaffected by transient systematic errors that would be of consequence to a calibration based on any single frame. Projectively unmodeled, persistent systematic errors can assume prominence in the large sample of residuals produced by a SMAC reduction of a moderate number of frames each containing a moderate number of images. Thus empirical modeling of residual systematic error can emerge as a practical refinement of the SMAC calibration. So too, can the derivation of radial and tangential weighting functions. In view of this expanded scope of the process of calibration, one should not strive to suppress certain sources of systematic error as is customarily done. Quite the contrary, one should deliberately exercise sources of persistent, unknown systematic error in order that their influence may be revealed. For this reason, we now appreciate that in the calibration of mapping cameras, plates should not be substituted for film. The magazine and film platen are integral parts of the mapping camera and their contribution to systematic errors should not be, and need not be, slighted. Similarly, if empirical weighting functions are to have validity for general operational applications, they must be derived from observational material appropriate to such applications. Thus if a camera does not employ a reseau, corrections for film deformation for that particular camera should be limited to what can be obtained from measurements of fiducial marks. Calibration should be as consistent as possible with operation.

We shall postpone making specific recommendations for future lines of investigation into the metric properties of the KC-6A cameras until after we have explored still other applications of SMAC.

3.3 Application of SMAC to Calibration of Lunar Orbiter Cameras

3.3.1 Background

Having reviewed applications of SMAC to aerial and stellar calibrations, we shall now direct our attention to the application of SMAC to laboratory calibrations of three, high resolution Lunar Orbiter Cameras. These cameras have focal lengths of 24 inches and subtend 5° x 20° formats on 70 mm film. The calibrations were performed at Cape Kennedy for Boeing Company, NASA's prime contractor for the Lunar Orbiter Project. A key requirement of the calibration was that the operational environment of the camera had to be simulated. This meant that the camera had to be operated from within its space capsule which, in turn, had to be placed in a vacuum chamber. These constraints ruled out any conventional approach to calibration (e.g., goniometer or standard collimator bank). Although the vacuum chamber itself was fairly small and had a high quality optical window, it was not permissible to remove the chamber from the clean room at Cape Kennedy. This ruled out the possibility of a stellar calibration. Moreover, less than a month was available from the approval by NASA to proceed and the cutoff date dictated by the launch schedule. Only a minimal laboratory set up could therefore be considered. Accordingly, NASA and Boeing decided to settle on a calibration leading primarily to a precise determination of focal length; all other potentially obtainable results were to be considered to be of secondary importance. This guideline led to an experimental set up limited to photographs of a single pair of collimators subtending a precisely known angle of nominally 10° (or about half the horizontal field).

Inasmuch as up to eighteen frames could be allotted to each camera for the calibration, we suggested a SMAC calibration wherein the pair of collimators, mounted on a horizontal rotary table, would be rotated about one half degree between exposures on successive frames so that the pair of collimator images would proceed from one extremity of the horizontal field to opposite extremity. Thus if all frames were superimposed to produce a single composite frame, the eighteen pairs of collimator images would be fairly uniformily distributed across the format with all images very nearly lying on a common straight line passing through the center of the frame in the long

(or x) direction of the format. Clearly, a more desirable distribution would have been one with images arrayed across both diagonals of the format. Unfortunately this could not be considered, in view of the time available, because of the severe physical constraints imposed on the operation.

A computer simulation of the SMAC reduction appropriate to proposed experiment showed that focal length could theoretically be recovered to an accuracy (one sigma) of about 30 microns. Thus, the desired result was potentially attainable. The simulation also showed that coefficients of radial distortion (K_1, K_2) and one of the coordinates (x_p) of the principal point could be recovered to meaningful accuracies. The second coordinate of the principal point y_p was found to be inherently unrecoverable because the distribution of control points produced no variation in the y coordinates of the images. The recovery of decentering distortion could not be effected because it was found to require a minimum of three control points per frame as well as variation in both x and y coordinates. Despite the fact that only a partial calibration could be achieved, the results theoretically obtainable were considered sufficient to warrant implementation of the experiment.

3.3.2 Results

The experiment was successfully executed and the results turned out to be consistent with expectations. They are reported in detail in Brown (1967a). Table 8 and Figure 15 below are reproduced from this reference. Our concern here is not so much with results themselves as with the implications of the results to laboratory calibrations.

Although a pair of collimators was used for the calibration, the reduction appropriate to the experiment was, in fact, a Stellar SMAC reduction. The pivotal consideration is that a pair of collimators may be viewed as a pair of artificial stars subtending a known angle α^*. One is therefore at liberty to assign one collimator coordinates in right ascension and declination of (0,0) and the second collimator coordinates (α^*,0). Equally admissible, in fact, would be assignment of any arbitrary pair of stellar coordinates (α_1, δ_1), (α_2,δ_2) satisfying the relation

$$\cos \alpha^* = \sin \delta_1 \sin \delta_2 + \cos \delta_1 \cos \delta_2 \cos (\alpha_1 - \alpha_2).$$

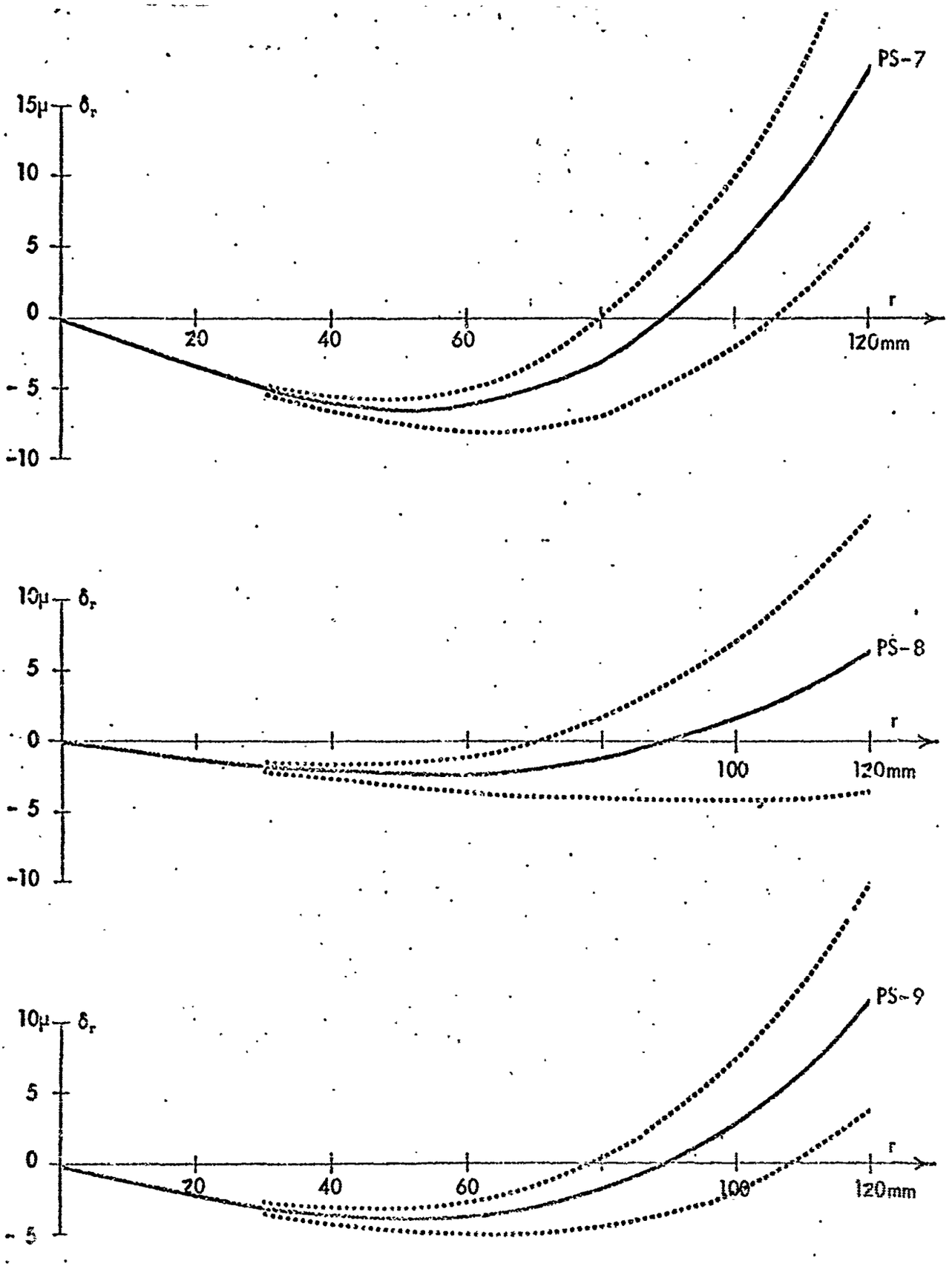

Figure 15. Distortion curves and one sigma error bounds of radial distortion curves produced by dual collimator SMAC calibration of Lunar Orbiter Cameras.

Table 8. Results of dual collimator SMAC calibration of Lunar Orbiter Cameras.

QUANTITY	PS-7 .9990011	PS-8	PS-9
1. Gaussian Focal Length: c	608.816 ± .030mm	610.812 ± .027mm	609.374 ± .022mm
2. Horizontal Coord. of Principal Pt.: x_p	.867 ± .100mm	1.547 ± .090mm	1.705 ± .074mm
3. Gaussian Third Order Coefficient of Radial Distortion: K_1 ($\delta_r = K_1 r^3$, δ_r = distortion in meters r = radial distance in meters)	.0231 ± .0063m^{-2}	.0082 ± .0056m^{-2}	.0141 ± .0047m^{-2}
4. Calibrated Focal Length: c' (adjusted to make distortion zero at r = 90mm)	608.702 ± .030mm	610.771 ± .027mm	609.305 ± .022mm
5. Transformed Coefficients of Balanced Distortion Curve: K_0'	- .000187	- .000067	- .000114
K_1' ($\delta_r' = K_0' r + K_1' r^3$)	.0231 ± .0063m^{-2}	.0082 ± .0056m^{-2}	.0141 ± .0047m^{-2}
6. Balanced Distortion at r = 0 mm	0.0 ± 0.00 microns	0.0 ± 0.00 microns	0.0 ± 0.00 microns
10	-1.9 ± 0.01	-0.7 ± 0.01	-1.1 ± 0.00
20	-3.6 ± 0.05	-1.3 ± 0.04	-2.2 ± 0.04
30	-5.0 ± 0.17	-1.8 ± 0.15	-3.0 ± 0.13
40	-6.0 ± 0.41	-2.1 ± 0.36	-3.7 ± 0.30
50	-6.5 ± 0.79	-2.3 ± 0.70	-3.9 ± 0.58
60	-6.3 ± 1.37	-2.2 ± 1.21	-3.8 ± 1.01
70	-5.2 ± 2.17	-1.8 ± 1.92	-3.2 ± 1.60
80	-3.2 ± 3.24	-1.1 ± 2.89	-1.9 ± 2.39
90	0.0 ± 4.62	0.0 ± 4.08	0.0 ± 3.41
100	4.4 ± 6.32	1.6 ± 5.60	2.7 ± 4.67
110	10.2 ± 8.42	3.6 ± 7.44	6.2 ± 6.21
120	17.5 ± 10.93	6.2 ± 9.67	10.7 ± 8.06

Now, although in the experiment itself the pair of collimators was actually rotated slightly from one exposure to the next, one could equally well regard the collimators as remaining fixed and the camera as having undergone the rotation. Under this interpretation, the Stellar SMAC reduction becomes immediately and directly applicable to calibrations based on a series of photographs of two or more collimators.

Considering the skimpiness of the observational material, the results produced by SMAC for the Lunar Orbiter Cameras are indeed impressive. It should be appreciated that on any given frame the observations consisted of merely the plate coordinates (x,y) of each of a pair of artificial stars (i.e., the collimator images). These coordinates give rise to four observational equations from the i^{th} frame involving

a) the determinable parameters of the inner cone, namely:

   (i) c, the principal distance;
   (ii) x_p, the horizontal component of the principal point;
   (iii) K_1, K_2, coefficients of radial distortion;

b) the angular elements of orientation for the frame: α_i, ω_i, κ_i.

Consistent with the SMAC concept, the parameters under group (a) are considered to be common to all frames, whereas those under group (b) are considered to vary from frame to frame inasmuch as the orientation of the camera in the 'stellar' coordinate system is altered between exposures. Hence, three of the four available equations from a given frame are, in effect, used up in establishing the angular elements of orientation peculiar to that frame; this leaves only one redundant observation per frame to be applied to the recovery of the parameters of the inner cone that are common to all frames. All told, the eighteen available frames generate a total of $4 \times 18 = 72$ observational equations involving a total of 57 or 58 unknowns consisting of $3 \times 18 = 54$ angular elements of orientation (three per frame) plus 3 or 4 parameters of the inner cone depending on whether one or two coefficients are needed for the radial distortion function. Inasmuch as a single coefficient turned out to be sufficient, the simultaneous adjustment of all observations generates a general system of normal equations of order 57, involving 14 statistical degrees of freedom. This is hardly a strong adjustment, but it is the best that can be done with the limited observational material and is, as Table 8 and Figure 15 indicate, sufficient to produce useful

results. Although the Lunar Orbiter experiment did not permit the recovery of the y_p or of parameters of decentering distortion, the converse propcsition holds that these unrecoverable parameters of the inner cone can have no effect on the values obtained for the recoverable parameters of the inner cone. Hence, the results of the calibration are in no way contaminated by the enforced values (zero) of the unrecoverable parameters.

3.4 General Application of SMAC to Multicollimator Calibrations

3.4.1 Application to Conventional Collimator Banks

We have seen that the pair of collimators employed in the Lunar Orbiter calibrations was successfully treated in the SMAC reduction as a pair of artificial stars. If follows that a bank of collimators employed in conventional laboratory calibrations may also be regarded as an artificial star field. Accordingly, sets of photographic observations of mu'ticollimators may be directly processed through a Stellar SMAC reduction. In conventional multicollimator calibrations, a time consuming and painstaking process of autocollimation must be performed in order to orient the camera so that the axis of the central collimator is precisely perpendicular to the focal plane. This process can be totally bypassed when a Stellar SMAC reduction is performed; here, it is sufficient merely to position the camera so that its entrance pupil intercepts the converging beams of the collimators. This, in turn, makes it practical to avoid the use of plates (if desired) by exercising the film magazine (or magazines) of the camera in the photography of the collimator bank. Because precise alignment is not required, a large number of frames can be quickly exposed with the camera being rotated about its axis between frames. This procedure would generate a very large number of collimator images having an overall distribution far superior to that obtainable from any one frame. Carried in a SMAC reduction, the measurements of all such images would contribute to a common calibration of the interior projective parameters. The large sample of measuring residuals that could thus be generated would provide the material necessary for sound empirical modeling of residual systematic error and for the derivation of weighting functions appropriate to the camera.

From the foregoing, it is clear that by applying Stellar SMAC to multicollimator calibrations, one can not only greatly simplify set up procedures but, by admitting the use of film and the exercise of several frames at different swing angles, one can also expect to obtain a more meaningful, more accurate and more thorough calibration. Such a calibration could be extended to take into account errors in the directions of the collimators. In principle, it would suffice if the angle subtended by but a single pair of collimators were accurately known; the directions of all other collimators could then be established within the reduction itself.

3.4.2 Implications of SMAC to the Design of New Multicollimators

As we have just seen, SMAC is directly applicable to the reduction of photographs of conventional multicollimators. The first of the modern collimator banks, designed and constructed by the National Bureau of Standards in 1949, incorporates a total of 25 collimators arrayed to span both diagonals of the photographic format. A multicollimator later developed for the U.S. Geological Survey is of similar general design but incorporates almost twice as many (49) collimators. A multicollimator recently developed by the National Research Council in Canada employs a total of 43 collimators evenly spaced at increments of 2.8125 and arrayed across a single diagonal. A multicollimator soon to be developed for the U. S. Air Force will incorporate about 150 collimators.

It is clear from the foregoing that the trend is towards larger and larger collimator banks containing more and more collimators. It is thus also clear that little, if any, consideration has been given to the possibility that a superior calibration could conceivably result from a combination of fewer collimators and a more advanced approach to data reduction. We demonstrated in the Lunar Orbiter calibrations that if decentering distortion is ignored (as indeed it is in conventional multicollimator calibrations) a single pair of collimators is sufficient for the accomplishment of a SMAC calibration. The recovery of decentering distortion requires that a third collimator be added. In principle, then, a minimum of three collimators can provide a full calibration of a camera, provided that a moderately large number of frames is exposed and a good distribution of images is realized. While more than three can provide a superior result, it does not

follow that a single frame containing a large number of collimator images is necessarily to be preferred over several frames each recording a relatively small number of collimator images. Indeed, quite the opposite could be true. We shall consider here how the computational tradeoffs made possible by the SMAC reduction might be exploited in the design of a simplified multicollimator capable of producing superior results. A SMAC multicollimator suitable for the calibration of six inch mapping cameras is shown schematically in Figure 16. The nine collimators in the array are considered to be of a diffraction limited, catadioptric type of moderate (about 10 cm) aperture. As shown in Figure 16a, the axes of the collimators are all horizontal and all are nominally in the same plane. The camera is mounted vertically (i.e., in its normal operating position),and the collimator rays are reflected to the entrance pupil by means of an adjustable, optically flat mirror (Figure 16b). The mirror tilts about a horizontal axis that is nominally perpendicular to the axis of the central collimator. With each tilt of the mirror, the point of intersection of the bundle of collimator rays assumes a different position along the arc PQ (Figure b). A simple linkage between the mirror support and the camera platform can be provided to reposition the camera automatically so that the entrance pupil is always at the proper location and the camera axis is always maintained in a nominally vertical orientation. In a typical calibration , eleven exposures of the multicollimator would be made with the mirror tilted as follows: -18°, -16°, -12°, -8°, -4°, 0, 4°, 8°, 12°, 16°, 18°, in which 0° corresponds to the case in which the mirror is inclined 45° to the horizontal. These angles need not be established with great accuracy. The composite frame for $\kappa = 0°$ would have the appearance indicated in Figure 17a. For higher accuracies, the process could be repeated at different swing angles (e.g., $\kappa = 90°$, 180°, 270°). The overlay of all exposures at $\kappa = 0°$ and $\kappa = 90°$ (Fig. 17b), would generate the pattern of images shown in Figure 17c. In still another mode of operation, one could produce a supplemental radially symmetric distribution of images by holding the camera fixed in its midposition of 0° and altering the swing angle of the camera between exposures. Figure 17d shows the composite pattern of 108 images that would be generated by this procedure if increments of 15° in swing angle were exercised over the range $\kappa = 0$ to $\kappa = 165°$. From these examples it is clear that the suggested SMAC Multicollimator can provide a most satisfactory overall distribution of images from a moderate number of exposures. The addition of two pairs of

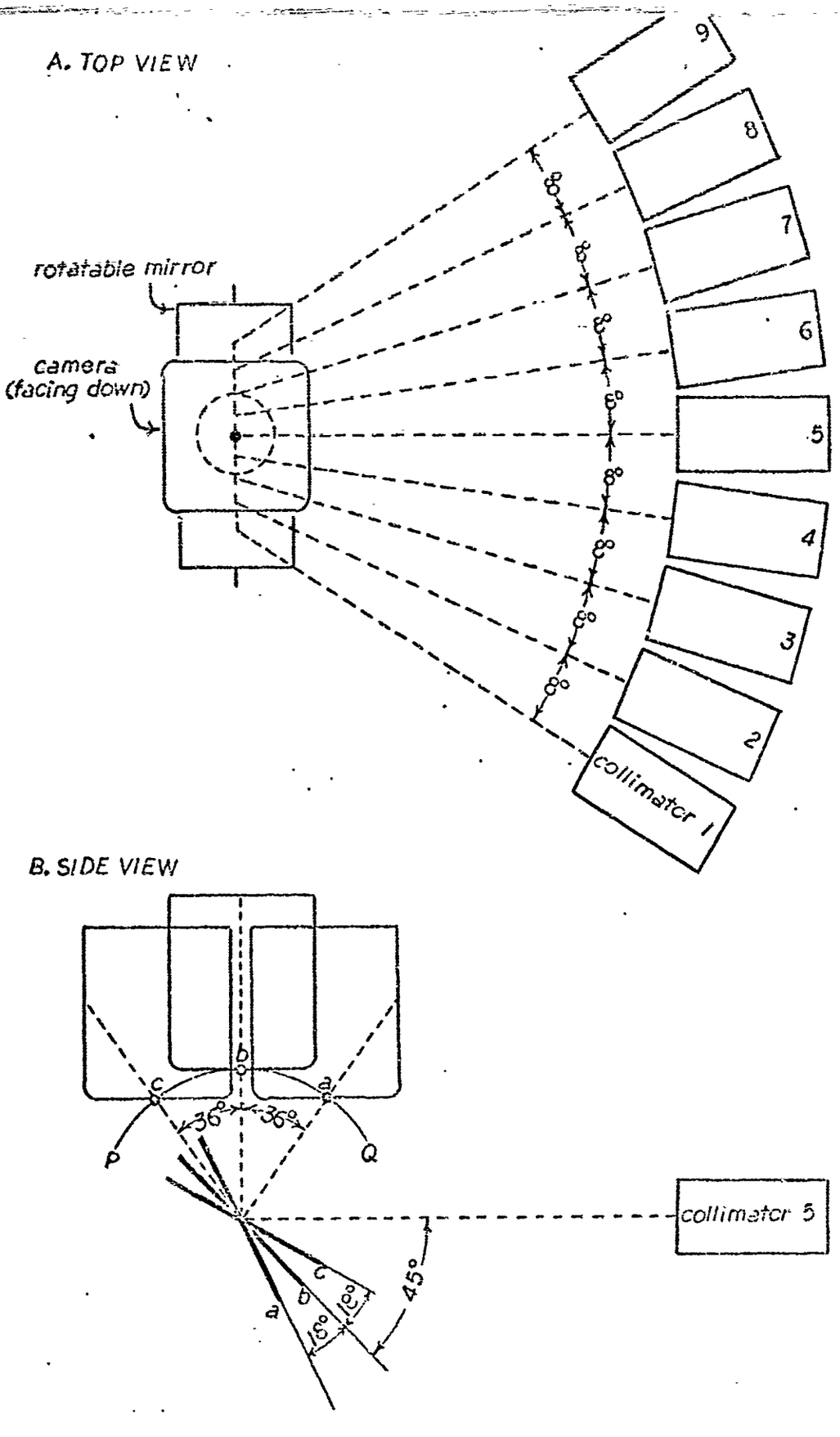

Figure 16. Illustrating concept of SMAC Multicollimator for calibration of mapping cameras.

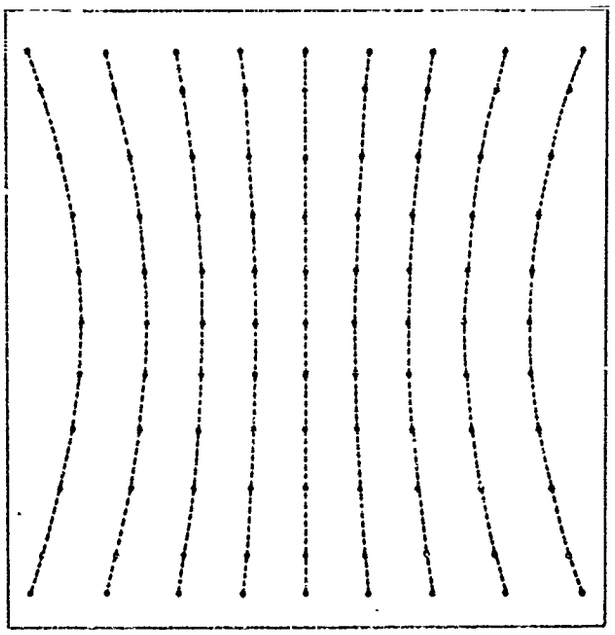

Fig. 17a. $\alpha=0$, $\chi=0$, $\omega=36°, 32°, 24°, 16°, 8°, 0°, -8°, -16°, -24°, -32°, -36°$

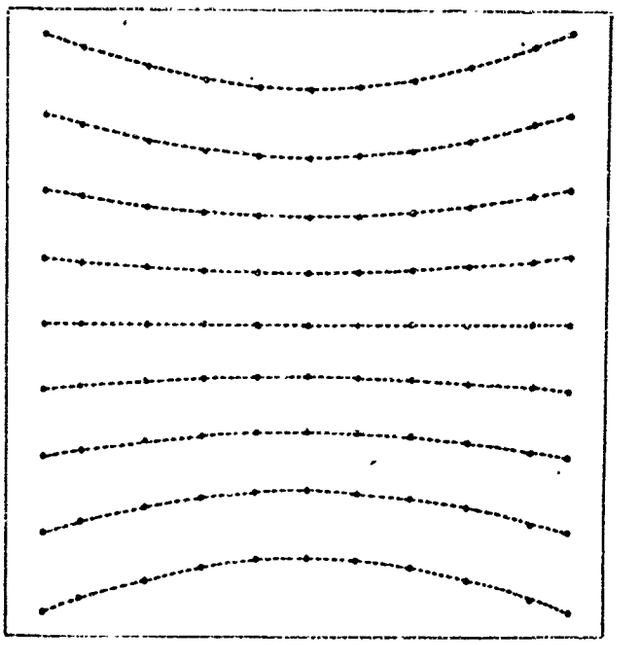

Fig. 17b. Same as Fig. 16a, except $\chi=90°$.

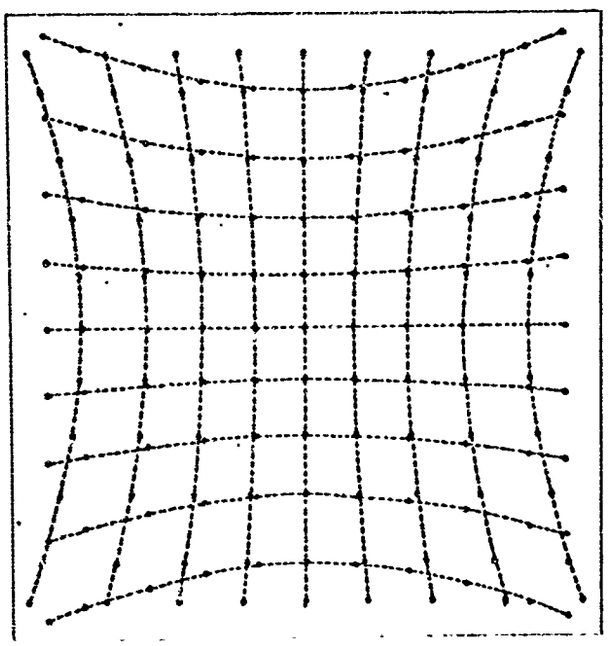

Fig. 17c. Overlay of Figs. 17a and 17b.

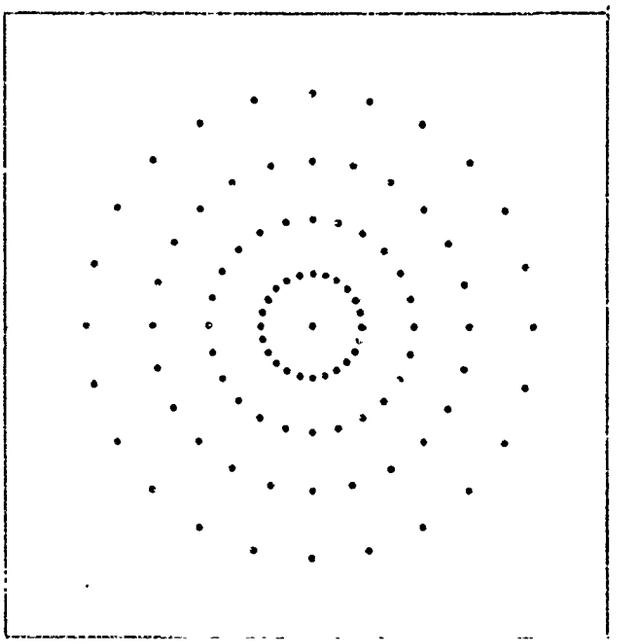

Fig. 17d. $\alpha=0°$, $\omega=0°$, $\chi=0, 15°, 30°, \ldots, 165°$.

Figure 17. Illustrating some of the various patterns of control that can be generated by superimposing exposures of SMAC multicollimator illustrated in Fig. 16.

collimators to the array shown in Figure 16a would make the instrument well suited to the calibration of super wide angle cameras.

Relative to conventional multicollimators subjected to conventional data reduction, a specifically designed SMAC Multicollimator has a number of advantages:

(a) Because of the small number of collimators involved and because of their simple arrangement, the cost of the instrument would be relatively low.

(b) Accordingly, it would be possible to invest appreciably more in collimators of wider aperture and superior optical performance.

(c) The relative simplicity of a SMAC Multicollimator would facilitate maintenance and adjustment of the instrument.

(d) Despite the fact that several exposures must be produced, appreciably less time would be required for data gathering operation because the tedious process of autocollimation is dispensed with.

(e) By virtue of (c) the results of the calibration are in no way compromised by lack of precision in set up procedures (thus the 'point of symmetry', an artifice used to compensate in part for the deficiencies of conventional procedures , has no role in a SMAC Multicollimator calibration).

(f) Also by virtue of (c) it becomes practical, when desired, to use film instead of plates, thereby allowing the camera magazine and platen to influence the results.

(g) As in any SMAC calibration, there is no limit to the number of frames that can be processed in a simultaneous reduction; thus specific schedules of exposures can be tailored to produce specific levels of accuracy.

(h) By exercising a straightforward extension of the SMAC reduction, one could on occasion accurately determine (and thus check) the directions of all collimators relative to the adopted angle between an arbitrary pair of collimators; thus periodic physical monitoring of collimator angles could be limited to measurements of the angle between a selected (preferably widespaced) pair of collimators.

(i) If the two selected collimators were designed to function also as autocollimators, the adjustment of their subtended angle to a desired value θ could be rapidly and accurately accomplished by autocollimation on the faces of a prism subtending an angle of $180° - \theta$. Thus a single calibrated prism could provide the ultimate standard of angular measure for a SMAC Multicollimator.

The concept of the SMAC Multicollimator provides still another example of how hardware can be simplified and improved when sophisticated techniques of data reduction are allowed a major role in establishing design. Previous examples of this approach include the Multilaterative

Plate Measuring Comparator (Brown. 1967c, 1968c) and the Satellite Surveying Utility (Brown, 1968b). Further examples are discussed in Brown 1967b.

3.5 Application of SMAC to Analysis of Ballistic Camera Stability

3.5.1 Introduction

We have already noted that by exercising SMAC in the stellar calibration of cameras, one eliminates all requirements for precise timing of exposures and for physical stability of the camera over the series of exposures. On the other hand, when precise timing of exposures is available, the application of SMAC enables one to determine with great accuracy the physical stability of the camera. Such an application of SMAC has particular merit in ballistic camera operations, for here stability is all important. Accordingly, the evaluation of stability that automatically emerges from the SMAC calibration of a ballistic camera provides information of considerable value.

3.5.2 Example

To illustrate the concept of SMAC analysis of stability, we shall consider the results of an experiment performed on observations made by a PC-1000 camera in December 1966 at Goddard Space Flight Center. Zenithal exposures were recorded with the camera placed on a concrete pad. The exposures were precisely timed and were made at five minute intervals over a period of more than half an hour. In the SMAC reduction, a common set of interior projective parameters (x_p, y_p, c, K_1, K_2, P_1, P_2) was recovered for eight successive exposures, and a separate set of angular elements was recovered for each of the eight exposures. The adopted angular elements consisted of the hour angle and declination (H, δ) of the camera axis and the swing angle κ referred to the line of intersection of the photographic plate and the equatorial plane. Approximately 25 stellar images from each exposure were carried in the SMAC reduction.

Our interest here is not with the interior projective elements resulting from the reduction, but rather with the variation displayed by the angular elements. The variation in each of the angular elements about its mean is indicated in Figure 18. The plotted results for hour angle have

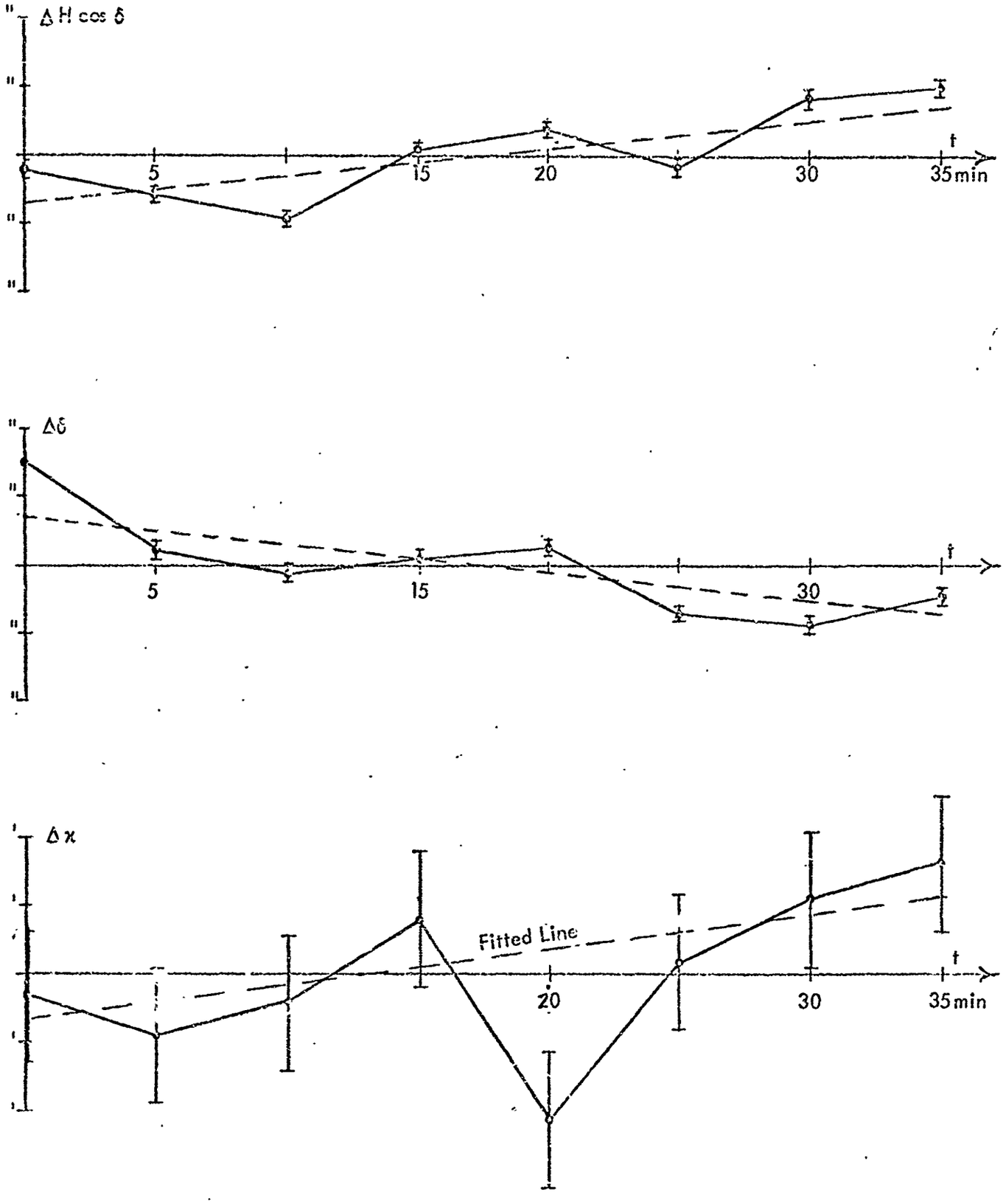

Figure 18. Variation in angular stability of PC-1000 camera over period of 35 minutes as established by Stellar SMAC reduction.

been normalized by the customary process of multiplication by the cosine of declination. Each point is accompanied by a vertical bar defining its plus and minus one sigma confidence intervals. The one sigma values for normalized hour angle and declination are slightly less than 0.2 seconds of arc; for swing angle, they are generally about ten times greater, averaging close to 2 seconds of arc. This disparity in sigmas is attributable to the fact that the focal length (1000 mm) of the PC-1000 is about 10 times greater than the semi-diagonal of the plate format. The projective effect of an error of 0.2 seconds of arc in the direction of the camera axis is equivalent to that of an error of about one micron on the plate. By the same token, the projective effect of an error of 2 seconds of arc in swing angle is equivalent to that of an error of about one micron near the edge of the plate. Thus, there is no actual projective disparity in the relative sigmas of the angular elements.

From Figure 18 we see that several of the variations in orientation differ significantly from zero at the two sigma level. Specifically, these consist of

(a) hour angles at t = 5, 10, 20, 30, and 35 minutes;

(b) declinations at t = 0, 20, 25, 30, and 35 minutes;

(c) swing at t = 20 minutes.

A few extreme excursions in the direction of the camera axis are seen to amount to as much as two seconds of arc in a five minute interval. For the most part, departures about the fitted straight lines in the figures are seen to be appreciably less than the departures about the means. This suggests the existence of slow secular trends upon which are superimposed small, short term changes that occasionally assume significance. With only a few exceptions, moving arc linear functions can accommodate variations over ten minute intervals to accuracies consistent with those of the plotted points.

Many experiments along the above lines would have to be performed in order to establish solid conclusions. The present results indicate that significant, nonabrupt changes in orientation can occur over fairly short periods of time. For this reason, in routine tracking operations the total sequence of exposures should be limited to as short an interval as possible consistent with acquisition

of a sufficient number of control points. A suitable observational schedule for satellite observations is recommended in Brown (1964); it spans a period of just over five minutes and allows each star to generate four sets of punctiform images. It is true that the results of our experiment indicate that camera orientation can vary significantly over a five minute period. However, it is also true that the variation over such a short interval is generally likely to be sufficiently linear to admit the representation of the angular elements as

$$\alpha = \alpha_o + \dot{\alpha}_o (t - t_o) ,$$
$$\omega = \omega_o + \dot{\omega}_o (t - t_o) ,$$
$$\kappa = \kappa_o + \dot{\kappa}_o (t - t_o) ,$$

in which t denotes the time of the exposure, t_o is the mean time of all exposures, and $\dot{\alpha}_o$, $\dot{\omega}_o$, $\dot{\kappa}_o$ are the unknown rates of change of the angular elements about their respective means α_o, ω_o, κ_o. The advanced plate reduction developed in Brown (1964) can readily be extended to incorporare $\dot{\alpha}_o$, $\dot{\omega}_o$, $\dot{\kappa}_o$ as additional parameters to be recovered. Our experience over the past few years indicates that such an extension would be especially worthwhile if accompanied by a statistical testing procedure designed to suppress $\dot{\alpha}_o$, $\dot{\omega}_o$, or $\dot{\kappa}_o$ automatically to zero if it were found to differ insignificantly from zero. In such a reduction, instantaneous orientation matrices generated by the α, ω, and κ's corresponding to times of satellite observations would be used in computing satellite directions.

We believe that instability is, in many instances, the predominant source of error in PC-1000 observations. When virtually perfect stability is maintained throughout the observational period and average atmospheric shimmer is experienced, one can expect the PC-1000 to produce directional accuracies of about 0.6 to 0.7 seconds of arc for individual flashes from a satellite (Brown, 1966). Indications are, however, that this level of accuracy is actually achieved in general operations only with about one plate in three, the others being compromised to a small, but significant degree by instability. The extended reduction discussed above would, in most cases, undo the damage induced by instability and would thus upgrade PC-1000 accuracies. The implementation of such a reduction is therefore to be recommended. In addition, a statistical study of instability by means of SMAC reductions of a large number of plates exposed over extended

periods should be undertaken to establish a clearer understanding of the problem and to generate realistic a priori constraints to be exercised for the angular rates $\dot{\alpha}_o$, $\dot{\omega}_o$, $\dot{\kappa}_o$.

4. CONCLUSIONS AND RECOMMENDATIONS

Our earlier statement concerning the flexibility and universality of the SMAC reduction is well supported by the various examples given in Section 3. We have seen that SMAC is equally applicable to aerial calibrations, to stellar calibrations, and to laboratory calibrations. In a special application to laboratory calibrations, we have seen that SMAC can provide the basis for the design of much simplified, yet possibly more effective, multicollimators.

Because SMAC can be exploited as a common method of reduction for all of the basic approaches to calibration, it provides the logical basis for the intercomparison of different processes. We recommend therefore that further studies be undertaken to determine the precise degree of validity of various approaches to laboratory and stellar calibration by employing comprehensive operational Aerial SMAC calibrations as standards. The limited comparisons made so far suggest that conventional laboratory calibrations of radial distortion can be effectively in error by as much as ten microns near the corners of the format. Some of this error may well be attributable to insufficiently flat plates, some to the small number of available control points (i.e., small relative to the expanded number made possible through a SMAC reduction), some to errors in alignment of the camera, and some to the method of data reduction. We suggest that in future tests laboratory calibrations be performed not only in the usual manner, but also in a manner appropriate to a SMAC reduction. Inasmuch as further flight testing of the USQ-28 System is now being planned, we recommend that one phase of the testing be devoted to a thorough comparative analysis of as many different methods of calibration as is practicable.

Specifically, we recommend that a pair of KC-6A Cameras be subjected to the following testing program:

A. Laboratory Calibrations:

(1) Standard calibrations on at least three different multicollimators (e.g., those at National Bureau of Standards, U. S. Geological Survey and Fairchild).

(2) SMAC calibrations with some multicollimators as (1) using film and a series of exposures on different frames at 15° increments in swing angle from $\kappa = 0°$ to $\kappa = 345°$ (a total of 24 frames per camera).

B. Stellar SMAC Calibrations

(1) Stellar calibration with camera facing upward, using film and the following operational sequence: on the first frame, expose star trails for 60 seconds, close the shutter for 30 seconds, expose stars for one second; advance to next frame, rotate camera 15° in swing angle and repeat same exposures as first frame; continue in this manner at 15° increments in swing angle until a total of 24 frames has been exposed.

(2) Same procedures as above but with camera facing downward into large, optically flat mirror (at least 24" in diameter) or a large, well damped mercury pool.

C. Aerial SMAC Calibrations: Clover leaf flights over McLure or Casa Grande Ranges in accord with following specifications:

(1a) Night flight, illuminated targets, ballistic camera tracking, Shiran tracking, cycling rate of one frame per three seconds, Image Motion Compensation exercised, positive x axis of film always nominally aligned with direction of flight.

(1b) Same as (1a), but performed on a different night.

(2) Same as (1a), but with IMC not exercised.

(3) Same as (1a), but with camera rotated 180° in swing angle between direct and reverse runs on each path.

(4) Daytime flight, no ballistic camera tracking or illuminated targets, but otherwise same as (1a).

On each of these five tests, 24 frames (6 from each flight leg) are to be used in the Aerial SMAC Calibration.

The wealth of material gathered in such a testing program would permit a most thorough evaluation of the various processes of camera calibration. Each of the SMAC calibrations would yield a sufficiently large sample of residuals to permit both the extraction of empirical models for residual systematic error and the determination of empirical weighting functions. The degree of test-to-test consistency obtained for such empirical models and weighting functions would help to establish the degree of confidence to be placed in these concepts.

In all of the above tests involving film, the first ten frames of the roll should be expended immediately prior to the data gathering exposures in accordance with recommendations made by Carman (1968). Carman found that the first few frames on a roll may be subject to excessive film deformation attributable to effects of atmospheric humidity. Normal film deformation should present no problems in the recommended testing program, for it can be thoroughly compensated for by the platen reseau of the KC-6A.

If it could be arranged, we would recommend that still another operational approach to camera calibration be evaluated in conjunction with the above testing program. This approach involves the recovery of radial and decentering distortion parameters within the process of aerotriangulation. An adequate test could be based on a 49 photo block consisting of 7 strips each containing 7 photos with 60% forward overlap and 60% side overlap. A pattern of 25 pass points would be measured on each photo. All absolute control would be withheld, except for the minimum needed for determinacy. As is discussed in Brown (1968a), the normal equations for the simultaneous adjustment of conventional photogrammetric blocks can be made to assume a patterned, banded-bordered form as indicated in Figure 19 . Although the system of normal equations for the proposed experiment would involve the simultaneous recovery of $6 \times 49 = 294$ unknown elements of exterior orientation plus perhaps as many as 6 distortion parameters, its solution can be effected with extraordinary efficiency by means of a special algorithm called Recurrent Partitioning. If it should turn out, as we suspect might well be the case, that a satisfactory camera calibration can be produced as an incidental byproduct of analytical aerotriangulation of a suitably designed block, such a process might ultimately emerge as the method generally to be preferred in aerial photogrammetry. In view of this, we urge that calibration by aerotriangulation be tried and evaluated as part of the recommended testing program.

Our expectation of achieving success with the method just described is based on the fact that over the past six years we have successfully employed a variation of it with plate cameras used for photogrammetric triangulation of points on large structures such as radio telescopes. This application differs from the proposed application to aerial cameras in that (a) highly

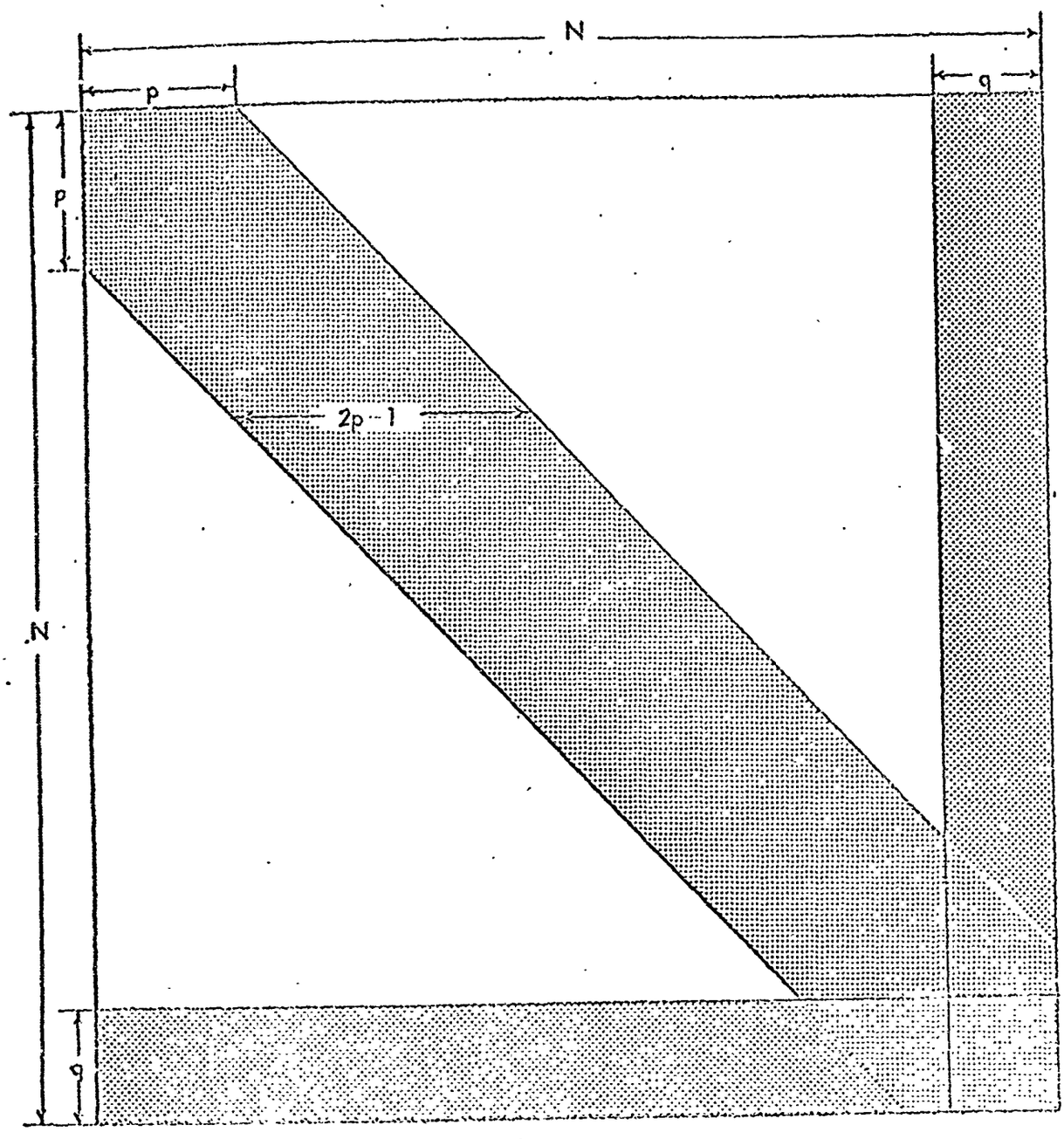

FIGURE 19. General form of banded-bordered coefficient matrix.

convergent geometry is exercised, (b) only from three to five plates having 100 percent overlap are carried in the reduction, and (c) a minimum of about a hundred pass points per plate are employed in the analytical aerotriangulation. The proposed test would establish whether or not equally satisfactory results could be obtained from a block of vertical aerial photographs having fewer points per photo (e.g., the 25 suggested), less overlap, but many more photos (e.g., the 49 suggested).

Our final recommendation is that the concept of the SMAC Multicollimator be explored more deeply in future investigations. In particular, a computer simulation should be performed to determine the minimum number of frames and distribution of images needed for the self-calibration of the directions of the collimators relative to the adopted angle between a selected pair of collimators. Other simulations should be performed to ascertain accuracies to be expected from various distributions of images. Should the outcome of such computer studies be favorable, we would recommend that the approach be tested further by means of a temporary laboratory set up of minimal cost. Such an investigation is especially warranted, we feel, by the fact that a large scale multicollimator currently being considered by the Air Force could well cost close to a million dollars. In our view, a SMAC Multicollimator costing a small fraction of this amount could conceivably produce equal, if not superior, results.

REFERENCES

Brown, D.C., 1956. The Simultaneous Determination of Lens Distortion of a Photogrammetric Camera, AF Missile Test Center Technical Report No. 56-20, Patrick AFB, Florida.

Brown, D.C., 1957. A Treatment of Analytical Photogrammetry with Emphasis on Ballistic Camera Applications, AF Missile Test Center Technical Report No. 57-22, Patrick AFB, Florida.

Brown, D.C., 1958. A Solution to the General Problem of Multiple Station Analytical Stereotriangulation, AF Missile Test Center Technical Report No. 58-8, Patrick AFB, Florida.

Brown, D.C., 1964. An Advanced Plate Reduction for Photogrammetric Cameras, AF Cambridge Research Laboratories Report No. 64-40.

Brown, D.C., 1965. Decentering Distortion of Lenses, Presented at Annual Convention of American Society of Photogrammetry, March 1965. Also published in Photogrammetric Engineering, May, 1966.

Brown, D.C., 1966. Stellar Triangulation (Rockets and Satellites), an article in the International Dictionary of Geophysics, Pergamon Press.

Brown, D.C., 1967a. Calibration of Three High Resolution Lunar Orbiter Cameras, Final Report, May, 1967, to the Boeing Company, Boeing P.O. N-721860-7631.

Brown, D.C., 1967b. Review of Current Geodetic Satellite Programs and Recommendations for Future Programs, Final Report, June, 1967, to NASA Headquarters, Contract No. NASW-1469.

Brown, D.C., 1967c. Computational Tradeoffs in the Design of a One Micron Plate Comparator, Presented at the Semi-Annual Convention of the American Society of Photogrammetry, St. Louis, October, 1967. Also to be published in February 1969 issue of Photogrammetric Engineering.

Brown, D.C., 1968a. Establishment of a Unified Lunar Control Net, Presented at the Annual Convention of the American Society of Photogrammetry, March 1968. Also published in December, 1968 issue of Photogrammetric Engineering.

Brown, D.C., 1968b. Feasibility of a Satellite Surveying Utility, Presented at the 49th Annual Meeting of the American Geophysical Union, April, 1968, Washington, D.C.

Brown, D.C., 1968c. The Self-Calibrating Multilaterative Plate Comparator, Presented to the Eleventh Congress of the International Society of Photogrammetry, July,1968, Lausanne, Switzerland.

Brown, D.C., Davis, R.G., Johnson, F.C., 1964. The Practical and Rigorous Adjustment of Large Photogrammetric Nets. Rome Air Development Center Report No. RADC-TDR-64-353.

Carman, P.D., 1968. The Camera Calibration Laboratory of the National Research Council of Canada. Presented at the Annual Convention of the American Society of Photogrammetry, March,1968, Washington, D.C.

Carman, P.D., Martis, J.F., 1968. Causes of Dimensional Changes in Estar Base Aerial Film Under Simulated Service Conditions, The Canadian Surveyor, June,1968.

Conrady, A., 1919. Decentered Lens Systems, Monthly Notices of the Royal Astronomical Society, Vol. 79, pp. 384-390.

Gambino, L.A., 1967. A Definitive Calibration of an Aerial Camera in its Operating Environment, Presented at the Thirteenth Conference on the Design of Experiments in Army Research, November,1967, Fort Belvoir, Virginia.

Hallert, B., 1954. A New Method for the Determination of the Distortion and the Inner Orientation of Cameras and Projectors, Photogrammetria XI:3 (1954-1955).

Livingstone, R.G., 1966. Airborne Mapping Equipment Quality Development, Photogrammetric Engineering, May,1966.

Morén, A., 1965. A Summary of Tests of Aerial Photographs of the Öland Test Field. Photogrammetric, No. 20, 1965.

Schmid, H., 1953. An Analytical Treatment of the Orientation of a Photogrammetric Camera, Ballistic Research Laboratories Report No. 880. Aberdeen Proving Ground, Maryland.

APPENDIX A

LINEARIZATION OF THE PROJECTIVE EQUATIONS

We assume that possibly nonzero approximations are available for the distortion parameters and set

$$\hat{x} = \bar{x} + \bar{x}(K_1^{00} r^2 + K_2^{00} r^4 + K_3^{00} r^6) + [P_1^{00}(r^2 + 2\bar{x}^2) + 2P_2^{00}\bar{x}\bar{y}][1 + P_3^{00} r^2]$$

$$\hat{y} = \bar{y} + \bar{y}(K_1^{00} r^2 + K_2^{00} r^4 + K_3^{00} r^6) + [2P_1^{00}\bar{x}\bar{y} + P_2^{00}(r^2 + 2\bar{y}^2)][1 + P_3^{00} r^2] \quad \text{(A.1)}$$

in which

$$\bar{x} = x^0 - x_p^{00}$$

$$\bar{y} = y^0 - y_p^{00} \quad \text{(A.2)}$$

$$r = (\bar{x}^2 + \bar{y}^2)^{\frac{1}{2}}.$$

The quantities $\hat{x}, \hat{y}$ then represent values of the measured plate coordinates referred to the approximate principal point and corrected approximately for radial and decentering distortion.

The orientation matrix to be used in the projective equations can assume various forms depending on the choice of angular elements of orientation. We shall limit our consideration here to two specific forms, namely to the expressions given by equations (2.92) and 2.98) in Volume 1 of the Third Edition of the Manual of Photogrammetry. These expressions are

$$(A.3)\quad \begin{bmatrix} A & B & C \\ A' & B' & C' \\ D & E & F \end{bmatrix} = \begin{bmatrix} \cos\alpha\cos\chi & \cos\omega\sin\chi + \sin\alpha\sin\omega\cos\chi & \sin\omega\sin\chi - \sin\alpha\cos\omega\cos\chi \\ -\cos\alpha\cos\chi & \cos\omega\cos\chi - \sin\alpha\sin\omega\sin\chi & \sin\omega\sin\chi + \sin\alpha\cos\omega\sin\chi \\ \sin\alpha & -\cos\alpha\sin\omega & \cos\alpha\cos\omega \end{bmatrix},$$

and

$$(A.4)\quad \begin{bmatrix} A & B & C \\ A' & B' & C' \\ D & E & F \end{bmatrix} = \begin{bmatrix} -\cos\alpha\cos\chi - \sin\alpha\sin\omega\sin\chi & \sin\alpha\cos\chi - \cos\alpha\sin\omega\sin\chi & \cos\omega\sin\chi \\ \cos\alpha\sin\chi - \sin\alpha\sin\omega\cos\chi & -\sin\alpha\sin\chi - \cos\alpha\sin\omega\cos\chi & \cos\omega\cos\chi \\ \sin\alpha\cos\omega & \cos\alpha\cos\omega & \sin\omega \end{bmatrix}.$$

The orientation matrix is applied to rotate the direction cosines λ, μ, ν defining a ray in object space into the corresponding direction cosines m, n, q in image space:

$$(A.5)\quad \begin{bmatrix} m \\ n \\ q \end{bmatrix} = \begin{bmatrix} A & B & C \\ A' & B' & C' \\ D & E & F \end{bmatrix} \begin{bmatrix} \lambda \\ \mu \\ \nu \end{bmatrix}.$$

In the process of linearization of the observational equations, we shall require the matrix

$$(A.6)\quad \frac{\partial(m,n,q)}{\partial(\alpha,\omega,\chi)} = \begin{bmatrix} \frac{\partial m}{\partial\alpha} & \frac{\partial m}{\partial\omega} & \frac{\partial m}{\partial\chi} \\ \frac{\partial n}{\partial\alpha} & \frac{\partial n}{\partial\omega} & \frac{\partial n}{\partial\chi} \\ \frac{\partial q}{\partial\alpha} & \frac{\partial q}{\partial\omega} & \frac{\partial q}{\partial\chi} \end{bmatrix}.$$

When the orientation matrix is defined by (A.3) this matrix is of the form

$$(A.7)\quad \frac{\partial(m,n,q)}{\partial(\alpha,\omega,\varkappa)} = \begin{bmatrix} -q\cos\varkappa & -C\mu + B\nu & n \\ q\sin\varkappa & -C'\mu + B'\nu & -m \\ p & -F\mu + E\nu & 0 \end{bmatrix},$$

in which

$$(A.8)\quad p = \lambda\cos\alpha + \mu\sin\alpha\sin\omega - \nu\sin\alpha\cos\omega.$$

Alternatively, when (A.4) is used, it becomes

$$(A.9)\quad \frac{\partial(m,n,q)}{\partial(\alpha,\omega,\varkappa)} = \begin{bmatrix} B\lambda - A\mu & -q\sin\varkappa & n \\ B'\lambda - A'\mu & -q\cos\varkappa & -m \\ E\lambda - D\mu & p & 0 \end{bmatrix},$$

in which

$$(A.10)\quad p = -\lambda\sin\alpha\sin\omega - \mu\cos\alpha\sin\omega + \nu\cos\omega.$$

At this point, we shall assume that approximations $\alpha^{00}, \omega^{00}, \varkappa^{00}$ have been employed in the evaluation of the orientation matrix and that the resulting orientation matrix is used in (A.5) to generate approximate direction cosines m^{00}, n^{00}, q^{00}. We then define

$$(A.11)\quad \begin{aligned} x^{00} &= c^{00}(m^{00}/q^{00}) \\ y^{00} &= c^{00}(n^{00}/q^{00}) \end{aligned}$$

in which c^{00} denotes an approximation to the principal distance. The quantities x^{00}, y^{00} denote the computed values of the plate coordinates referred to the principal point. The

differences between (A. 1) and (A. 11) generate the observational equations for the adjustment

$$
\begin{aligned}
f_1^0 &= \hat{x} - x^{00} \\
f_2^0 &= \hat{y} - y^{00} \quad .
\end{aligned}
\tag{A. 12}
$$

The elements of the discrepancy vector of the linearized observational equations are given simply by

$$
\epsilon = \begin{bmatrix} -f_1^0 \\ -f_2^0 \end{bmatrix} = - \begin{bmatrix} \hat{x} - x^{00} \\ \hat{y} - y^{00} \end{bmatrix} . \tag{A. 13}
$$

The elements of the A matrix are provided by

$$
A = \frac{\partial(f_1^0, f_2^0)}{\partial(x^0, y^0)} = \begin{bmatrix} 1+\xi_{11} & 0+\xi_{12} \\ 0+\xi_{21} & 1+\xi_{22} \end{bmatrix} , \tag{A. 14}
$$

in which the quantities ξ_{ij} are first order functions of the approximate distortion parameters and are obtained from the differentiation of (A. 1) with respect to x^0, y^0. Inasmuch as these first order quantities generate second order quantities when multiplied by the first order variations in the plate coordinates (i.e., the residuals v_x, v_y), they may ordinarily be neglected.

To express the elements of the $\dot{B}$ matrix compactly, we find it convenient to introduce the auxiliaries:

$$
\begin{aligned}
M &= m^{00}/q^{00} \\
N &= n^{00}/q^{00} \\
Q &= c^{00}/q^{00}
\end{aligned}
\tag{A. 15}
$$

$$U = P_1^{00}(r^2 + 2\bar{x}^2) + 2P_2^{00}\bar{x}\bar{y}$$

(A.16) $$V = 2P_1^{00}\bar{x}\bar{y} + P_2^{00}(r^2 + 2\bar{y}^2)$$

$$W = 1 + P_3^{00}\, r^2$$

The expressions for the elements of the $\dot{B}$ matrix then become

(A.17) $$\dot{B}^T = \begin{bmatrix} b_1 & b_1' \\ b_2 & b_2' \\ b_3 & b_3' \\ b_4 & b_4' \\ b_5 & b_5' \\ b_6 & b_6' \\ b_7 & b_7' \\ b_8 & b_8' \\ b_9 & b_9' \end{bmatrix} = \begin{bmatrix} -1-\xi_{11} & 0-\xi_{12} \\ 0-\xi_{12} & -1-\xi_{22} \\ -M & -N \\ \bar{x}r^2 & \bar{y}r^2 \\ \bar{x}r^4 & \bar{y}r^4 \\ \bar{x}r^6 & \bar{y}r^6 \\ (r^2+2\bar{x}^2)W & 2\bar{x}\bar{y}W \\ 2\bar{x}\bar{y}W & (r^2+2\bar{y}^2)W \\ Ur^2 & Vr^2 \end{bmatrix},$$

in which the ξ_{ij} are the same negligible quantities as those appearing in the A matrix.

Those elements of the $\ddot{B}$ matrix pertaining to the angular elements of orientation can be computed from

$$\begin{bmatrix} \ddot{b}_1 & \ddot{b}_1' \\ \ddot{b}_2 & \ddot{b}_2' \\ \ddot{b}_3 & \ddot{b}_3' \end{bmatrix} = Q \begin{bmatrix} \frac{\partial m}{\partial \alpha} & \frac{\partial m}{\partial \omega} & \frac{\partial m}{\partial \kappa} \\ \frac{\partial n}{\partial \alpha} & \frac{\partial n}{\partial \omega} & \frac{\partial n}{\partial \kappa} \\ \frac{\partial q}{\partial \alpha} & \frac{\partial q}{\partial \omega} & \frac{\partial q}{\partial \kappa} \end{bmatrix}^{00} \begin{bmatrix} 1 & 0 \\ 0 & 1 \\ -M & -N \end{bmatrix},$$

in which the superscript '00' denotes that the elements of the matrix are computed from approximations.

In cases where the coordinates of the exposure station are to be recovered, the remainder of the $\ddot{B}$ matrix can be computed from

$$\begin{bmatrix} \ddot{b}_4 & \ddot{b}'_4 \\ \ddot{b}_5 & \ddot{b}'_5 \\ \ddot{b}_6 & \ddot{b}'_6 \end{bmatrix} = \frac{Q}{R^{00}} \begin{bmatrix} A & A' & D \\ B & B' & E \\ C & C' & F \end{bmatrix}^{00} \begin{bmatrix} 1 & 0 \\ 0 & 1 \\ -M & -N \end{bmatrix},$$

in which R^{00} denotes the approximate distance between the control point and the exposure station, namely

$$R^{00} = \{[X-(X^c)^{00}]^2 + [Y-(Y^c)^{00}]^2 + [Z-(Z^c)^{00}]^2\}^{\frac{1}{2}}.$$

APPENDIX B

RESULTS OF AERIAL SMAC CALIBRATIONS FOR KC-6A CAMERAS 005 AND 008

In the main body of the report the results of two Aerial SMAC calibrations of Camera 006 were discussed and analyzed in considerable detail. Though of secondary interest in the flight testing program, Cameras 005 and 008 were also subjected to Aerial SMAC calibrations. Key results of those calibrations are summarized below in Table and Figure

For the most part, the results for 005 and 008 are comparable with those obtained for Camera 006. Thus, rather large displacements of the principal point, particularly in x_p, are experienced, and one sigma accuracies of one micron or better are obtained for the distortion functions over most of the format. However, unlike the decentering distortion for Camera 006 which had been found to be unusually low, that for Camera 005 (Fig. 20) turned out to be decidedly on the high side, growing to as much as 15 microns within the format. Decentering distortion for Camera 008 (Fig. 20) was found to be more nearly typical of the average modern mapping lens.

Comparisons between results from Aerial SMAC and results from conventional multicollimator calibrations are given in the main body of the report. There, too, are given the results of the Stellar SMAC calibration of Camera 008.

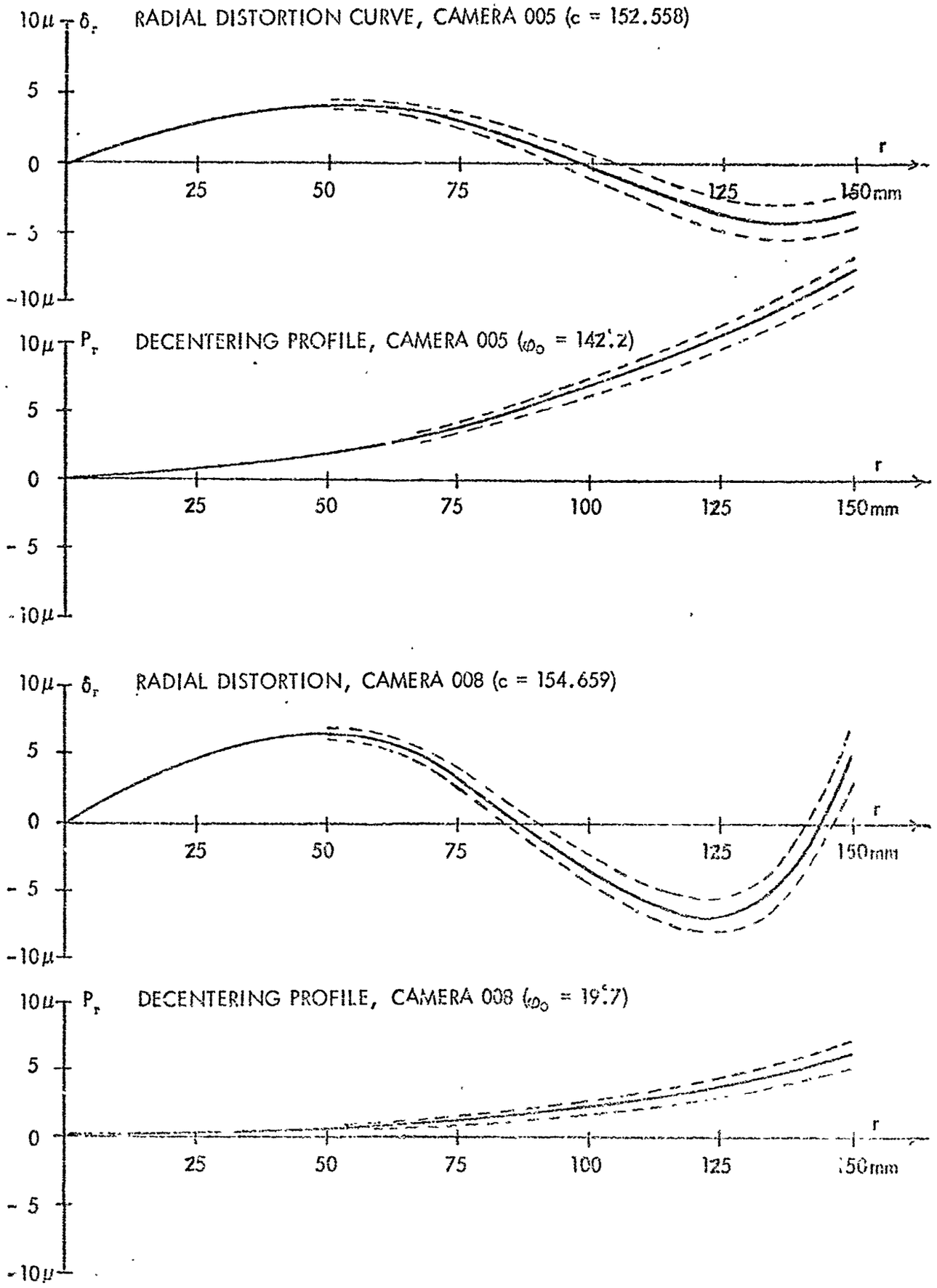

Figure 20. Radial distortion curves and decentering profiles resulting from Aerial SMAC calibrations of Cameras 005 and 008.

TABLE 9. Summary of Results of Aerial SMAC Calibrations of Cameras 005 and 008.

CAMERA 005 (Test No. 2)		CAMERA 008 (Test No. 1)	
Parameter	Value	Parameter	Value
x_p (mm)	.167±.004	x_p (mm)	.175±.003
y_p (mm)	-.045±.004	y_p (mm)	-.052±.003
c (mm)	152.539±.002	c (mm)	154.626±.002
K_1 (mm/mm^3)	$(-.180\pm.018)\times 10^{-7}$	K_1 (mm/mm^3)	$(-.385\pm.015)\times 10^{-7}$
K_2 (mm/mm^5)	$(.503\pm.079)\times 10^{-12}$	K_2 (mm/mm^5)	$(1.347\pm.063)\times 10^{-12}$
J_1 (mm/mm^2)	$(6.808\pm.434)\times 10^{-7}$	J_1 (mm/mm^2)	$(2.550\pm.359)\times 10^{-7}$
Φ_0 (deg)	142.2±3.7	Φ_0 (deg)	19.7±7.7

POINTS ON RADIAL AND DECENTERING DISTORTION CURVES

CAMERA 005			CAMERA 008		
r (mm)	δ_r[a] (Microns)	P_r (Microns)	r (mm)	δ_r[b] (Microns)	P_r (Microns)
0	0	0	0	0	0
20	2.4±0.01	0.27±0.02	20	4.0±0.01	0.10±0.01
40	4.0±0.11	1.09±0.07	40	6.4±0.09	0.41±0.06
60	4.2±0.20	2.45±0.16	60	5.8±0.27	0.92±0.13
80	2.7±0.67	4.36±0.28	80	2.1±0.56	1.63±0.23
100	-0.1±1.05	6.81±0.43	100	-3.3±0.88	2.55±0.36
120	-3.1±1.31	9.80±0.63	120	-6.9±1.12	3.67±0.52
140	-4.3±1.41	13.34±0.98	140	-2.7±1.20	5.00±0.70

(a) referred to value of c of 151.262mm

(b) referred to value of c of 151.255mm

Unclassified
Security Classification

DOCUMENT CONTROL DATA - R&D
(Security classification of title, body of abstract and indexing annotation must be entered when the overall report is classified)

1. ORIGINATING ACTIVITY *(Corporate author)*
DBA Systems, Inc., P.O. Drawer 550
Melbourne, Florida 32901

2a. REPORT SECURITY CLASSIFICATION
Unclassified

2b. GROUP

3. REPORT TITLE
ADVANCED METHODS FOR THE CALIBRATION OF METRIC CAMERAS

4. DESCRIPTIVE NOTES *(Type of report and inclusive dates)*
Final Technical Report, Part 1

5. AUTHOR(S) *(Last name, first name, initial)*
Duane C. Brown

6. REPORT DATE	7a. TOTAL NO. OF PAGES	7b. NO. OF REFS
9 December 1968	117	21

8a. CONTRACT OR GRANT NO.
DA-44-009-AMC-1457(X)

b. PROJECT NO. 4A 00145001A52C

c. 01

d. 006

9a. ORIGINATOR'S REPORT NUMBER(S)
N/A

9b. OTHER REPORT NO(S) *(Any other numbers that may be assigned this report)*
N/A

10. AVAILABILITY/LIMITATION NOTICES
Distribution of this document is unlimited. It may be released to the Clearinghouse, Department of Commerce, for sale to general public.

11. SUPPLEMENTARY NOTES

12. SPONSORING MILITARY ACTIVITY
U.S. Army Engineer Topographic Laboratories
Fort Belvoir, Virginia

13. ABSTRACT

A new analytical approach to the problem of the accurate calibration of metric cameras is developed and specific applications are reported. The method permits an indefinitely large number of frames from a given camera to be reduced simultaneously, yet efficiently, to produce common parameters of the inner cone for all frames, as well as independent elements of exterior orientation for each frame. Because control points may be exercised repeatedly in a common reduction, very large sets of well distributed residuals can be generated from a relatively small set of control points (in principle, a complete and accurate calibration could be performed from as few as three control points). From such large sets of residuals empirical functions can be derived to account for persistent, unmodelled systematic error. In addition, it becomes feasible to establish the variation in the accuracies of the radial and tangential components of plate coordinates throughout the format and thus to establish appropriate empirical weighting functions for subsequent applications. The method is of universal applicability and encompasses (a) calibrations from aerial photographs, (b) calibrations from stellar photographs, and (c) calibrations from multicollimator photographs. Applied to stellar calibrations, the method leads to improved accuracies and convenience by completely doing away with conventional requirements for precise timing of the shutter and for stability of the camera throughout successive exposures. Applied to multicollimator calibrations, the method has far reaching implications concerning both the use of existing multicollimators and the design of future multicollimators.

DD FORM 1 JAN 64 1473

Unclassified
Security Classification

Unclassified

Security Classification

14 KEY WORDS	LINK A		LINK B		LINK C	
	ROLE	WT	ROLE	WT	ROLE	WT
camera calibration photogrammetry analytical photogrammetry least squares						

INSTRUCTIONS

1. ORIGINATING ACTIVITY: Enter the name and address of the contractor, subcontractor, grantee, Department of Defense activity or other organization *(corporate author)* issuing the report.

2a. REPORT SECURITY CLASSIFICATION: Enter the overall security classification of the report. Indicate whether "Restricted Data" is included. Marking is to be in accordance with appropriate security regulations.

2b. GROUP: Automatic downgrading is specified in DoD Directive 5200 10 and Armed Forces Industrial Manual. Enter the group number Also, when applicable, show that optional markings have been used for Group 3 and Group 4 as authorized.

3. REPORT TITLE: Enter the complete report title in all capital letters. Titles in all cases should be unclassified. If a meaningful title cannot be selected without classification, show title classification in all capitals in parenthesis immediately following the title.

4. DESCRIPTIVE NOTES: If appropriate, enter the type of report, e.g., interim, progress, summary, annual, or final. Give the inclusive dates when a specific reporting period is covered.

5. AUTHOR(S): Enter the name(s) of author(s) as shown on or in the report. Enter last name, first name, middle initial. If military, show rank and branch of service. The name of the principal author is an absolute minimum requirement.

6. REPORT DATE: Enter the date of the report as day, month, year; or month, year. If more than one date appears on the report, use date of publication.

7a. TOTAL NUMBER OF PAGES: The total page count should follow normal pagination procedures, i.e., enter the number of pages containing information.

7b. NUMBER OF REFERENCES: Enter the total number of references cited in the report.

8a. CONTRACT OR GRANT NUMBER: If appropriate, enter the applicable number of the contract or grant under which the report was written.

8b, 8c, & 8d. PROJECT NUMBER: Enter the appropriate military department identification, such as project number, subproject number, system numbers, task number, etc.

9a. ORIGINATOR'S REPORT NUMBER(S): Enter the official report number by which the document will be identified and controlled by the originating activity. This number must be unique to this report.

9b. OTHER REPORT NUMBER(S): If the report has been assigned any other report numbers *(either by the originator or by the sponsor)*, also enter this number(s).

10. AVAILABILITY/LIMITATION NOTICES: Enter any limitations on further dissemination of the report, other than those imposed by security classification, using standard statemen such as:

(1) "Qualified requesters may obtain copies of this report from DDC."

(2) "Foreign announcement and dissemination of this report by DDC is not authorized."

(3) "U. S. Government agencies may obtain copies of this report directly from DDC. Other qualified DDC users shall request through

_____."

(4) "U. S. military agencies may obtain copies of this report directly from DDC. Other qualified users shall request through

_____."

(5) "All distribution of this report is controlled. Qualified DDC users shall request through

_____."

If the report has been furnished to the Office of Technic Services, Department of Commerce, for sale to the public, in cate this fact and enter the price, if known.

11. SUPPLEMENTARY NOTES: Use for additional explana tory notes.

12. SPONSORING MILITARY ACTIVITY: Enter the name o the departmental project office or laboratory sponsoring *(pay ing for)* the research and development. Include address.

13. ABSTRACT: Enter an abstract giving a brief and factu summary of the document indicative of the report, even thou it may also appear elsewhere in the body of the technical re port. If additional space is required, a continuation sheet sl be attached.

It is highly desirable that the abstract of classified rep be unclassified. Each paragraph of the abstract shall end w an indication of the military security classification of the in formation in the paragraph, represented as *(TS), (S), (C), or (*

There is no limitation on the length of the abstract. Ho ever, the suggested length is from 150 to 225 words.

14 KEY WORDS: Key words are technically meaningful ter or short phrases that characterize a report and may be used index entries for cataloging the report. Key words must be selected so that no security classification is required. Ident fiers, such as equipment model designation, trade name, mili project code name, geographic location, may be used as key words but will be followed by an indication of technical con text The assignment of links, rules, and weights is optiona

GPO 886-551

Unclassified

Security Classification